BIOSYSMO

Deliverable D3.6

Report on aggregated and immobilized consortia and biofilms

Deliverable information	
Responsible Partner:	JSI
Work Package	3 - Development and optimization of consortia and plant-microbe biosystems
Author(s):	Dmitrii Deev, Tomaž Rijavec, Kristian Gašpirc, Maja Zugan, Tayebeh Sharifi, Aleš Lapanje, Diana Losantos, Andre Granadeiro.
Contributing Partner(s):	JSI, LEITAT
Dissemination Level:	PU - public
Type:	R – Document, report
Due Date:	31/08/2025
Submission Date:	29/08/2025
Version:	V 1.0

Funded by the European Union under the GA no **101060211**.
Views and opinions expressed are however those of the author(s) only and do not necessarily reflect those of the European Union or REA. Neither the European Union nor the granting authority can be held responsible for them.

Project Profile

Programme	Horizon Europe
Call	HORIZON-CL6-2021-ZEROPOLLUTION-01
Topic	HORIZON-CL6-2021-ZEROPOLLUTION-01-10
Number	101060211
Acronym	BIOSYSMO
Title	BIOremediation systems exploiting SYnergieS for improved removal of Mixed pOllutants
Start Date	1 September 2022
Duration	48 months

Document History

Version	Date	Author	Remarks
0.0	25/07/2025	JSI	Prepared Outline
0.1	26/07/2025	JSI	Prepared draft
0.2	28/07/2025	LEITAT	Updated document and added contribution
0.3	27/08/2025	JSI	Preparing the final version
1.0	29/08/2025	JSI	Final version

Disclaimer

All the contributors to this deliverable declare that they:

- *Are aware that plagiarism and/or literal utilisation (copy) of materials and texts from other Projects, works and deliverables must be avoided and may be subject to disciplinary actions against the related partners and/or the Project consortium by the EU.*
- *Confirm that all their individual contributions to this deliverable are genuine and their own work or the work of their teams working in the Project, except where is explicitly indicated otherwise.*
- *Have followed the required conventions in referencing the thoughts, ideas and texts made outside the Project.*

Executive Summary

This deliverable (D3.6) presents the final results of Task 3.2 within Work Package 3 of the BIOSYSMO project, focusing on strategies for enhancing microbial consortia biodegradation through spatial structuring via synthetic aggregates and biofilms, including electroactive variants. Building on methodologies from intermediate report D3.2 and incorporating consortia from WP1 Task 1.3, it integrates JSI and LEITAT efforts, linking to metabolic modelling (WP2 Task 2.2) and bioremediation applications (WP4, WP5) for surface water, estuarine sediments, and groundwater.

Subtask 3.2.1 (JSI-led) details consortia design with microgeographic placement, including protocols for multicellular aggregates enabling aerobic-anaerobic niches, vaterite-based carriers for hydrophobic pollutants like PAHs and pesticides, planar biofilm attachment to plant roots (e.g., Phragmites australis), controlled electrostatic aggregation, and flow cytometry assays for GMO strain growth on atrazine/lindane.

Subtask 3.2.2 (JSI and LEITAT collaboration) covers electroactive biofilm development, with polypyrrole electrode modifications enhancing bacterial attachment, polyelectrolyte layering for multilayered structures, carbon brush optimizations, and redox potential modulation protocols for BES targeting metals (three/two-electrode configurations), hydrocarbons (H-type/flat-plate reactors with kerosene), and chlorinated ethenes (electrolysis cells with bioaugmentation).

Table of Contents

List of Figures

List of Tables

Table of Abbreviations

Abbreviation	Definition
CV	Cyclic Voltammetry
EET	Extracellular Electron Transfer
PPY	Polypyrrole
OD	Optical Density
PEI	Polyethylenimine
BES	Bioelectrochemical Systems
ORR	Oxygen Reduction Reactions
SRB	Sulfate-Reducing Bacteria
GW	Groundwater
HC	Hydrocarbons
TPH	Total Petroleum Hydrocarbons
CE	Chlorinated Ethenes
TCE	Trichloroethene
PCE	Perchloroethene
VC	Vinyl Chloride
SSW	Stainless Steel Wool
µLUME	Micro-Lure, Microfluidics And Entrapment
PAH	Polycyclic Aromatic Hydrocarbons
M9	Minimal Growth Medium Formulation
ELS	Electro Light Scattering
OCP	Open Circuit Potential
LE	Loading Efficiency
BES-M	Bioelectrochemical System For Metals
OCV	Open Circuit Voltammetry
LSV	Linear Sweep Voltammetry
EIS	Electrochemical Impedance Spectroscopy
SEM	Scanning Electron Microscopy
PAH	Poly(Allylamine Hydrochloride)
PSS	Poly(Sodium 4-Styrenesulfonate)
CFU	Colony Forming Unit
DSM 720	Desulfitobacterium Hafniense Medium
LB	Luria-Bertani Medium
PGPR	Plant Growth-Promoting Rhizobacteria
CLSM	Confocal Laser Scanning Microscopy
GFP	Green Fluorescent Protein
PDI	Polydispersity Index

WCA	Water Contact Angle
OHRB	Organohalide-Respiring Bacteria
LBL	Layer-By-Layer
Rct	Charge Transfer Resistance
TAP	Tris-Acetate-Phosphate Medium
AC	Air-Diffusion Cathodes
LC	Liquid Cathodes
CEM	Cathion Exchange Membrane
MMO	Mixed Metal Oxide
BTEX	Benzene, Toluene, Ethylbenzene, Xylenes
GC-MS	Gas Chromatography-Mass Spectrometry
GC-FID	Gas Chromatography With Flame Ionization Detector
MFC	Microbial Fuel Cell

1 General Introduction

This deliverable presents the final results of strategies for enhancing biodegradation capabilities of microbial consortia through controlled spatial distribution via synthetic aggregates and biofilms. The work represents the culmination of activities within WP3 Task 3.2, building upon methodological foundations established in the intermediate report D3.2 and integrating bacterial consortia isolated during WP1 Task 1.3.

The activities are structured within two complementary subtasks: T3.2.1, which explores the effects of spatial structuring on intercellular interactions within microbial communities, and T3.2.2, which focuses on spatial distribution and immobilization strategies for enhancing biodegradation activity in Bioelectrochemical Systems (BES). This work is integral to the broader BIOSYSMO framework, connecting microbial resource acquisition (WP1 T1.3), metabolic modelling (WP2 T2.2), and downstream applications in bioremediation systems (WP4, WP5).

The developed methodologies target applications in surface water bioremediation, estuarine sediment treatment, and groundwater remediation using BES technologies. These spatially-engineered microbial systems will be implemented in rhizosphere-based phytoremediation (T4.1), estuarine sediment treatment (T4.3), and bioelectrochemical groundwater treatment (T4.4).

During this last reporting period, JSI concentrated on developing robust methods for spatial structuring of multicellular biofilms, construction of defined microenvironments with versatile metabolic pathways for pollutant biodegradation, and assessment of the efficacy of these strategies. Moreover, to extend the applicability of the developed new methods JSI developed (i) protocols for efficient delivery of bacterial cell to plant rhizospheres as engineered biofilms that can be applied to different plants and (ii) elaborated innovative strategies based on iACME and µLUME concepts for enhanced electroactive consortia performance. Concurrently, LEITAT focused on engineering BES systems for metal precipitation, hydrocarbon degradation, and chlorinated ethene remediation and determine the electrochemical conditions to guarantee a successful inoculation of electroactive biofilms.

JSI's work encompassed five primary research directions: (1) Development of methods for constructing robust multicellular aggregates that are enabling separation of aerobic (oxidative) and anaerobic (reductive) niches i.e. composed of strictly anaerobic sulphate-reducing bacteria (SRB) and aerobic bacteria *Cobetia marina* and determining their metabolic activity through the metal reduction assay vanadate during the incubation under the aerobic conditions. (2) Enhancement of aggregation methods to achieve precise structural control, enabling defined biofilm architecture with established protocols for construction, characterization, and performance evaluation. (3) Development of the µLUME approach for handling hydrophobic pollutants, allowing controlled planktonic phase management while serving as a carrier platform for polycyclic aromatic hydrocarbons (PAHs), pesticides including lindane and atrazine, with demonstrated platform stability and validated methods for assessing genetically modified pesticide-degrading organism growth. (4) Extension of two-dimensional structural approaches through development of protocols for constructing robust multi-layered bacterial biofilms and novel protocols for bacterial cell delivery to plant roots, developed in collaboration with CIIMAR. (5) Investigation of novel approaches for modifying conductive graphite electrodes to enhance bacterial attachment, with successful application to large-surface electrodes including carbon brushes.

JSI and LEITAT collaboratively developed and validated BES prototypes maintaining anaerobic conditions while enabling continuous monitoring of biofilm structure and activity without system disassembly.

Within the context of WP3 activities, LEITAT developed three distinct reactor inoculation strategies: (i) Metal removal systems utilizing biofilms as electron donors through organic matter degradation, with electrons driving cathodic metal removal, either by electrodeposition or indirect by-product precipitation due to oxygen reduction reactions (ORR), in three-chamber flat-plate reactors operated under controlled electrochemical potential. (ii) Hydrocarbon removal systems promoting weak electrogens capable of electrode interaction to assist indigenous hydrocarbon-degrading microorganisms, implemented in single-chamber H-type reactors with air cathodes, subsequently modified to include liquid cathode strategies. (iii) Chlorinated ethene remediation systems for both oxidative (in the anode) and reductive dichlorination (cathode), with ongoing enrichment and CE degradation in flat-plate microbial electrolysis cells and a posterior membrane-less tubular reactor.

The integration of JSI and LEITAT efforts will focus on implementing validated methodologies with isolated strains from T1.3, integrating activities across WP4 and WP5 to optimize bioelectrochemical and phyto-bioelectrochemical systems for enhanced field-scale bioremediation applications.

2 Subtask 3.2.1. Design of consortia with microgeographic placement and redistribution of microbial cells

2.1 Construction of multispecies bacterial 3D structures and assessment of their spatiotemporal dynamics

2.1.1 Introduction

This section presents protocols for creating functional anaerobic microenvironments within aerated systems, enabling controlled spatial organization of microbial communities with complementary metabolic capabilities.

Initial random aggregation experiments were established and reported in D3.2. The current work extends these approaches through controlled aggregation strategies, comparing four experimental configurations: non-precise random aggregation, aggregation around SRB cores, multi-species cores (SRB + *Cobetia marina* interior coated with an additional *Cobetia* layer), and SRB suspensions without aggregation in aerated conditions as negative controls. These systems utilized sulfate-reducing bacteria (*Desulfovibrio africanus* DSM2603, *Desulfosporosinus hippei* DSM8344, *Desulfitobacterium* sp. G1-2) with *Cobetia marina*, with electrogenic activity validated through vanadium reduction assays.

In addition to developing cell–cell spatially organized 3D structures such as granules and flocs, JSI is advancing methods to engineer 2D and 3D planar architectures. These approaches serve two purposes: (i) structuring biofilms directly on electrodes, and (ii) minimizing biofilm size for high-throughput testing in microfluidic assays, where vaterite-based core–shell particles can be applied. Moreover, since many pollutants are hydrophobic and insoluble in polar solvents, they cannot be

directly used in biodegradation assays. Incorporating such pollutants into vaterite particles bridges this gap by avoiding the need for emulsifiers (which can themselves serve as additional carbon sources) while providing pollutant-loaded particles with a high surface area for efficient bacterial contact. .PAH-loading protocols and vaterite synthesis are described in D4.2 (Annex III), while aggregation protocols on vaterite are detailed in the current deliverable. Six bacterial consortia isolated from BIOSYSMO sampling sites 6 and 7 using the µLUME (micro-Lure, Microfluidics and Entrapment) approach were previously tested for PAH degradation as reported in D3.2. Based on 16S rRNA gene sequencing and phylogenetic analysis, two consortia candidates were selected for evaluation using the vaterite system, assessing both electrogenic activity via vanadium reduction and PAH degradation capabilities. The objective is to construct core-shell aggregate structures with anaerobically-isolated consortia forming the oxygen-depleted core and aerobically-isolated consortia constituting the outer layer, optimizing both PAH degradation efficiency and electrogenicity for integration into BES hydrocarbon removal systems (WP4 and WP5).

Given the novelty of µLUME-based consortium isolation, community stability represents a critical parameter for controlled system development. The temporal stability of a selected µLUME-derived PAH-degrading bacterial consortium I18-S0211, previously isolated during T1.3 activities and subjected to microcosm experiments reported in D4.2, was assessed over a 14-day cultivation period using 16S rRNA gene sequencing. Results demonstrated that while minor taxonomic groups exhibited temporal variation, major genera remained stable throughout the cultivation period, indicating robust community structure suitable for controlled biofilm applications.

2.1.2 Methods

2.1.2.1 Assessment of different aggregation strategies for building multispecies aggregates

Considering the morphological diversity and physiological variability of sulfate-reducing bacteria, aggregation strategies were evaluated using three representative SRB strains: *Desulfovibrio africanus* DSM2603, Desulfosporosinus *hippei* DSM8400, and *Desulfitobacterium* sp. G1-2. *D. africanus* DSM2603 and *D. hippei* DSM8400 were cultivated in DSM 641 medium, while *Desulfitobacterium* sp. G1-2 was grown in DSM 720 medium. All SRB cultures were maintained under strict anaerobic conditions at 28°C for 21 days to achieve stationary phase biomass.

The marine aerobe *Cobetia marina* DSM50416 served as the model aerobic strain. Cultivation was performed in DSM 79 medium at 28°C for 48 hours under continuous agitation (180 rpm). Biomass was harvested by centrifugation (7,000 × g, 5 min) and washed twice in sterile 0.9% NaCl solution. Prior to aggregation experiments, washed biomass was fluorescently labelled using SYTO 11 (green) for aerobic strains and SYTO 64 (red) for SRB strains according to manufacturer specifications.

Based on previous findings reported in D3.2 demonstrating the critical importance of aggregation protocols and cultivation strategies for system stability, four distinct aggregation configurations were developed to assess electrostatic cell interactions and anaerobic microenvironment formation (Figure 1):

- Case I (Negative Control): Non-aggregated planktonic suspensions of SRB strains maintained in aerated conditions to establish baseline anaerobic activity loss.
- Case II (Positive Control): Standard random aggregation using polyethyleneimine (PEI) coating as previously described in D3.2, where one cell population was electrostatically modified to promote non-specific aggregation with uncoated cells.

- Case III (Mixed Core Configuration): Multi-species cores containing both SRB and *C. marina* in the interior, with an additional external C. marina layer to establish gradient oxygen conditions.
- Case IV (SRB Core Configuration): Dense SRB cores formed through controlled aggregation, subsequently coated with an external layer of *C. marina* cells to create defined core-shell architectures.

Constructed aggregation systems were inoculated in media appropriate for the respective SRB strains and supplemented with 3 mM V_2O_5 as an electron acceptor for anaerobic respiration. Incubation was performed under aerated conditions (28°C, 180 rpm) for 7 days to simulate realistic environmental oxygen exposure. Samples were collected at 24 hours, 6 days, and 7 days for temporal analysis.

Aggregate integrity and spatial organization were monitored using fluorescence microscopy to track the distribution of fluorescently-labelled cell populations. Ongoing anaerobic metabolic activity within constructed aggregates was quantified through V^{5+} concentration measurements using a modified diphenylcarbazide (DPC) colorimetric assay as detailed in D3.2. This approach enables direct assessment of vanadium reduction as a proxy for maintained anaerobic respiratory activity despite aerobic environmental conditions.

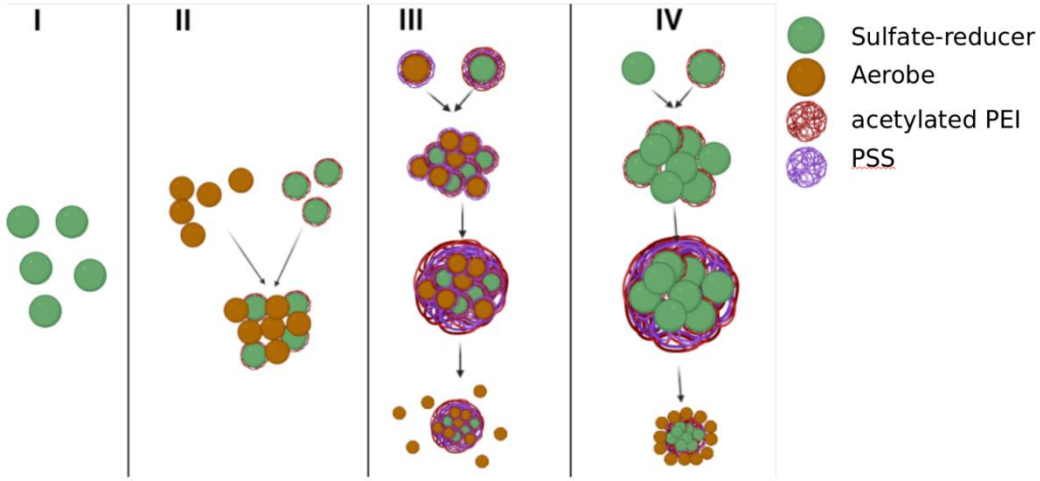

Figure 1. Scheme of tested cases for construction of multi-species aggregates

2.1.2.2 Vaterite-based carrier systems for constructing controlled aerobic-anaerobic aggregates

Selected bacterial candidates were attached to 6 µm vaterite particles pre-loaded with a mixture of pyrene and benzo-a-pyrene. Detailed protocols for particle synthesis and PAH-loading procedures are described in Annex III of D4.2. Bacterial candidates were recovered from -80°C glycerol stocks and inoculated into minimal medium (MM) supplemented with 3.8 mM V_2O_5 and containing 10 mg of PAH-loaded vaterite particles as the sole carbon source. Anaerobic candidates were cultivated in medium purged with N_2 gas and maintained under anoxic conditions throughout the experiment.

Abiotic controls consisting of MM containing PAH-loaded vaterite particles without bacterial inoculation were included to monitor potential chemical reduction of vanadate in the absence of

biological activity. All experimental systems were incubated for 14 days at 28°C under continuous agitation (180 rpm).

Sample aliquots (2 mL) were collected at 3-, 7-, and 14-days post-inoculation for temporal analysis. Each sample was divided for parallel analyses: 1 mL was allocated for PAH degradation profiling using Gas Chromatography with Flame Ionization Detection (GC-FID), and 1 mL was used for V^{5+} concentration measurements via the diphenylcarbazide (DPC) colorimetric method. All measurements were performed in biological duplicates with technical triplicates, and V^{5+} concentrations were determined against a calibration curve prepared from standard solutions.

2.1.2.3 Phylogenetic characterization and community stability assessment

2.1.2.3.1 Electrogenic Consortium Characterization

Six bacterial consortia candidates, previously isolated using the µLUME approach and reported in D3.2, were subjected to phylogenetic analysis to guide selection for vaterite-based experiments. These consortia represent candidates with demonstrated PAH degradation/electrogenic activity capabilities under different environmental conditions and were characterized to assess their taxonomic composition and potential electrogenic properties.

2.1.2.3.2 Temporal Stability Analysis of PAH-Degrading Community

The stability of the PAH-degrading consortium I18-S0211, previously characterized and reported in D4.2, was evaluated over an extended cultivation period. The consortium was cultivated according to protocols detailed in Annex III of D4.2, using minimal medium supplemented with PAH-loaded vaterite particles. Samples were collected at 3, 5, 10, and 14 days of cultivation to assess temporal changes in community composition and detect potential population shifts that could affect degradation performance.

2.1.2.3.3 16S rRNA Gene Sequencing and Analysis

Bacterial communities in all samples were characterized through 16S rRNA gene sequencing following the comprehensive methodology described in deliverable D1.2, Annex II: Protocols of Microfluidic Enrichment, encompassing "Sample preparation and pre-treatment", "DNA isolation", "PCR amplification, library prep and sequencing" and "Bioinformatics analyses" sections. For bioinformatics analyses, updated software versions were employed: BLAST+ (v2.16.0+), 16_ribosomal_RNA database (2025-04-01), and MEGAN6 (v6.25.10) to ensure current taxonomic assignments and enhanced analysis precision.

2.1.3 Results

2.1.3.1 Aggregate structure formation and spatial organization

The applied aggregation strategies successfully generated distinct multicellular structures with characteristic spatial organization patterns. Fluorescence microscopy analysis revealed clear differentiation in cellular distribution for each aggregation protocol, demonstrating controlled assembly of aerobic-anaerobic interfaces.

Non-precise aggregation (case II,Figure 1) resulted in heterogeneous cellular distribution with mixed fluorescent signals uniformly dispersed across the aggregate surface (Figure 2 - A and D), indicating random intercellular associations without defined spatial organization. Mixed-core aggregates (case

III, Figure 1) exhibited preferential concentration of red-labelled SRB in central regions with interspersed green-labelled aerobic cells (Figure 2 - B and E), suggesting partial spatial segregation but incomplete core-shell formation.

In contrast, SRB-core structures (case IV, Figure 1) displayed highly concentrated red fluorescence exclusively in central regions, while aerobic cells formed a distinct outer layer, effectively creating a protective barrier against oxygen exposure for the anaerobic core (Figure 2 - C and F). This architecture demonstrates successful establishment of defined aerobic-anaerobic gradients within engineered multicellular systems.

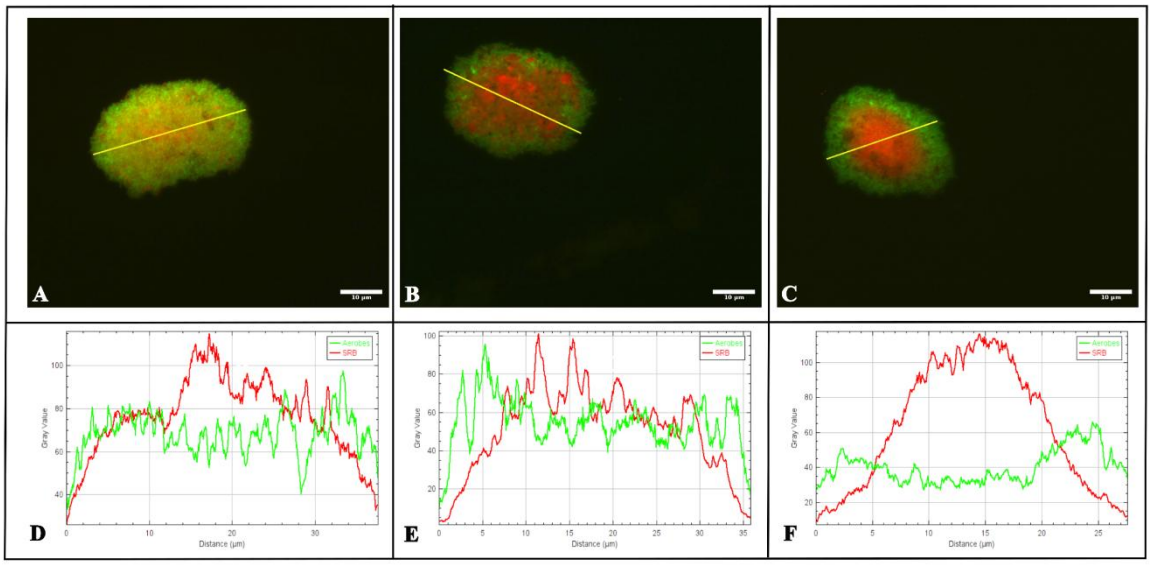

Figure 2. A – Fluorescence microscopy of bacterial aggregates formed using (A) non-precise, (B) mixed-core, and (C) SRB-core aggregation protocols. Lower panels (D-F) represent normalized fluorescence intensity histograms for red-stained SRB and green-stained aerobic cells along selected regions of interest (yellow line). Scale bars represent 50 µm.

2.1.3.2 Temporal dynamics and microenvironment development

2.1.3.2.1 Aggregate evolution under aerated conditions

The temporal dynamics of constructed aggregates during cultivation under aerated conditions revealed distinct patterns of cellular redistribution for both aerobic and anaerobic populations. As aggregates increased in size over the incubation period, multiple discrete anaerobic microenvironments emerged within the enlarged structures (Figure 3). Red-labelled SRB cells formed localized clusters distributed throughout the expanded aggregates, indicating the spontaneous formation of oxygen-depleted niches despite external aerobic conditions.

Maintenance of SRB viability was indirectly confirmed through sustained fluorescence intensity equilibrium between red and green signals throughout the cultivation period. The consistent fluorescence levels demonstrate preserved cellular integrity and DNA stability, as SYTO dyes specifically bind nucleic acids and exhibit diminished emission upon cell death or membrane compromise. This fluorometric stability indicates that the formed microenvironments successfully protect anaerobic bacteria from oxygen toxicity while maintaining metabolic viability.

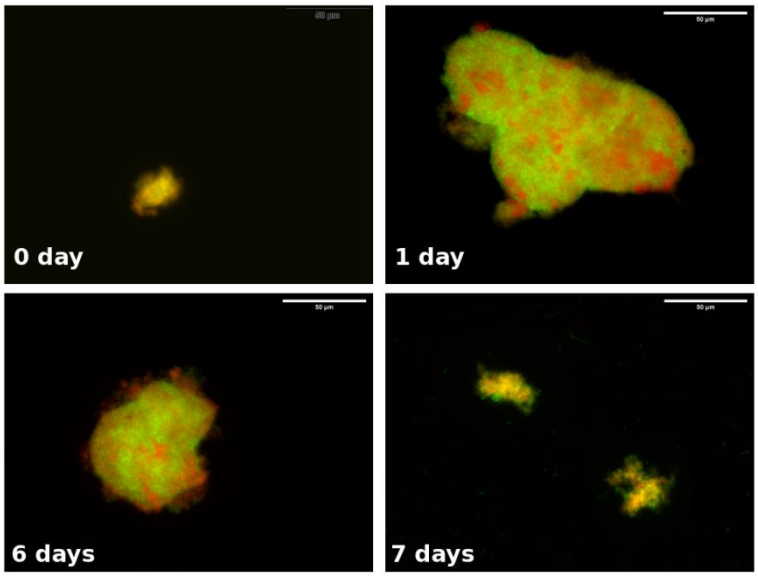

Figure 3. Temporal fluorescence microscopy of bacterial aggregates formed using non-precise assembly protocol with *D. hippei* DSM8344 and *C. marina* DSM50416 during cultivation under aerated conditions. Images show the development of multiple anaerobic microenvironments (red clusters) within expanding aggregate structures over time. Scale bar = 50 µm

2.1.3.3 Anaerobic activity assessment via vanadate reduction

2.1.3.3.1 Strain-specific performance in aggregated systems

Assessment of anaerobic metabolic activity was conducted through quantification of SRB-mediated vanadate reduction using the DPC colorimetric method. All aggregation configurations demonstrated significant V^{5+} reduction compared to planktonic controls, confirming maintained anaerobic respiratory activity within the constructed microenvironments (Figure 4).

However, vanadate reduction efficiency exhibited pronounced strain-specific differences. *Desulfitobacterium* sp. G1-2 and *D. hippei* DSM8344 showed comparable reduction rates across all aggregation strategies, with average V^{5+} decreases of 273 ± 2.8 µM and 283 ± 3.5 µM, respectively, compared to planktonic SRB cultures under aerated conditions. In contrast, *D. africanus* DSM2603 demonstrated markedly enhanced performance in non-precise aggregates, achieving 760 µM V^{5+} reduction, substantially exceeding the activity observed in more structured aggregation configurations.

2.1.3.3.2 Morphological and physiological factors

The superior performance of *D. africanus* in loosely structured aggregates suggests that self-organization capacity and reduced physical constraints (fewer polyelectrolyte layers) provide enhanced cellular freedom, potentially facilitating more efficient metabolic processes. This observation indicates that optimal aggregation strategies may be strain-dependent and should account for bacterial morphological characteristics.

Notably, *D. hippei* and *Desulfitobacterium* sp. are both spore-forming, rod-shaped organisms, while *D. africanus* exhibits a curved-rod morphology without spore-forming capability. Additionally, *Desulfitobacterium* sp. is Gram-positive, contrasting with the Gram-negative cell wall architecture of the other strains. These morphological and physiological differences likely influence cellular behavior within aggregated structures and represent critical parameters for optimizing future aggregation protocols and strain selection strategies.

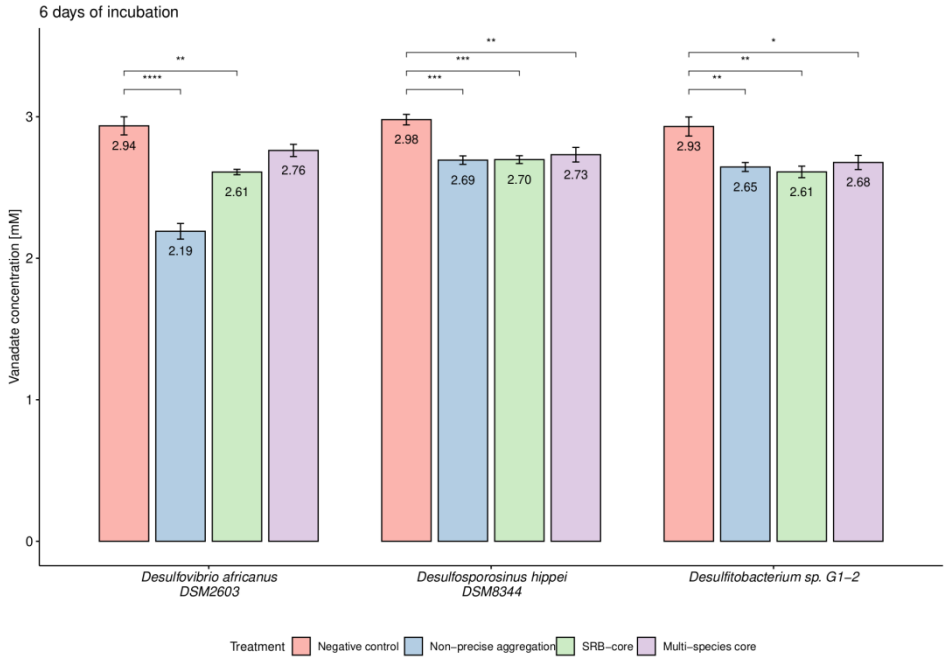

Figure 4. Vanadate reduction by artificial bacterial aggregates after 6 days of cultivation using different aggregation strategies. Data represent mean V^{5+} reduction ± standard deviation (n=3). Statistical significance was determined using two-tailed t-tests with planktonic SRB cultures (negative control) as the reference group (*p < 0.05, **p < 0.01, *p < 0.001)

2.1.3.4 Vaterite-based consortia selection and performance assessment

2.1.3.4.1 Phylogenetic characterization and candidate selection

Enhancement of protocols for constructing aerobic-anaerobic systems targeting hydrophobic compounds required identification of bacterial candidates exhibiting both efficient PAH degradation and electrogenic activity. Six consortia candidates, previously isolated and reported in D3.2, were subjected to comprehensive 16S rRNA gene analysis to determine their taxonomic composition and guide selection for vaterite-based applications.

Phylogenetic analysis revealed distinct community dynamics dependent on initial isolation conditions (Figure 5). Consortia isolated under aerated conditions from both sampling sites (S6II and S7II) exhibited the highest taxonomic diversity, with site 6 consortia demonstrating greater genus-level richness than site 7. Under anoxic conditions, selective pressure varied significantly between sites: isolates from site 7 (S7IIA) showed pronounced enrichment of *Ralstonia* species, while anaerobic consortia from site 6 (S6IIA) maintained substantial genus-level diversity.

Sequential reinoculation of aerobic isolates under anoxic conditions imposed additional selective pressure, resulting in dramatic community simplification. Both sites converged to three dominant genera: *Ralstonia*, *Cupriavidus*, and *Polynucleobacter*. This convergence reflects the exceptional metabolic versatility of *Ralstonia* and *Cupriavidus*, which exhibit robust facultative anaerobic growth, extensive heavy metal resistance mechanisms, and broad hydrocarbon degradation capabilities, positioning them as effective environmental remediators. *Polynucleobacter*, while primarily aerobic, includes facultatively anaerobic strains specialized in freshwater carbon cycling through dissolved organic matter utilization.

The observed taxonomic distribution reveals functional specialization: *Ralstonia* and *Cupriavidus* function as broad-spectrum "pollution specialists" adept at processing anthropogenic contaminants, while *Polynucleobacter* serves as a "natural cycle specialist" focused on simpler carbon compounds in aquatic environments. Based on this analysis, consortia S6IIA and S7II were selected as anaerobic and aerobic candidates, respectively, for subsequent vaterite-based experiments.

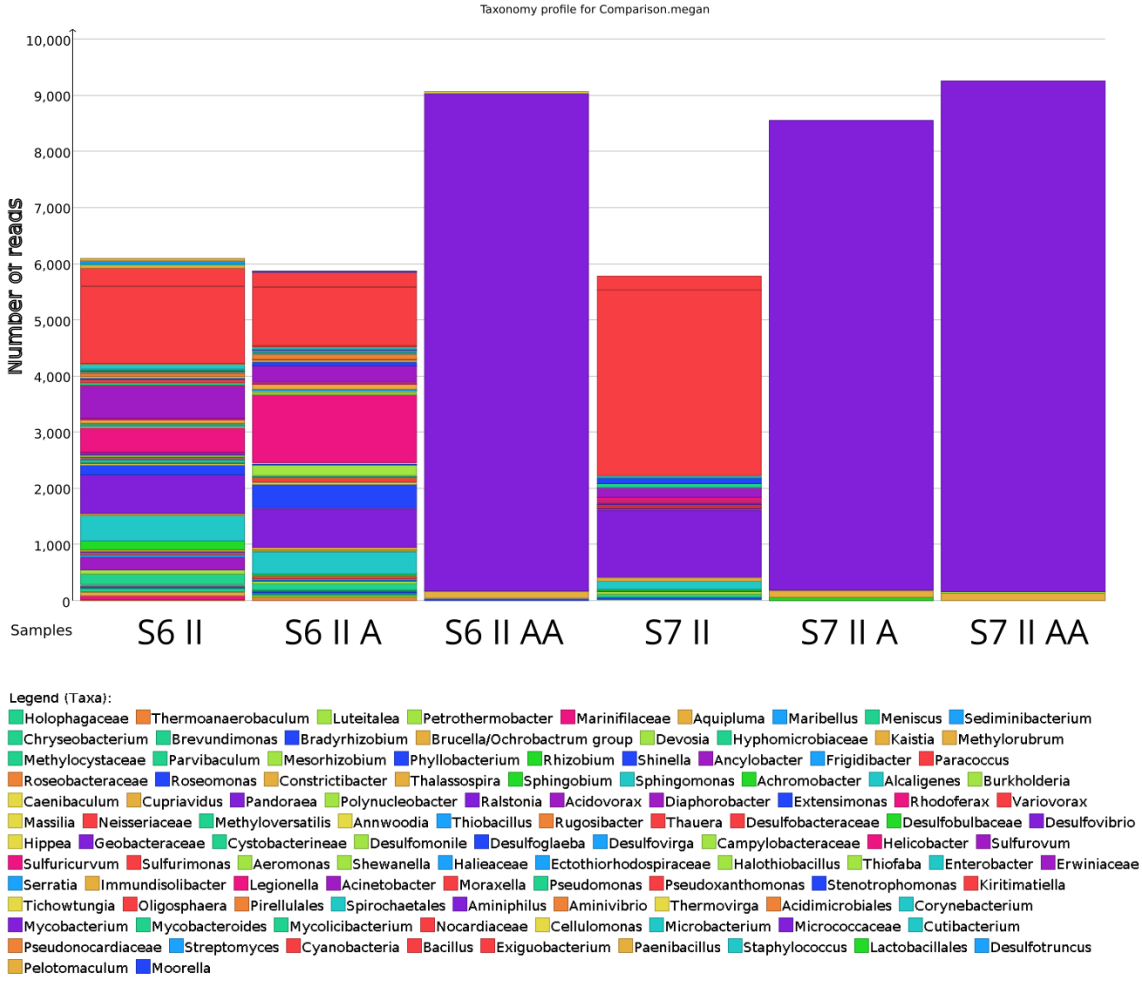

Figure 5. Taxonomic distribution of bacterial genera among isolated consortia from sites 6 and 7 under different cultivation conditions. Letters indicate cultivation conditions: no letter = aerobic, A = anaerobic, AA = aerobic followed by anaerobic cultivation

2.1.3.4.2 Vaterite-particle system development

The development of this system is based on two presumptions: (i) in nature the hydrophobic pollutants are attached on particles and here we aimed to simulate natural bacterial community organization around solid particles in e.g. PAH-contaminated environments and (ii) to enable high-throughput construction and monitoring biofilms which can be engineered on the surface of small particles and monitored by using flow cytometry. Therefore a novel approach was developed utilizing vaterite microparticles, metastable $CaCO_3$ crystals, that are loaded with pyrene and benzo-a-pyrene as model pollutants (detailed protocols in D4.2, Annex III). Selected consortia were inoculated in minimal medium containing PAH-loaded vaterite particles and 3.8 mM V_2O_5 under aerobic or

anaerobic conditions. Performance assessment encompassed PAH degradation analysis via GC-FID and vanadium reduction quantification through DPC colorimetry at 3-, 7-, and 14-days post-inoculation.

2.1.3.4.3 Electrogenic activity assessment

Vanadium reduction analysis revealed temporal patterns in electrogenic activity (Figure 6). Initial incubation (3 days) showed minimal V^{5+} concentration changes across all configurations, with the exception of S6IIA under anaerobic conditions, which exhibited slight V^{5+} increase. After 7 days, significant V^{5+} reduction was detected in all configurations except S7II consortia under aerobic conditions. Following 14 days of incubation, only S7II consortia under anaerobic conditions maintained significant reduction activity.

The observed temporal variability likely reflects the metabolic flexibility of generalist species such as *Cupriavidus* and *Ralstonia*, combined with dynamic community restructuring around vaterite particles. Cell attachment-detachment processes may generate non-uniform metal ion distribution within bacterial communities, potentially influencing measurement consistency. Complete system characterization awaits integration with PAH degradation profiles from GC-FID analysis, which will provide comprehensive insight into the metabolic processes within these engineered systems.

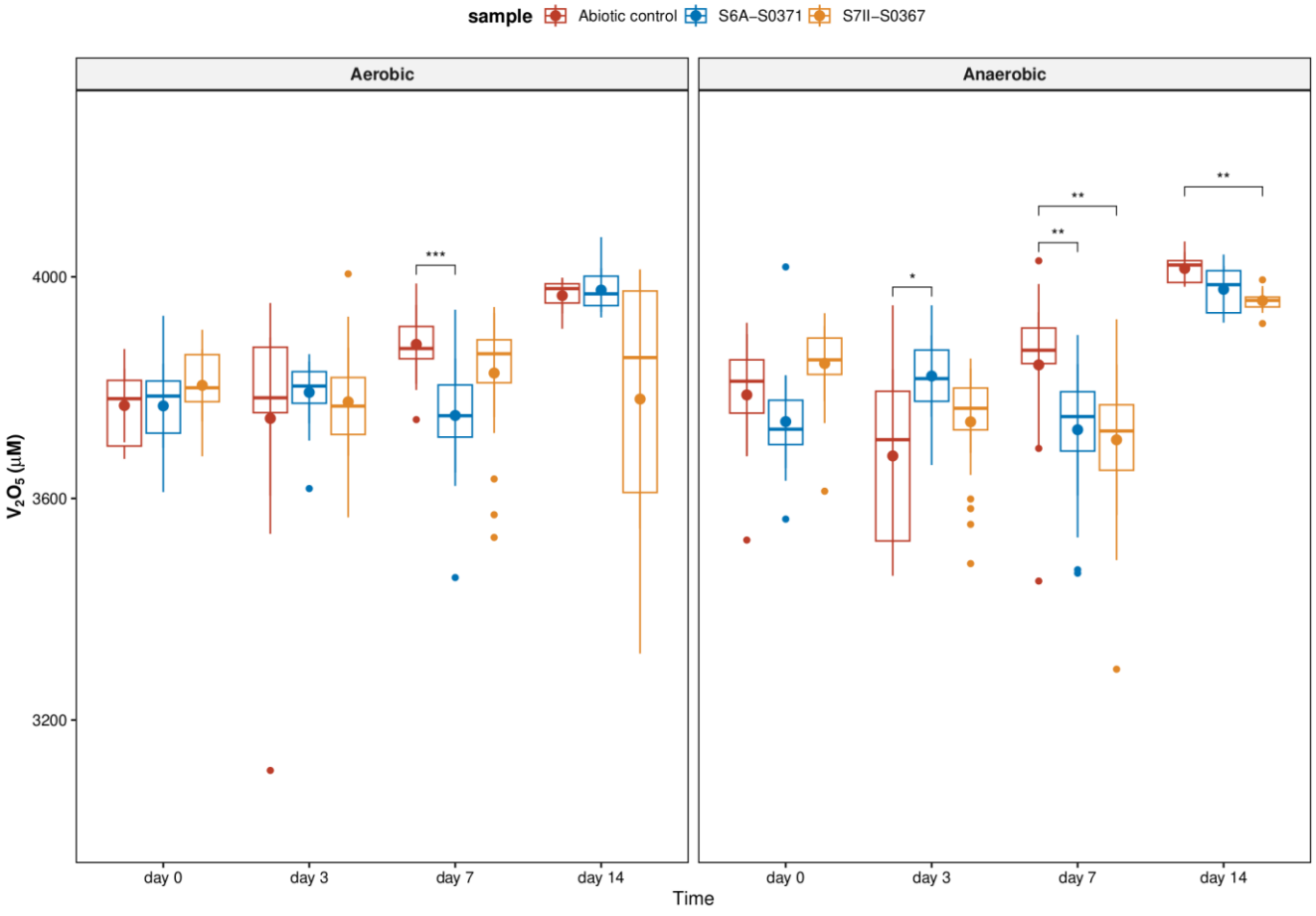

Figure 6. Temporal vanadium reduction activity of selected consortia (S6IIA and S7II) inoculated with PAH-loaded vaterite particles under aerobic and anaerobic conditions. Data represent mean V^{5+} concentration ± standard deviation. Statistical significance determined by two-tailed t-test compared to abiotic controls (*p < 0.05, p < 0.01)

2.1.3.5 Temporal stability and spatial organization of PAH-Degrading consortium I18-S0211

Community stability represents a critical parameter for successful implementation of µLUME-derived isolates in downstream bioelectrochemical applications (WP4 and WP5). Given the stochastic nature of bacterial cell aggregation and detachment dynamics during cultivation, comprehensive characterization of community composition within engineered aggregates is essential. The PAH-degrading consortium I18-S0211 (previously designated as BPC5 in D4.2) was selected as the most promising µLUME candidate based on its demonstrated hydrocarbon degradation efficiency and subjected to temporal stability analysis over a 14-day cultivation period.

2.1.3.5.1 Spatial distribution and cellular viability within aggregates

Fluorescence microscopy analysis using Live/Dead viability staining (Invitrogen) revealed distinct spatial organization patterns within mature bacterial aggregates (Figure 7). Viable cells (green fluorescence) were predominantly localized in close proximity to vaterite particles containing residual PAH substrates (blue autofluorescence), while regions depleted of carbon sources exhibited concentrated dead biomass (red fluorescence). This spatial segregation suggests metabolite gradient-driven cellular distribution, with viable populations maintained through direct access to hydrophobic substrates embedded within the vaterite matrix.

The formation of localized necrotic zones within aggregate structures correlates with heterogeneous substrate availability and may partially explain the temporal variability observed in vanadium reduction assays (Figure 6) through cyclic processes of bacterial growth, death, detachment, and recolonization on vaterite surfaces. These findings indicate that aggregate architecture directly influences metabolic activity distribution, with implications for bioelectrochemical system design and optimization.

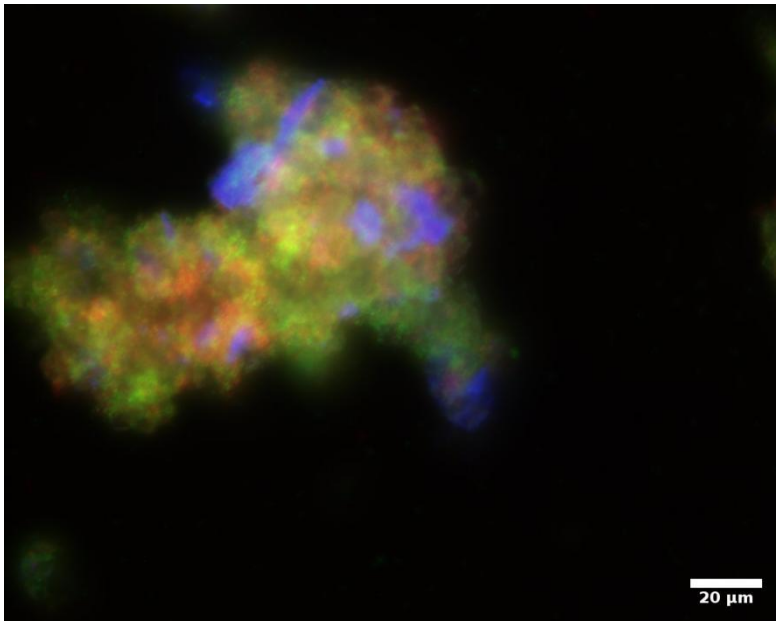

Figure 7. Fluorescence microscopy of I18-S0211 bacterial aggregates cultivated on vaterite particles loaded with pyrene and benzo-a-pyrene (blue autofluorescence). Live/Dead staining shows viable cells (green) and dead biomass (red). Scale bar = 20 µm

2.1.3.5.2 Temporal community dynamics and taxonomic stability

16S rRNA gene sequencing analysis revealed dynamic shifts in community composition while maintaining functional stability throughout the cultivation period (Figure 8). The consortium exhibited a core taxonomic structure comprising three dominant genera: *Microbacterium*, *Methylorubrum*, and *Xanthomonas*.

Notably, *Xanthomonas* demonstrated rapid ecological succession, transitioning from a minor constituent at inoculation to the dominant genus by day 3 of cultivation. This expansion likely reflects the metabolic versatility of *Xanthomonas* species in hydrocarbon degradation and their competitive advantage under the established cultivation conditions.

Temporal analysis revealed distinct colonization patterns among minority taxa. Late-emerging genera including *Pseudomonas*, *Sphingomonas*, and *Methylobacterium* appeared exclusively during extended cultivation (days 10-14), suggesting their role in secondary metabolite utilization or biofilm maturation processes. Conversely, certain minority populations such as *Leucobacter* experienced local extinction during prolonged incubation, indicating competitive exclusion or niche specialization.

Microvirga exhibited transient presence, appearing at day 10 before declining by day 14, potentially reflecting its involvement in specific degradation intermediates or biofilm developmental stages.

The observed community dynamics support the hypothesis of spatiotemporal metabolic complementarity within aggregated bacterial consortia. Despite considerable taxonomic flux among minority populations, the persistence of core hydrocarbon-degrading genera throughout the cultivation period demonstrates functional redundancy essential for stable PAH biodegradation performance.

These findings provide critical insights for optimizing µLUME-derived consortia integration into bioelectrochemical systems, emphasizing the importance of maintaining substrate gradients and aggregate architecture for sustained metabolic activity and community stability.

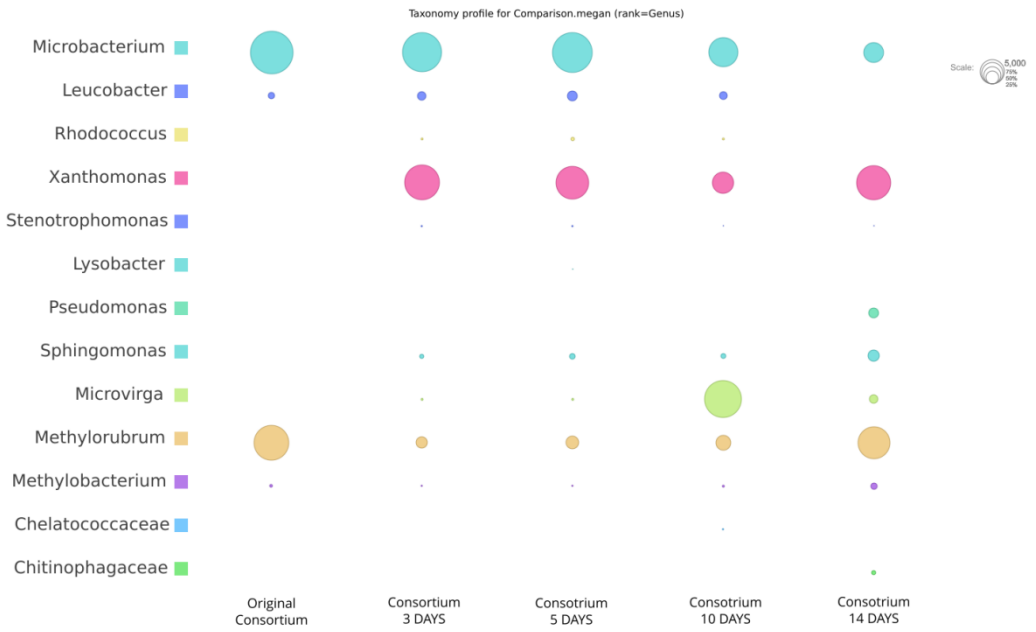

Figure 8. Succession of bacterial community observed through the changes of the 16S rRNA gene abundance of consortium I18-S0211 at the genus level. Bubble size represents relative abundance (%)

2.2 Methods for attachment of planar biofilms on plant root surfaces

2.2.1 Introduction

The primary objectives of Work Packages 4 and 5 focus on developing enhanced pollutant remediation strategies through integration of multiple complementary technologies. Higher remediation efficiency can be achieved by combining phytoremediation, bioelectrochemical systems (BES), and bacterial bioaugmentation for water treatment targeting contaminants including pharmaceuticals, metals, and hydrocarbons. Within this integrated approach, bacterial communities with plant growth-promoting (PGP) properties play a crucial role in system performance.

While previous reports have characterized the individual components of this integrated system, the challenge of effectively combining these three elements remains. Specifically, controlled deposition of bacterial cells with PGP properties in proximity to plant root systems represents a critical technical requirement. Therefore, within the framework of Task 3.2.1, JSI collaborated with CIIMAR to develop and evaluate multiple approaches for depositing model bacterial consortia onto *Phragmites australis* roots, leveraging knowledge and expertise acquired from previous tasks.

2.2.2 Methods

A synthetic bacterial consortium was constructed from 57 individual strains previously isolated from sampling site 4 (Lima estuary), as described and reported in deliverables D1.2 and D3.5. Individual strains were cultivated at 28°C under continuous agitation (180 rpm) for 48 hours, after which biomass was harvested by centrifugation and washed with sterile saline solution.

Individual isolates were normalized to equivalent cell concentrations using flow cytometry quantification, then combined in equal ratios (1:1) to ensure uniform species representation within the consortium. The prepared artificial consortium was labelled with SYTO 11 green nucleic acid stain according to manufacturer protocols. The deposition of the cells and formation of films and coats using biopolymers are described in the Annex I within the D4.2.

2.2.3 Results

Alginate demonstrates several advantageous properties as a bacterial delivery matrix: (i) Physical cell entrapment maintains bacterial cells in close proximity to root surfaces for extended periods, with cell density readily manipulated through high-concentration bacterial suspensions. (ii) The porous hydrogel structure facilitates efficient transport of small molecules, enabling nutrient exchange and signal transduction between PGPR cells and plant tissues. (iii) The soft material properties ensure minimal physical constraint on P. australis root development, preserving natural growth characteristics.

Evaluation of multiple alginate configurations, varying in both layer number and concentration, revealed consistent loading efficiency patterns (Figure 9). Flow cytometry quantification demonstrated that most experimental conditions achieved loading efficiencies below 2% of the initial cell suspension. The optimal configuration (2 mg/mL alginate, double-layer application) yielded the highest cell retention, with 1.7×10^8 cells/mL remaining on root surfaces. Considering the initial suspension concentration of 7×10^9 cells/mL, this represents a two-order-of-magnitude reduction. However, the resulting cell density (10^7 cells/mL) remains within the typical range of rhizosphere bacterial abundance, indicating biological relevance for plant-microbe interactions. Importantly, these

calculations reflect cells recovered from the wash phase; actual concentrations at the root-coating interface may be substantially higher due to spatial concentration gradients within the alginate matrix.

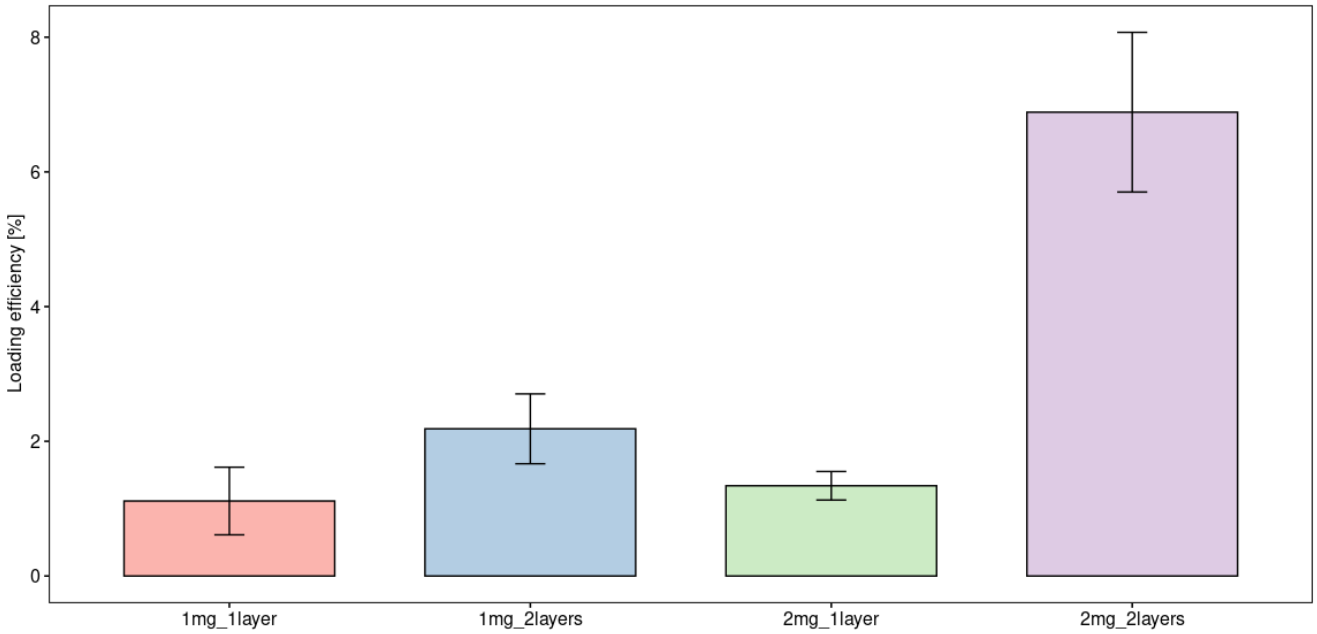

Figure 9. Loading efficiency comparison across different alginate treatment protocols. Data represent mean cell retention ± standard deviation (n=3).

Confocal microscopy analysis of treated root surfaces revealed two critical findings (Figure 10). First, alginate-treated samples demonstrated superior cell concentrations compared to both untreated controls and chitosan-treated reference samples, where few cells were observed in proximity to root surfaces. Second, despite high cell concentrations within the alginate matrix, significant distances persisted between the root surface and entrapped bacterial cells, potentially limiting direct plant-microbe interactions.

These results indicate the need for further protocol optimization to enhance plant-cell proximity. Future development should focus on alternative polyelectrolyte systems capable of reducing the spatial gap between bacterial cells and root surfaces. Ongoing performance assessments of *P. australis* plants treated with optimized protocols are in progress and will be reported in deliverable D4.5.

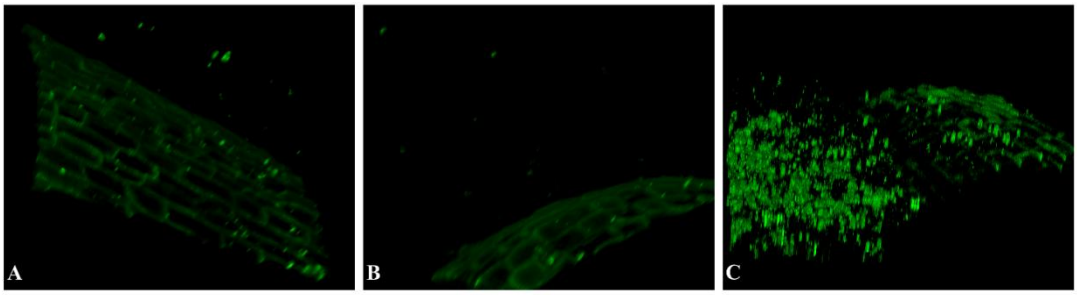

Figure 10. Three-dimensional confocal microscopy reconstruction of P. australis root surfaces showing bacterial distribution patterns. Images compare (A) untreated control, (B) chitosan-treated, and (C)

alginate-treated (2mg_1layer) samples. Green fluorescence indicates SYTO 11-labelled bacterial cells. Green autofluorescence mesh structure is representing surface of the root showing typical epithelial structure formed by the root epithelial cells.

2.3 Development of methods for controlled aggregation

2.3.1 Introduction

The potential of microbial spatial organization and niche formation remains poorly understood, limiting the effectiveness of current bioremediation strategies. In natural environments, microbes rarely exist as isolated cells; rather, they form aggregates within soil micro and macroaggregates, generating distinct microenvironments that promote metabolic cooperation. Such spatial heterogeneity is crucial for the degradation of complex pollutants, such as polycyclic aromatic hydrocarbons (PAHs), and also enables microbial growth in toxic environments containing mixtures of organic pollutants and heavy metals.

To investigate microbial interactions, two main approaches are commonly used: top-down (analysing whole communities) and bottom-up (cultivating defined strains). While informative, both have limitations in capturing spatial structure and functional dynamics. In response, this research proposes an intermediate strategy: controlling microbial aggregation to form structured microbial consortia.

As a form of top-down approach, method of controlled electrostatic aggregation proposed. This method will allow the formation of artificial aggregates where microbial interactions, spatial arrangements, and cross-feeding can be studied under defined conditions. These structured systems also support the creation of aerobic–anaerobic microenvironments, which are relevant for pollutant degradation processes. Altogether, this approach bridges the gap between simplified laboratory models and complex environmental systems, offering a practical platform for both fundamental ecological research and applied bioremediation development.

As a bottom-up approach, we use vaterite particles as solid supports to create controlled microenvironments for bacterial attachment and biofilm development. This system not only allows us to investigate layered structures formed by individual bacterial strains within a single construct but also extends to studying interactions between distinct populations attached to different vaterite particles. By developing a protocol for direct and controlled attachment of bacterial suspensions onto these particles—bypassing the planktonic phase—we ensure cells remain localized, enabling precise analysis of local biological processes, co-evolutionary dynamics, and pollutant transformation within and between structured microbial communities.

2.3.2 Methods

2.3.2.1 Controlled Electrostatic Aggregation

2.3.2.1.1 Experimental Setup and Principle

For specific placement of bacterial strains in the polymicrobial structures we hypothesise two approaches (i) by controlling sizes of aggregates and then establishing the sub-niches in structures through the biological succession and (ii) developing protocols based on controlling parameters such as hydrodynamics, cell shape, strength of electrostatic interactions and ratios of cells that are an object of the aggregation. The first approach (see 2.1.2.1) enables control of local environmental

conditions, and it is important to know in advance the metabolic interactions between cells and in the second approach the specific physicochemical conditions brings cells together into the particular in advance predefined structures which can enable testing stability and spatial distribution of different cells on the outcomes of the efficiencies of metabolic pathways. For specific assembly of multicellular structures in the past we developed the approaches for specific spatial distribution of two strains through empirical experimental testing (see D3.2). Here we advanced the method in order to determine parameters that can set the mechanistic guide for top-down specific aggregation protocols. Here we prepared an experimental setup for aggregation two distinct cell populations (Figure 11). Aggregation was achieved using a polyelectrolyte-based approach, which preliminary tests confirmed to reliably induce cell–cell interactions. The system consists of a reaction vessel containing the suspension of cell type A, equipped with a mixer to maintain homogeneity, flow of cells and formed aggregates as well as redistribution these two groups according to the centrifugal forces caused by the swirling of the suspension. Cell type B is introduced into the vessel through a needle connected to a flow regulator, allowing precise control of the addition rate. The suspension level in the vessel is maintained constant throughout the experiment. This setup enables fine control of physical parameters such as mixing speed and flow rate, providing a robust platform for systematic investigation of conditions affecting microbial aggregation Detailed approaches are described in the D1.2, D3.2 and Annex I-III of D4.2.

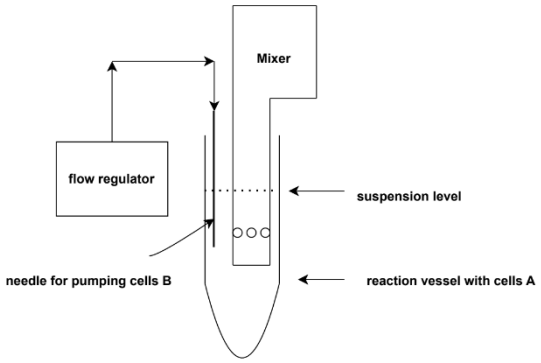

Figure 11. Schematic of the aggregation setup. Cell suspension A is placed in the reaction vessel, maintained at a constant level, and mixed with a submerged mixer. Cell suspension B is introduced at a controlled rate through a needle, regulated by a flow regulator

Cell Preparation and PEI Coating

To test the experimental setup, *Escherichia coli* TOP10, a well-characterized model organism, was selected. Two cell populations were prepared: natural *E. coli* cells and *E. coli* cells with a positive surface charge induced by polyethyleneimine (PEI) coating. An overnight culture of *E. coli* was harvested, washed with saline solution, and adjusted to the desired optical density. The coating procedure and stock preparation described by Rybkin et al. (2019).

Prior to the experiments, native and PEI-coated *E. coli* suspensions were adjusted to the desired optical densities. Aggregation experiments were conducted under controlled mixing conditions, with the coated bacteria introduced into the suspension at a constant flow rate. Samples were collected at regular time intervals and stored at 4 °C until analysis.

2.3.2.1.2 Protocol optimization

Identifying aggregation formation during preparation

Since PEI-coated bacteria showed a tendency to aggregate during the preparation process, the experiment was designed to identify the stages at which aggregation occurs and to optimize the protocol to minimize it. The goal was to keep the PEI-coated cells as well-dispersed as possible before the controlled aggregation assay.
An *E. coli* suspension was prepared, washed with saline solution, and adjusted to the desired optical density. Cells were mixed with the PEI solution, incubated under controlled conditions, and washed to remove excess PEI. At each preparation step, the size distribution of the bacterial suspension was monitored using an ELS device.

Optimizing Centrifugation and Washing Procedures

This experiment was conducted to evaluate how centrifugation and washing steps influence the aggregation of PEI-treated *E. coli*. The goal was to identify conditions that minimize unintended aggregation during cell preparation.

E. coli TOP10 cells were harvested, washed with saline, and adjusted to the desired optical density before PEI coating, performed as previously described. After treatment, two washing protocols using low centrifugal force (1000 × g) were compared to reduce aggregation. One protocol involved a single gentle wash, while the other included an additional centrifugation and wash step.

For both approaches, particle size distribution was measured at key preparation stages using an ELS device to monitor changes in aggregation.

Vaterite Particle Attachment

Determination of the optimal ratio between cells and vaterite particles allowing complete attachment was performed using *Lactococcus cremoris* MG1633 with inserted GFP plasmid. We used these cell to simulate acidification of the microenvironment that is the most affecting stability of the vaterite, which is prone to the dissolution in low pH conditions. Cells were cultivated in chemically defined medium (CDM) for 24 hours at 180 rpm and 30°C.

Vaterite particles were prepared by mixing calcium chloride and sodium carbonate under controlled conditions as described in Annex III of D4.2, followed by drying overnight at 60˚C.

Different vaterite concentrations were used combined with different concentrations of cells. Bacterial suspension was added to ultrapure water (MQw) containing vaterite particles and shaken in microtubes for 1 to 6 hours using IKA vortex. Subsamples were taken every hour and observed using an inverted fluorescent microscope (Zeiss AxioObserver Z1) equipped with a GFP filter. Attachment efficiency was determined by flow cytometry measurement of the planktonic fraction of *L. cremoris* cells that did not attach to the particles.

2.3.2.1.3 Detection and Analysis Methods

Fluorescent Staining Optimization

To evaluate the formation of aggregates under controlled induction conditions, we employed three complementary techniques: flow cytometry, size measurements using an ELS device (Zetasizer Nano), and microscopy. Since all three methods require well-stained cells for reliable detection and discrimination, we tested several fluorescent dyes. Specifically, we evaluated SYTO 11 and SYTO 21 (green fluorescence) and SYTO 59 and SYTO 64 (red fluorescence) to enable distinction between the

two cell populations in a mixed sample. Because our goal was to simultaneously detect the two populations using both flow cytometry and microscopy, it was essential to choose a pair of dyes that provided distinct, non-overlapping signals and performed reliably with a single staining protocol. The approach followed the methods described in D1.2, D3.2 of D4.2. The prepared samples were diluted 500-fold in 0.9% NaCl prior to analysis. Fluorescence of the stained cells was then evaluated using both a flow cytometer and a fluorescence microscope.

Validation of methods that enable interpretation of aggregations

After testing different dyes to distinguish bacterial populations, aggregation experiments were performed to evaluate whether SYTO 21 and SYTO 59 staining allows differentiation between single cells and aggregates using three analytical methods.

After testing different dyes to distinguish bacterial populations, aggregation experiments were performed to evaluate whether SYTO 21 and SYTO 59 staining allows differentiation between single cells and aggregates using three analytical methods.

The preparation of *E. coli* suspensions and PEI coating followed the method described in the supplementary section of D4.2. Stained cells were diluted to OD_{600} = 0.8 and adjusted as needed for aggregation experiments. Aggregation assays were then performed by mixing differently stained bacterial suspensions under controlled conditions, with samples collected at regular intervals and stored at 4 °C until further analysis.

2.3.3 Results

2.3.3.1 Development of detection methods

2.3.3.1.1 Fluorescent dye selection and optimization

Through preliminary experiments with different SYTO fluorescent dyes, we determined that SYTO 21 and SYTO 59 provided the best contrast for distinguishing the two *E. coli* populations (Figure 12). This dye combination allowed clear discrimination of the two cell types both under the fluorescence microscope and in flow cytometry analysis, enabling simultaneous monitoring of both populations in mixed samples with a single staining protocol

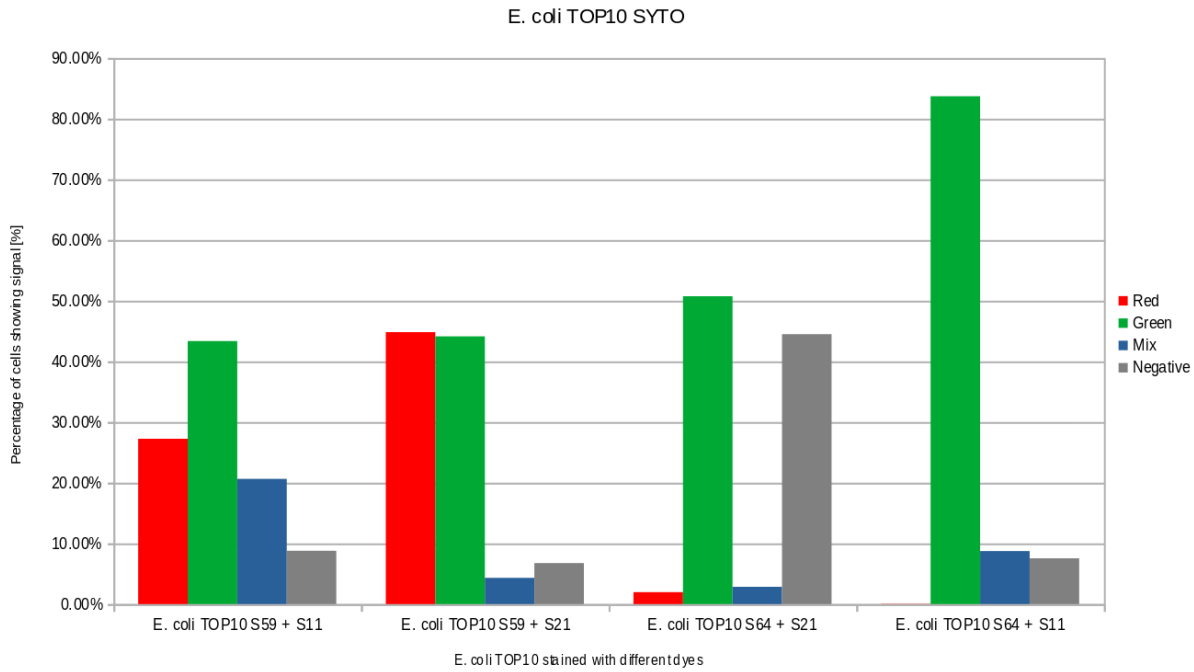

Figure 12. Fluorescence staining of *E. coli* TOP10 samples with different dyes. The bar graph shows the percentage of cells exhibiting red, green, mixed, or no fluorescence (Negative) in four *E. coli* TOP10 samples stained with different SYTO dyes. Each bar represents the proportion of cells in a given staining category, as indicated in the legend. Samples include combinations of SYTO dyes S59, S21, S64, and S11, as labelled on the x-axis. The y-axis indicates the percentage of cells showing fluorescent signal [%] (green FL1-A; red FL4-A). Percentages were calculated based on the number of detected events within each gated cell population (red, green, mixed, and negative), relative to the total cell population identified by size-based gating, with a high number of recorded events per sample ensuring statistical reliability

2.3.3.1.2 Validation of methodologies for characterisation of aggregates

Building on the observation that PEI-coated cells were already partially aggregated during preparation, we sought to optimize the final washing step during the preparation of PEI-coated cells, since earlier results indicated that this step strongly influenced the extent of aggregation. Using size distribution measurements (ELS), we compared two washing protocols (wash 1 and wash 2), but observed no substantial difference between them. Both protocols resulted in cell suspensions with a main population around ~1 µm in size, consistent with individual bacteria, but also with the presence of larger particles around ~30-50 µm, indicative of aggregates.

To further reduce aggregation, we tested additional approaches. Filtration through a 10 µm mesh effectively removed the largest aggregates, but the resulting suspension still contained clusters and did not achieve a completely single-cell distribution. We also varied the duration of the sweeping step during washing but again observed no significant differences in size distribution between samples.

Due to the protonation/deprotonation of polyelectrolytes as well as functional groups on the surface of bacterial cells by adjusting the pH of the suspension, we found that increasing the pH to 9 reduced aggregation significantly, resulting in a single peak in the size distribution at 1-1.6 µm. However, when the pH was subsequently lowered back to 5, as in the initial preparation conditions, the larger

aggregates reappeared, suggesting that the system reaches an equilibrium between dispersed cells and aggregates that is influenced by pH.

These findings indicate that the washing step in the preparation of PEI-coated cells has the greatest impact on their aggregation state, and that neither modified washing protocols, filtration, nor sweeping alone are sufficient to fully prevent aggregate formation. The observed pH effect suggests that charge interactions play a role in aggregate stability. These results highlight the importance of maintaining PEI-coated cell suspensions in a well-dispersed, single-cell state prior to controlled aggregation experiments. This was particularly evident in the initial apparatus test, where microscopy images clearly showed a gradual increase in aggregate size when starting from well-dispersed cells. Further optimization and additional strategies are therefore needed to obtain well-dispersed, single-cell suspensions of PEI-coated bacteria suitable for controlled aggregation assays.

2.3.3.1.3 Controlled electrostatic aggregation results

Proof-of-concept aggregation demonstration

In the initial test of the aggregation, we confirmed that it is possible to induce controlled aggregation of bacteria. Microscopy images clearly showed that at the beginning of the experiment the suspension consisted of individual cells, which gradually assembled into larger aggregates as PEI-coated bacterial cells were added (Figure 13). This progressive aggregation correlated with the controlled introduction of positively charged cells, demonstrating the functionality of the setup and the ability to monitor aggregation dynamics over time.

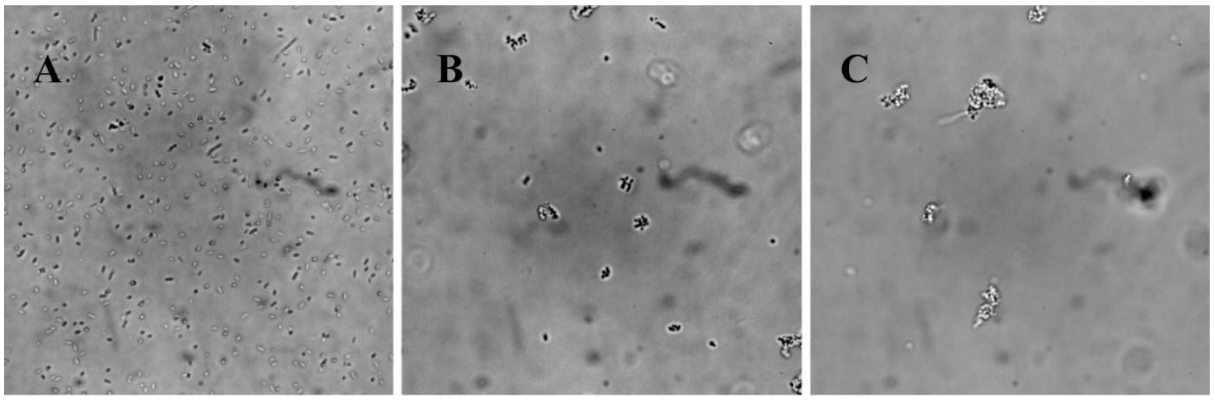

Figure 13. Microscopy images showing the progression of bacterial aggregation. (A) Suspension of single, dispersed cells before induction. (B) Formation of small aggregates after induction of aggregation. (C) Formation of larger aggregates at later stages.

Aggregation Analysis of Dual-Dye-Stained Cells

We demonstrated that the degree of aggregation can be reliably quantified using all three methods (ELS device, flow cytometry, and microscopy). Flow cytometry analysis revealed that larger aggregates could be distinguished by detecting aggregates containing both fluorescent signals (Figure 14). The higher the proportion of double-fluorescent events, the larger the aggregates are likely to be, as they consist of increasing numbers of both cell types.

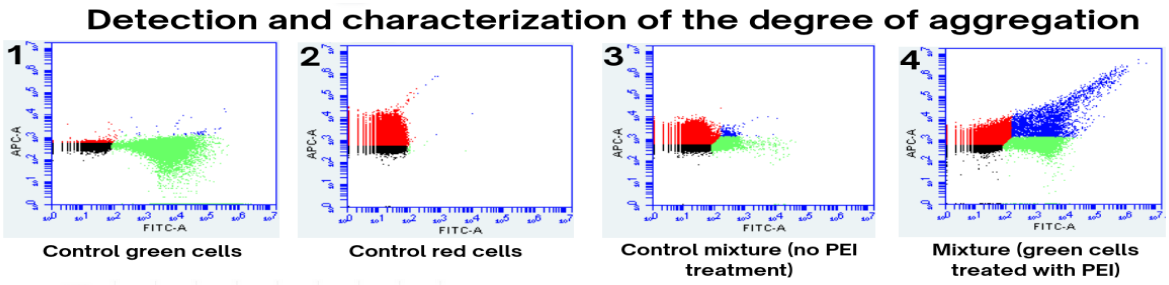

Figure 14. Flow cytometry analysis of stained bacterial populations. Figure 1: SYTO 21-stained E. coli cells (green). Figure 2: SYTO 59-stained E. coli cells (red). Figure 3: mixture of SYTO 21- and SYTO 59-stained E. coli cells without PEI treatment. Figure 4: mixture of SYTO 21-stained E. coli cells treated with PEI and SYTO 59-stained cells, showing the formation of aggregates (blue).

Quantitative aggregation analysis

In the subsequent comprehensive test of the aggregation setup, we demonstrated that bacterial aggregation can be induced and quantified in a controlled manner. Fluorescence microscopy images taken throughout the experiment revealed that the suspension initially contained only individual *E. coli* cells. As PEI-coated bacteria were gradually introduced, cells began to cluster, forming larger aggregates over time. These visual observations confirmed the effectiveness of the setup in supporting time-resolved analysis of aggregation dynamics.

We observed that large aggregates formed almost immediately after the introduction of PEI-coated *E. coli* into the vessel. This suggests that the PEI-coated cells were already partially aggregated during their preparation, leading to the introduction of larger clusters of cells into the suspension of the native *E. coli* cells As a result, large aggregates formed rapidly upon mixing. This was reflected in the average particle size distribution measured by ELS, which was already approximately three times higher at the first time point compared to the starting suspension and then showed little further change over time. The polydispersity index (PDI), which reflects the width of the particle size distribution (with higher values indicating a more heterogeneous population), was already ~1 at the first measurement and increased only slightly thereafter. In contrast, the control mixtures containing both cell populations without PEI modification maintained a consistent mean diameter of around 1 µm and a lower PDI of approximately 0.4, indicative of a more uniform size distribution, even after the addition of 1 mL of green-stained cells.

In flow cytometry, larger aggregates were removed by filtering the samples through a 100 µm mesh prior to measurement. This allowed us to focus on the distribution of smaller aggregates and single cells, revealing that the extent of aggregation increased progressively with higher numbers of PEI-coated cells. The proportion and size of aggregates increased consistently with increasing concentrations of PEI-coated cells in the sample, whereas in the control mixtures, where cells were not treated with PEI before mixing, this effect was not observed.

2.3.3.1.4 Vaterite microparticle-based sedimentation

The formation of attached biofilm structures enabling testing interactions between attached subpopulations of cells is mostly problematic since there is the dynamic attachment-detachment process. Here we needed to prepare a robust protocol that only attached cells on the vaterite particles are present. By our approach we demonstrated that that biofilm formation on surfaces can be

controlled, with the planktonic phase of cells potentially eliminated entirely. After 1 hour of incubation, vaterite particles coated by the PEI adsorbed most cells, localizing them on the particle surface (Figure 15). The interaction between cells and particles is stochastic, with the primary determining factor being the ratio between the number of cells present in solution and the surface area available for attachment. By manipulating these two parameters, conditions can be achieved where 100% of cells attach to the surface within 2 hours (10^4 cells/mL, Figure 16). However, excessive amounts of vaterite particles lead to decreased attachment efficiency due to increased frequency of physical contacts between cells and solid particles, as well as elevated shear stress (10^4 cells/mL, Figure 16). These findings provide insight into the nature of the sedimentation process and offer an approach for manipulating bacterial community formation on particle surfaces.

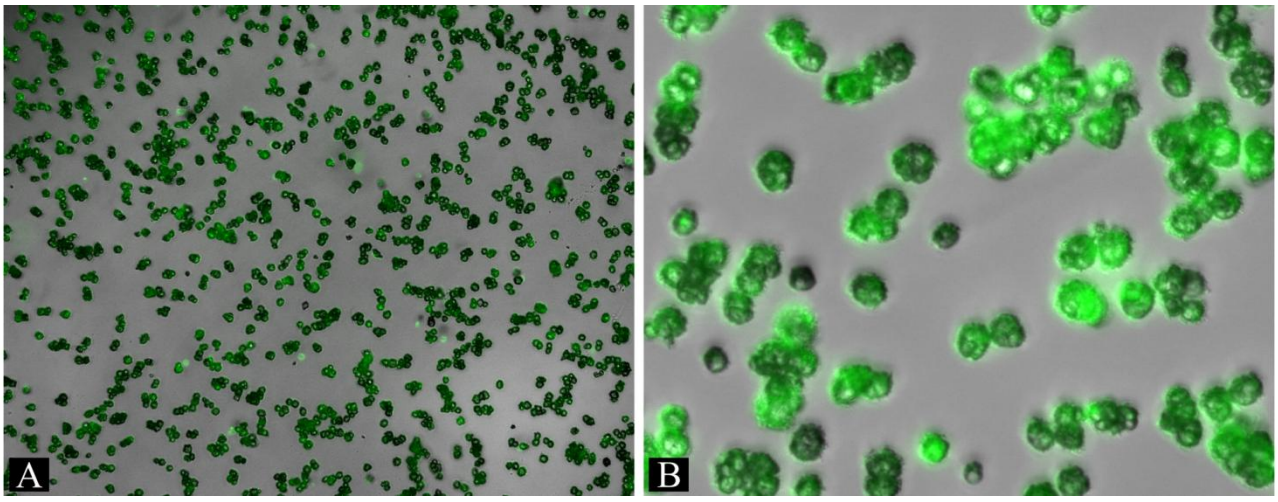

Figure 15. Fluorescence microscopy images showing GFP-labelled *L. cremoris* MG1633 cells (green channel) attached to vaterite particles (gray channel). Images were captured at 100× (A) and 400× (B) magnification

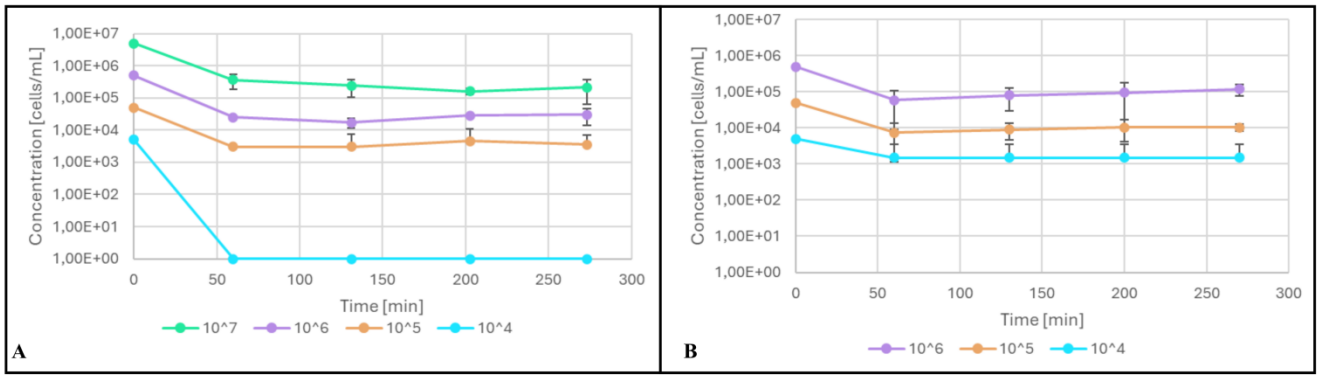

Figure 16. Attachment of bacterial cells to vaterite microparticles at concentrations of 7 mg/mL (A) and 70 mg/mL (B). Values represent the number of cells detected in the planktonic phase of the solution

2.4 Assessment of growth of GMO strains using novel approach based on flow cytometry

2.4.1 Introduction

For microbial cells to utilize potential carbon, nitrogen, or energy sources, they must come into direct contact with them before uptake can occur. This makes it difficult to study the transformation of pure hydrophobic or water-insoluble substances, as they require the addition of surfactants to disperse them. However, surfactants themselves can act as alternative energy or nutrient sources, which may obscure the actual growth and metabolic activity of the strains under study. This issue is particularly critical when assessing the growth of genetically modified, engineered, or knockout strains, where precise measurement of metabolic capacity is essential. In the BIOSYSMO the genetic constructs prepared by ICL where pathways for degradations for lindane and atrazine were prepared the main chalenge remained how strains can degrade these compounds.

To overcome these challenges, JSI developed a novel assay that enables detection and evaluation of microbial growth directly on hydrophobic compounds. In this method, described in detail in D1.2, D3.2, D3.4,D3.8 and D4.2, bacteria and pollutant carriers were combined and their growth measured by flow cytometry. the target pollutant on their surface. At this level we only used statistical probability that cells will get in contact with the loaded particles due to the (i) passive adsorption of cells on the vaterite particles, (ii) co-aggregation of cells with particles or (iii) due to the prolonged cell-particle exposure causing by dynamic impingement of cells on particles caused by continuous shaking and we did not electrostatically induce attachment on the surface. Since we could observe high adsorption rate on the particles the assay has been further complemented with fluorescent staining and flow cytometry to detect bacterial growth. The measurement is based on the fluorescence signal depletion due to the division. Cells stained with a fluorescent dye (SYTO) get fluorescent since dye get attached on the DNA and every division theoretically can decrease fluorescent signal for two times. since dye is distributed between daughter cells. This enables monitoring of growth directly on the particles by tracking the decrease in fluorescence signal over time. This method was applied to engineered *P. putida* strains carrying inserted genes for the degradation of atrazine and lindane, enabling detection of their capacity to degrade these hydrophobic compounds.

2.4.2 Methods

2.4.2.1 Cultivation of bacterial strains and preparation of vaterite particles

Bacterial strains used in this study were provided by ICL and included a wild-type (WT) reference strain (*Pseudomonas putida* KT24401), a strain carrying the empty plasmid vector without inserted genes , and engineered strains carrying genes for atrazine (ATR+) and lindane (Lin+) degradation. A detailed description of the strains is provided in D3.4. Strains carrying the plasmid vector harbours a kanamycin resistance gene. Strains were stored at –80 °C in 15 % glycerol and were revived on solid LB agar medium before use. Kanamycin was supplemented in the medium at a concentration of 50 µg/mL as needed to maintain plasmid-bearing strains. Pre-cultures were prepared by inoculating single colonies into LB broth and incubating 3-4 days at 30 °C with shaking at 250 rpm. Cells were then reinoculated into M9 medium supplemented with 0.02% glucose. The cells, prepared as described above, were then employed in the assay to test their ability to grow on hydrophobic compounds.

Determination of the optimal ratio between cells and carriers particles allowing complete attachment was based on the results of above-described experimental protocols using *Lactococcus cremoris* MG1633 with inserted GFP plasmid. Cells were cultivated in chemically defined medium (CDM) for 24 hours at 180 rpm and 30°C.

A method for detecting microbial growth on vaterite particles with atrazine was developed, subsequently optimized, and applied to *Pseudomonas putida* engineered strains. The optimization included determining the optimal initial cell concentration and evaluating the effect of SYTO dyes on cell staining and growth. The approach was then applied to the *Pseudomonas putida* GMO-engineered strains, provided by ICL. Detailed protocols are provided in method sections of D1.3, D3.2, D3.4 and D4.2.

2.4.3 Results

2.4.3.1 Optimal initial cell concentration

Preliminary tests with varying initial OD_{600} (0.2–1.2) showed that low cell densities rapidly lost detectable fluorescence due to cell division and dye dilution, even in media lacking carbon and nitrogen. In contrast, higher densities maintained stable signals, indicating that an initial OD_{600} above 0.5 is necessary for reliable detection of growth on vaterite particles.

2.4.3.2 Differentiation of bacterial growth patterns using flow cytometry

The wild-type (WT) strain and a strain carrying a plasmid encoding atrazine degradation genes (ATR+) were tested. The WT strain showed a clear decrease in fluorescence over time, corresponding to cell growth. Interestingly, even in the absence of nitrogen and carbon sources, a fluorescence decay was still observed, likely due to internal bacterial reserves or trace nutrient availability, which also highlights the high sensitivity of the method. This observation indicates that further optimization is needed to reduce background and to better distinguish true growth from residual activity. However, the growth rate of control mixtures was clearly lower compared to the conditions with added glucose, which significantly enhanced growth even in nitrogen-free medium (Figure 17). This suggests that nitrogen in the medium was not limiting under these conditions. Addition of atrazine did not influence WT growth, indicating it cannot utilize atrazine as a carbon or nitrogen source.

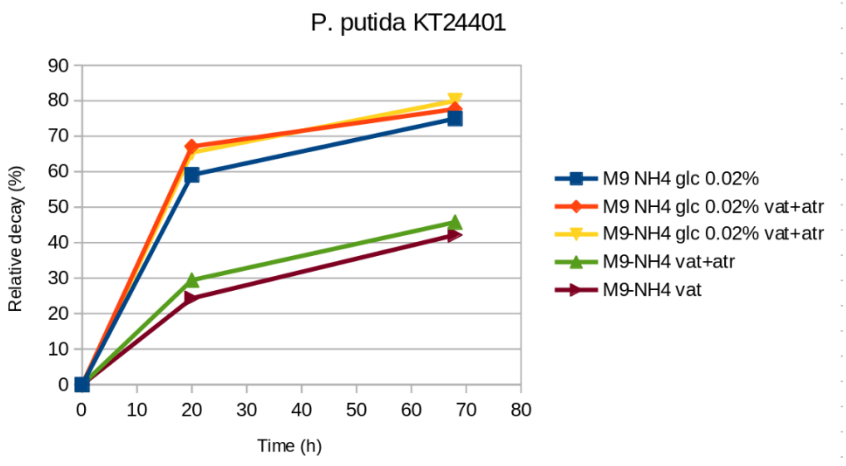

Figure 17. Relative fluorescence decay of P. putida KT24401 measured over time. Different growth conditions are indicated in the legend: M9 minimal medium supplemented with 0.02% glucose (dark

blue squares), M9 + 0.02% glucose + vaterite (vat) + atrazine (atr) (orange diamonds), M9 without NH4 + 0.02% glucose + vaterite + atrazine (yellow triangles), M9 without NH4 vaterite + atrazine (green triangles) and M9 without NH4 + vaterite (purple diamonds). Relative decay was calculated as the percentage decrease of mean FL1-A fluorescence from the initial time point (0 h) according to the formula described in Methods

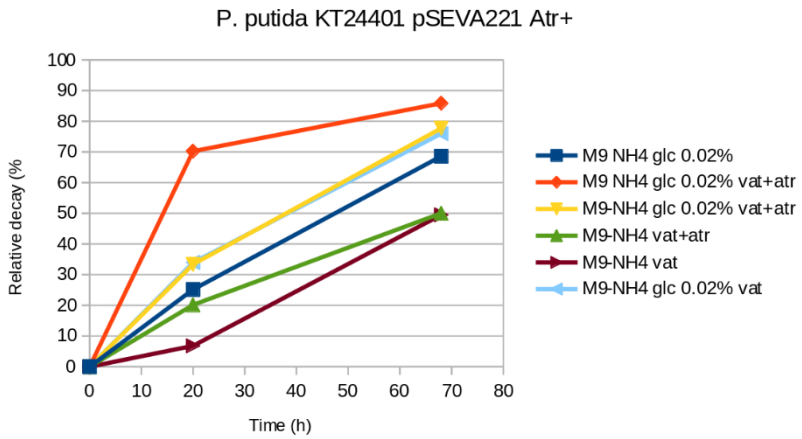

Figure 18. Relative fluorescence decay of P. putida KT24401 carrying pSEVA221 (Atr+) measured over time. Different growth conditions are indicated in the legend: M9 minimal medium supplemented with 0.02% glucose (dark blue squares), M9 + 0.02% glucose + vaterite (vat) + atrazine (atr) (orange diamonds), M9 without NH4 + 0.02% glucose + vaterite + atrazine (yellow triangles), M9 without NH4 vaterite + atrazine (green triangles), M9 + vaterite (purple diamonds), and M9 without NH4 + 0.02% glucose + vaterite (light blue arrows). Relative decay was calculated as the percentage decrease of mean FL1-A fluorescence from the initial time point (0 h) according to the formula described in Methods

In contrast, the ATR+ strain behaved differently. When provided with all nutrients (glucose, NH4, and atrazine), it grew well, and growth was improved compared to the condition without ATR, suggesting it may be capable of partial atrazine degradation (Figure 18). However, the ATR$^+$ strain grew more slowly than the WT in conditions with glucose and inorganic nitrogen, indicating a possible metabolic burden of the plasmid. In conditions without added carbon and nitrogen, the ATR$^+$ strain showed no significant growth, implying it requires an external source of C and N to utilize atrazine.

Overall, this method allows us to detect and measure bacterial growth; however, further optimization is needed to reduce background changes in control samples, which should not support growth, and thereby improve the sensitivity of the assay.

2.4.3.3 SYTO staining and fluorescence intensity

To address above mentioned issue, we tested the effect of different SYTO 11 concentrations on cell growth and staining. When testing SYTO staining at different concentrations, we found that cells stained well up to concentrations of 0.1 µM (Figure 19); however, at this level, a noticeable decrease in fluorescence intensity and in the number of detected cells was observed. Measurements taken after 2.5 hours indicated that cells gradually lost fluorescence over time, and the increase in the non-fluorescence fraction suggests that some cells may have lysed during incubation. At a concentration of 0.5 µM, these effects were less pronounced, indicating that SYTO at this concentration is likely less toxic to the cells and more suitable for this method. Based on these results, we conclude that lower SYTO concentrations are more appropriate for staining, as they result in less decline in the proportion of fluorescent events, while still providing sufficient fluorescence intensity for detection.

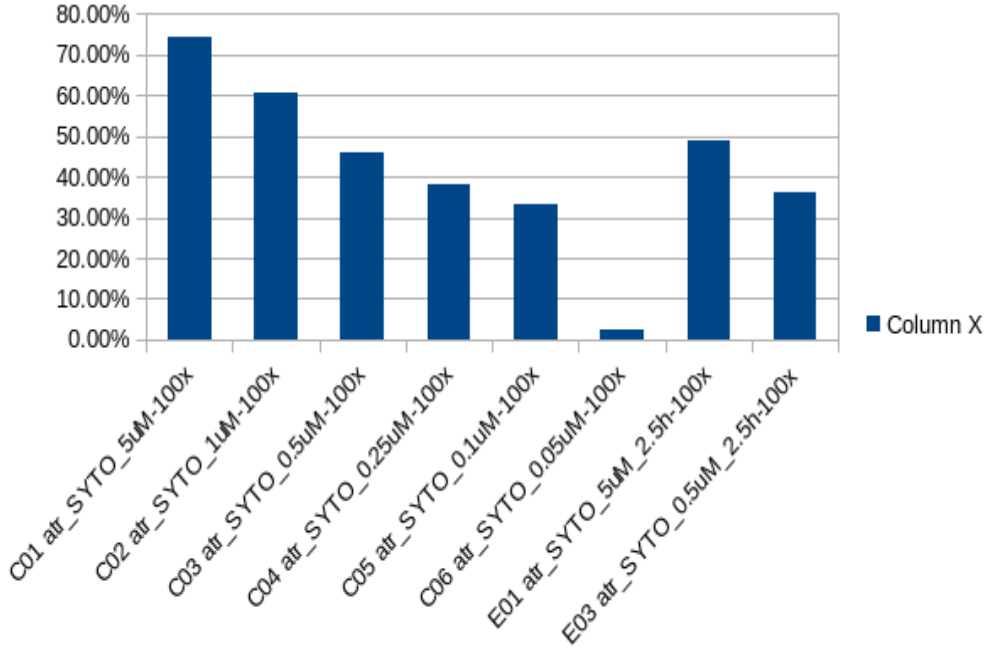

Figure 19. Percentage of detected fluorescent cells in the samples at different SYTO concentrations.

2.4.3.4 SYTO effect on bacterial growth

Cells grown in medium containing both glucose and NH_4 showed good growth; however, when SYTO was added growth rate was reduced, and cultures did not reach the same maximum OD as the control without SYTO, indicating cellular stress due to SYTO incorporation into DNA (Figure 20). When nitrogen was removed from the medium, cells were still able to grow, consistent with previous observations (Figure 21). When both the carbon and nitrogen sources were removed, growth was completely inhibited. SYTO did not enhance growth under any tested condition, confirming that it cannot be used by the cells as a source of carbon or nitrogen. The wild-type strain grew well without nitrogen but with glucose only at lower SYTO concentrations; lowering the SYTO concentration to 1 µM already improved growth considerably, while 5 µM strongly inhibited growth.

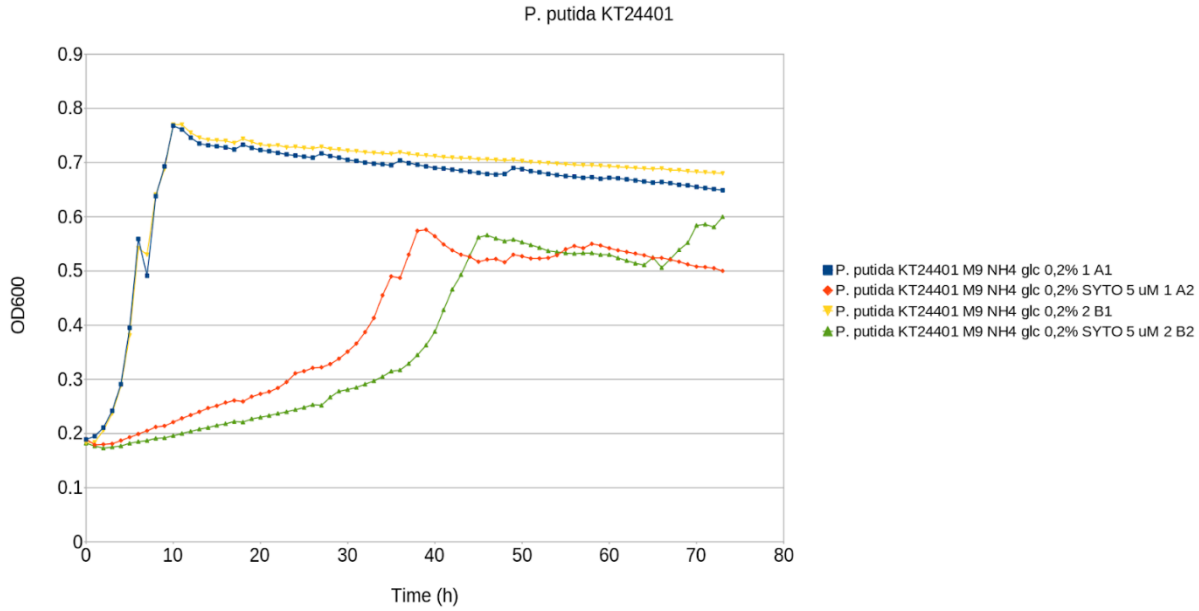

Figure 20. Growth of Pseudomonas putida KT2440 in M9 medium with glucose and addition of SYTO 11 5uM. OD_{600} was measured over 70 hours

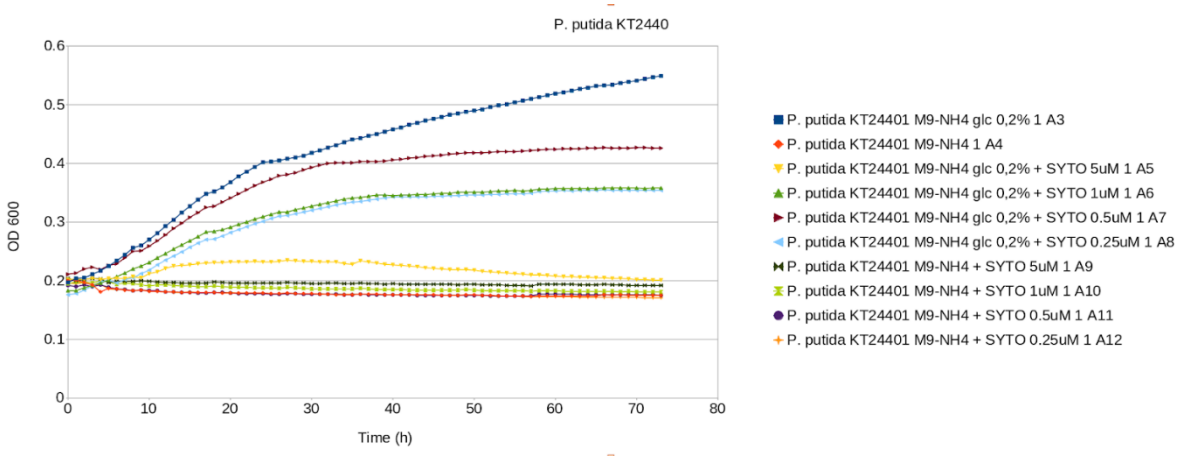

Figure 21. Growth of Pseudomonas putida KT2440 in M9 without NH4 medium with or without glucose and different concentrations of SYTO 11. OD_{600} was measured over 70 hours.

Our findings suggest that SYTO 11 concentration can be reduced to improve cell viability while maintaining adequate staining intensity for flow cytometry. Based on the data, concentrations below 0.5 µM resulted in weaker staining and unstable signals, while 5 µM was clearly toxic. Therefore, a concentration around 1 µM appears to offer the best compromise between strong signal and acceptable toxicity and is recommended for future experiments.

3 Subtask 3.2.2. Development of electroactive biofilms

3.1 Development and optimization of methods for efficient deposition of cells on the electrode surfaces

3.1.1 Introduction

Bioelectrochemical systems (BES) rely on electroactive biofilms to facilitate electron transfer at electrode surfaces. Traditional approaches allow biofilms to develop naturally over time, often leading to heterogeneous microbial communities. Here, we investigated whether pre-immobilized biofilms on modified graphite electrodes could accelerate biofilm formation and enhance system performance. We examined the effect of initial *Shewanella oneidensis* MR-1 attachment on modified graphite surfaces and its impact on the subsequent growth of electroactive biofilms. Unlike conventional bioelectrochemical or microbial fuel cell systems, which typically support mixed-species biofilms, this approach aimed to selectively enhance *Shewanella* attachment and accelerate biofilm stabilization.

In order to stimulate attachment of bacterial cells, graphite electrodes were modified to enhance hydrophilicity through plasma treatment and forming positive surface charge through the deposition of polyethyleneimine (PEI), or polypyrolle (PPy) by electrochemically induced polymerisation. The PPy was electrochemically polymerized on the surface of graphite electrodes using the cyclic voltammetry (CV) technique with a MultiEmStat4 Potentiostat/Galvanostat. Detailed methods are described in the D4.2 and D3.2

3.1.2 Results

3.1.2.1 Initial characterization of modified graphite electrodes

The LSV results (Figure 22) demonstrate enhanced electrochemical activity with PPy modification. Moreover, the current density increased with increasing PPy deposition, as indicated by the rise in current response in both LSV and CV results (Figure 23).

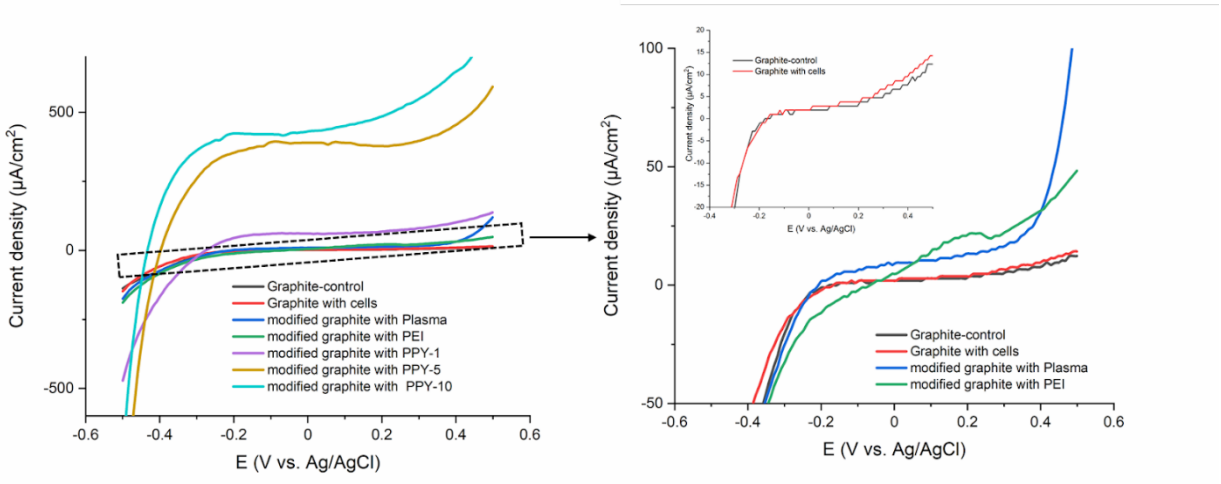

Figure 22. LSV plots of bare graphite electrode (control) and modified graphite electrode with plasma, PEI and polypyrolle

Nyquist plots recorded at 0.2 V vs. Ag/AgCl for graphite electrodes with different surface treatments (Figure 23 - B). The bare graphite (control) and graphite exposed only to bacterial cells exhibit the highest charge transfer resistance (Rct), as indicated by their large semicircular diameters. Plasma and PEI treatments reduce Rct, while subsequent polypyrrole (PPy) deposition via electrochemical polymerization significantly lowers Rct, especially with increasing scan cycles (PPY-1, PPY-5, PPY-10). These results indicate enhanced surface conductivity and improved electron transfer efficiency due to PPy modification.

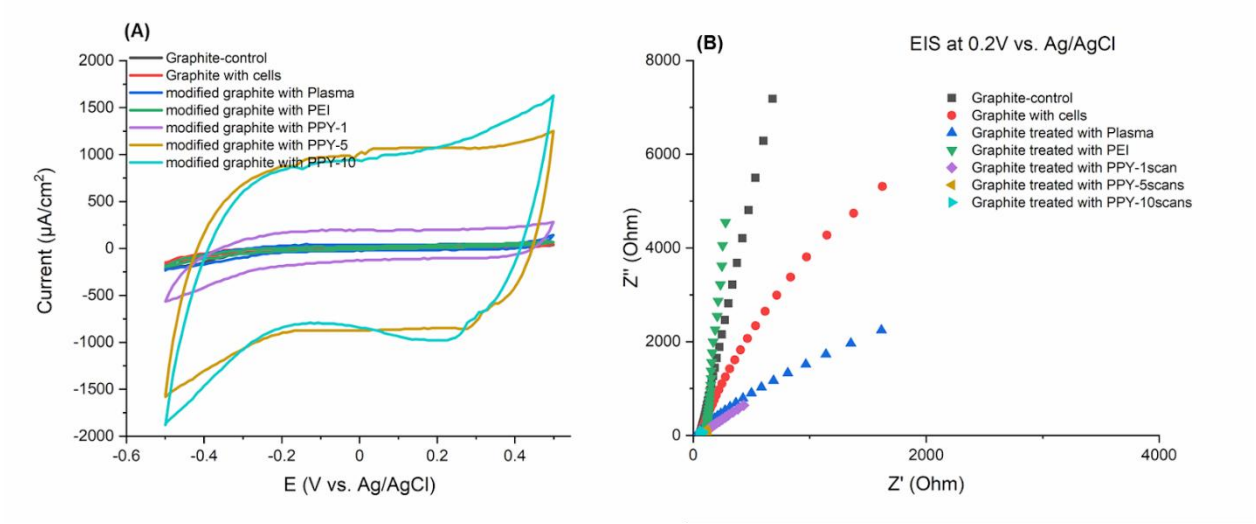

Figure 23. CV and Nyquist plots of bare graphite electrode (control) and modified graphite electrode with plasma, PEI and polypyrrole

Based on these comparative electrochemical characterization results, polypyrrole-modified electrodes demonstrated superior performance across all tested parameters, exhibiting the highest current density, lowest charge transfer resistance, and best overall electrochemical activity among all surface modifications tested. Consequently, subsequent bacteriological studies and detailed electrochemical characterization were focused exclusively on polypyrrole-modified electrodes to further optimize and understand this most promising surface modification approach.

3.1.2.2 Characterisation of PPy-modified electrodes

The cyclic voltammetry profiles during electrochemical pyrrole polymerization reveal a pronounced dependency of electrochemical characteristics on the number of polymerization cycles employed. The voltammograms demonstrate progressive enhancement of electrochemical activity with successive polymerization cycles, as evidenced by the systematic increase in current density and evolution of redox behaviour across the potential window examined (Figure 24).

For the single-cycle polymerization (PPy-1), the voltammogram exhibits a relatively modest current response with characteristic oxidation onset around 0.4 V vs. Ag/AgCl. The five-cycle modification (PPy-5) shows substantially enhanced electrochemical activity, with increased current density and more defined redox characteristics, indicating improved surface coverage and electroactive polymer deposition. The ten-cycle polymerization (PPy-10) demonstrates the most pronounced electrochemical enhancement, exhibiting significantly elevated current densities and well-developed redox features that suggest optimal polymer film formation and enhanced charge transfer kinetics.

This systematic progression illustrates the critical influence of polymerization cycle number on the electrochemical properties of polypyrrole-modified electrodes, with increasing cycles correlating directly with improved electrochemical performance. The evolution from single to multiple cycles appears to optimize polymer film thickness, surface morphology, and electronic properties, thereby creating increasingly favourable conditions for electrochemical processes.

Given these distinct electrochemical signatures corresponding to different polymerization cycle numbers (1, 5, and 10 cycles, given names PPy-1, PPy-5 and PPy-10), subsequent investigations will focus on evaluating bacterial cell interactions with these systematically varied surface modifications to elucidate the relationship between electrochemical properties and biological attachment efficiency.

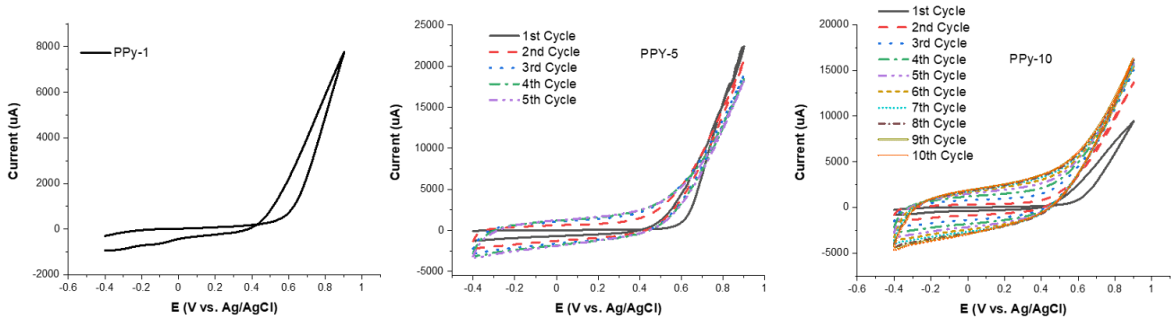

Figure 24. CV plots during electrochemical pyrrole polymerization in Na2SO4 (0.5 M) containing 1mM pyrrole at scan rate of 50 mV/s

The SEM images of bare graphite electrodes and after electropolymerization, PPy-1, PPy-5, and PPy-10, are presented in Figure 25. the smooth graphite electrodes is covered with polymer layer and the formation of aggregated globular shaped PPy is noticed for all the modified graphite despites of number of cycles during CV.

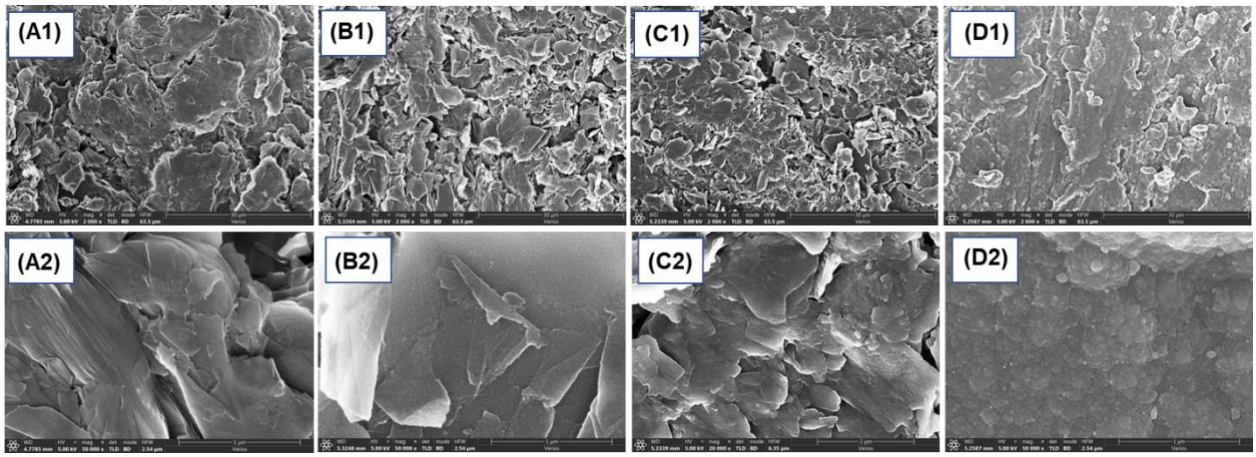

Figure 25. SEM images of bare graphite electrode (A1 and A2) and modified graphite electrodes electropolymerization with one (B1 and B2), five (C1 and C2), and ten cycles (D1 and D2) of cyclic voltammetry

3.1.2.3 Initial attachment efficiency on modified electrode surfaces

Fluorescence microscopy images revealed clear differences in cell attachment between polymerized and nonpolymerized graphite electrodes. Electrodes that underwent 5 or 10 cycles of cyclic voltammetry (CV) polymerization consistently showed a higher number of attached cells per field, indicating improved surface compatibility and enhanced initial cell adhesion compared to the untreated control.

Electrodes treated with only one CV cycle of polymerization exhibited greater variability. Among them, electrode I4 demonstrated cell densities similar to those observed on the 5 and 10 CV cycle polymerized electrodes, while electrode I1 showed considerably lower attachment, closely resembling the nonpolymerized control. These differences highlight the inconsistency of surface modification at low polymerization levels.

All modified graphite electrodes showed significantly higher cell attachment compared to the unmodified (bare) graphite electrode (Figure 26).

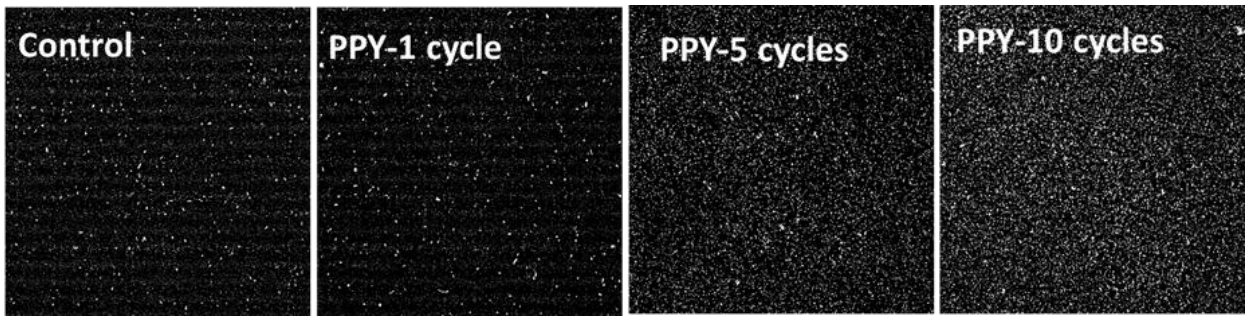

Figure 26. Comparison of *Shewanella oneidensis* MR-1 cell attachment (bright spots in the images) on untreated graphite (control) and modified graphite electrodes with PPy.

The distribution of attached cells across the electrode surface was also found to be spatially heterogeneous in samples with low or no polymerization. An increase in the number of polymerization cycles was associated with a more homogeneous distribution of cells across the electrode surface (Figure 27).

Together, these results confirm that surface polymerization via cyclic voltammetry promotes and stabilizes cell adhesion to graphite electrodes, with the effect becoming more pronounced and consistent as the number of polymerization cycles increases.

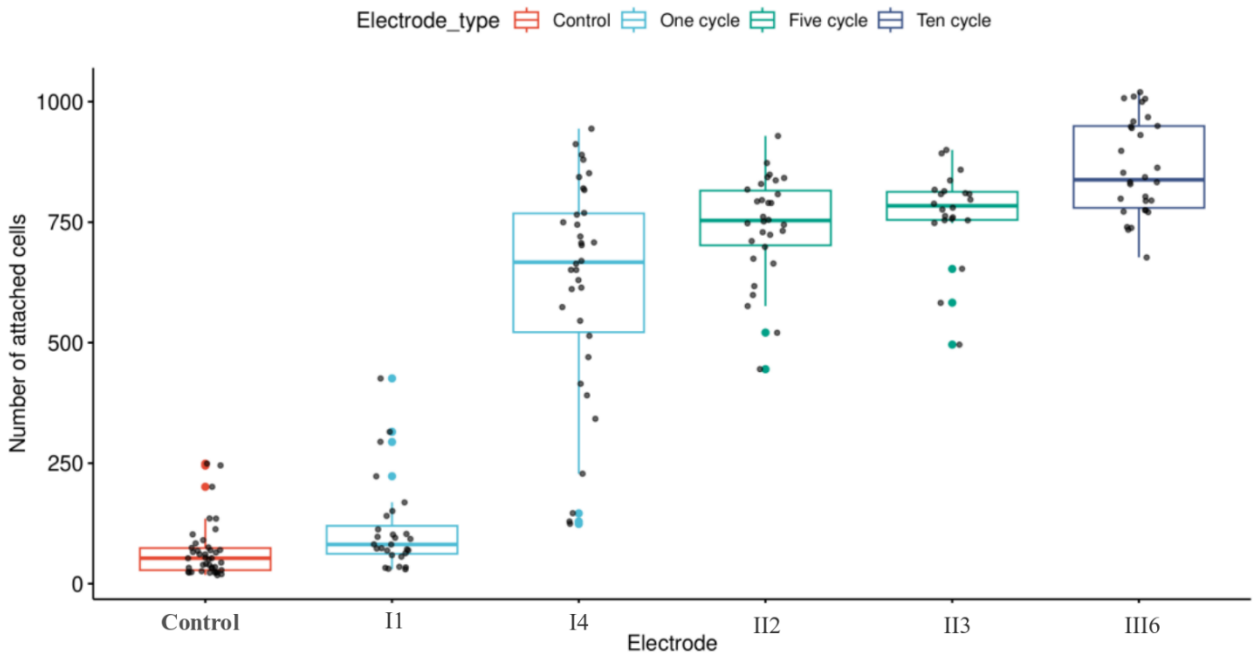

Figure 27. Number of attached cells per microscope field (400× magnification) on different electrodes. Each box plot represents data collected from individual fields of view for six electrode types, categorized by the degree of surface polymerization (control, (I1 in I4) 1 cycle, (II2 in II3) 5 cycles, and (III6) 10 cycles of cyclic voltammetry). Data points represent individual measurements, while box plots indicate the median, interquartile range, and data spread.

Scanning electron microscopy (SEM) images of both bare and modified electrodes (PPy-5), before and after cell attachment, are presented in Figure 28. The SEM images show very few cells attached to the surface of bare graphite, whereas PPy-5 electrodes exhibited a greater number of attached cells as well as larger colony sizes compared to all other modified graphite electrodes (images are not shown here).

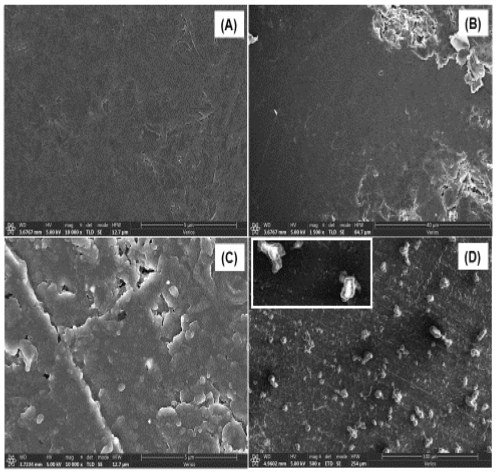

Figure 28. SEM images of bare graphite electrode before (A) and after cell attachment (B) and modified graphite electrode, PPy-5, before (C) and after cell attachment (D)

3.1.2.4 Cell growth dynamics during incubation in BES

Having established that polypyrrole modification enhances initial cell attachment, the subsequent phase investigated biofilm development dynamics under operational bioelectrochemical conditions. A custom-designed H-type BES reactor was fabricated via 3D printing as detailed in D3.2 to evaluate long-term microbial colonization and electrochemical performance.

Six electrodes representing different surface treatments were deployed: one unmodified control, two PPy-1 (single-cycle), two PPy-5 (five-cycle), and one PPy-10 (ten-cycle) electrode. These were immersed in LB medium inoculated with fluorescently labelled *S. oneidensis* MR-1 suspension. The sealed reactor maintained strict anaerobic conditions through N_2 purging (30 minutes every 3 hours) to simulate the oxygen-limited environment required for future applications with obligate anaerobic electrogens.

Biofilm development was monitored over 14 days using fluorescence microscopy while simultaneous electrochemical characterization tracked functional electrode performance.

Fluorescence imaging of the electrode surfaces after 8 and 14 days of incubation in the bioelectrochemical system (BES) revealed clear evidence of cell growth and surface colonization. Compared to time 0, the number of detected particles (representing individual cells, clusters, or colonies) increased on all electrodes, indicating successful cell proliferation (Figure 29). However, this trend varied depending on the degree of electrode surface modification.

Electrodes polymerized with 5 and 10 cycles of cyclic voltammetry showed a slight decrease in particle count after 8 days, but a notable increase in both average particle size and total covered area (Figure 30 and Figure 32). This suggests that cells had aggregated into larger clusters or colonies, reducing the number of individually distinguishable particles while increasing surface coverage. In contrast, the non-polymerized control exhibited a slightly higher number of small particles and lower average size, indicating less effective cell growth and possibly slower biofilm development.

Quantitative image analysis further supported these conclusions. Violin plots of covered area and particle size distributions revealed a clear shift toward higher values on polymerized electrodes by day 8, with the trend becoming even more pronounced by day 14. Electrodes II2 and II3, in particular, showed broader distributions skewed toward greater surface coverage and larger particle sizes. At time 0, particle sizes mostly ranged from 4–12 μm², while after 8 and 14 days, they reached 50 μm² or more on the polymerized electrodes. The control electrode, by contrast, consistently displayed lower and more uniform distributions across all fields of view.

After 14 days, the differences became more pronounced. Electrodes I1, II2, and II3 (all treated with surface polymerization) exhibited larger average particle sizes and greater coverage, reflecting advanced colonization. Among these, electrodes with 5 polymerization cycles (electrodes II2 and II3) showed the most consistent and favourable results across replicates, with higher values in all measured parameters. Electrode III6, despite having undergone 10 cycles, showed a decrease in average particle size and surface coverage between day 8 and day 14 (Figure 31 and Figure 33).

Electrodes polymerized with only one cycle (electrodes I1 and I4) showed considerable variability at all time points, which aligns with earlier findings of inconsistent and heterogeneous polymer formation at low cycle numbers. The heterogeneity of the surface was more pronounced in these cases, likely due to insufficient and uneven polymer coverage. In contrast, as the number of polymerization cycles

increased, particularly in the case of 10 CV cycles, distinct changes in surface structure were evident. Microscopy images revealed that these highly polymerized electrodes exhibited significantly more irregular surfaces, often requiring multiple focal planes to fully visualize a single field of view. This suggests a thicker and more complex polymer layer, consistent with increased polymer deposition. Such structural complexity may have contributed to the formation of microenvironments more favourable for microbial colonization and could help explain the enhanced growth patterns observed on these electrodes.

Altogether, the data indicate that surface polymerization of graphite electrodes enhances both initial cell attachment and longer-term microbial growth under BES conditions. Among the tested configurations, electrodes with 5 polymerization CV cycles offered the best balance between consistency, colonization efficiency, and reproducibility.

The precise mechanisms underlying these improvements remain to be fully elucidated. Potential contributing factors include enhanced initial colonization, increased surface conductivity, improved surface roughness, and the formation of microenvironments more suitable for microbial growth. It is likely that a combination of these effects plays a role. Further investigation will be required to determine their individual and combined contributions.

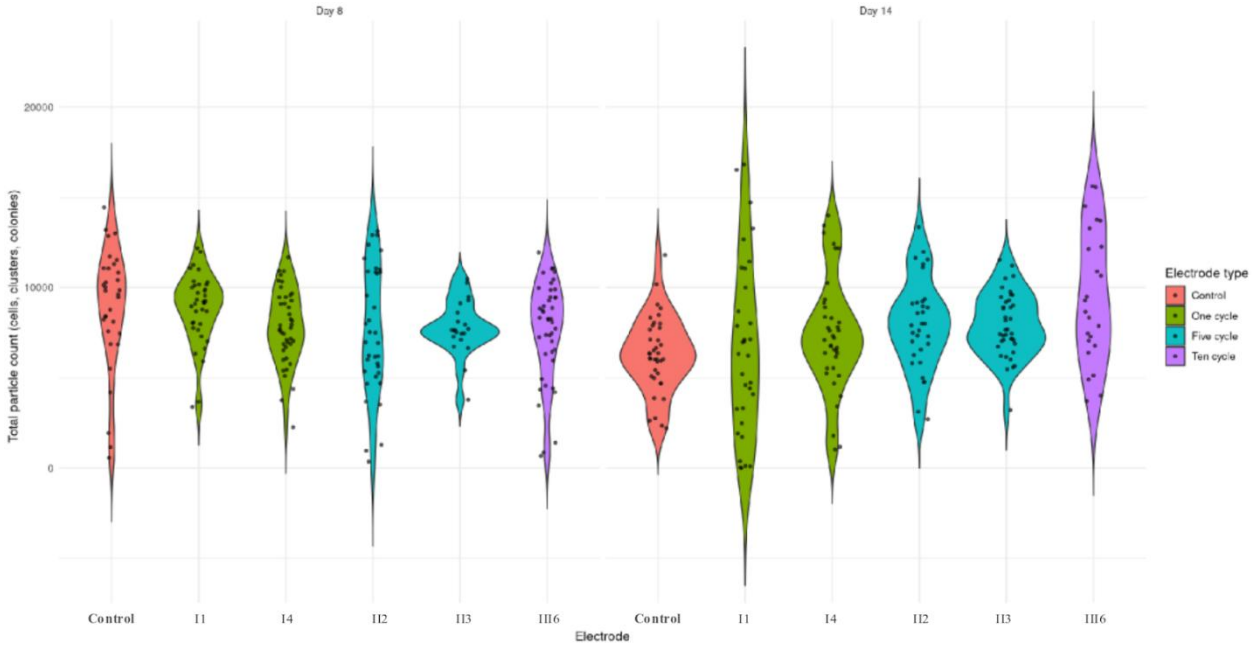

Figure 29. Distribution of total particle count (individual cells, clusters, or colonies) on different electrodes after 8 and 14 days of incubation in the bioelectrochemical system. Violin plots represent the density and spread of particle counts for each electrode, grouped by electrode type (control, 1 cycle, 5 cycles, 10 cycles of polymerization). Each point represents a single image field analysed under 100x magnification.

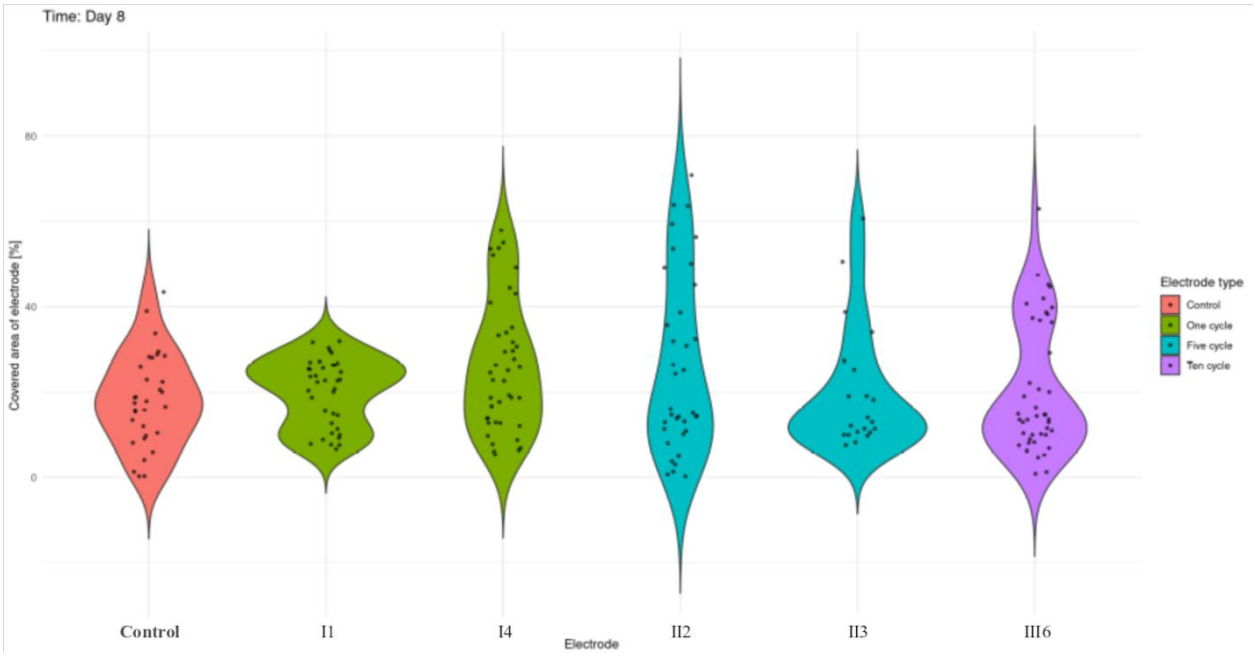

Figure 30. Distribution of surface coverage by detected particles on different electrodes after 8 days of incubation in the bioelectrochemical system. Violin plots show the percentage of the electrode area covered by cells, clusters, or colonies, based on image analysis. Each point represents a single image field analysed under 100x magnification. Electrodes are grouped by polymerization level (control, 1 cycle, 5 cycles, 10 cycles of CV polymerization).

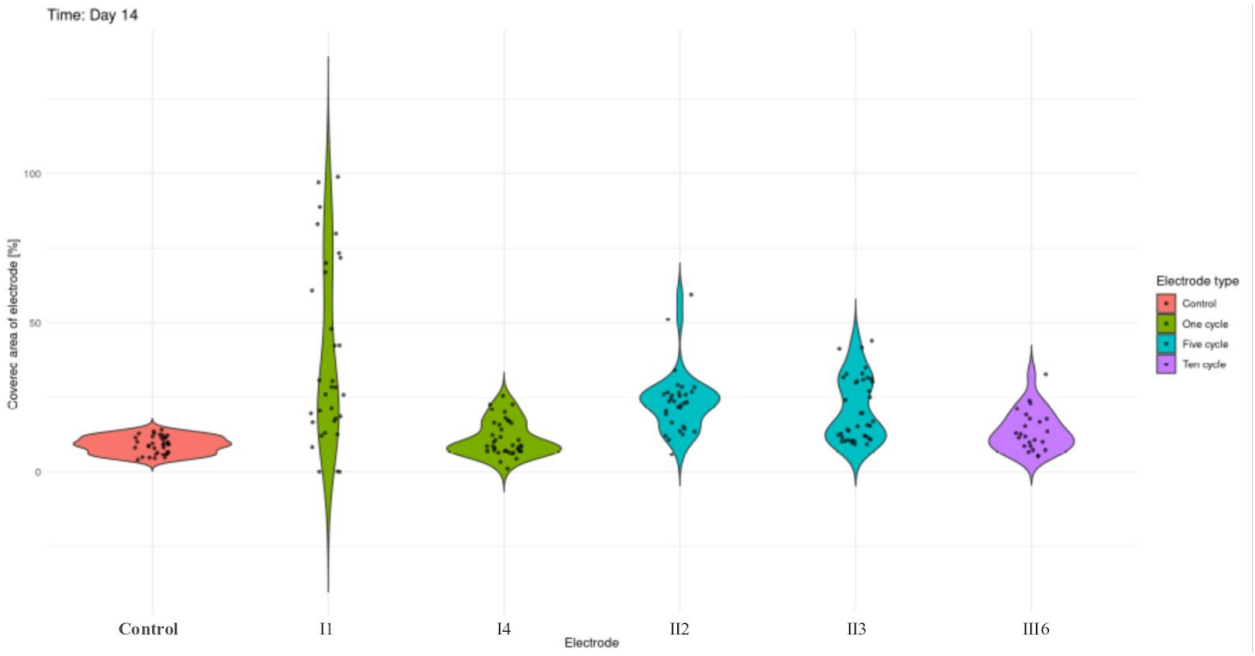

Figure 31. Distribution of surface coverage by detected particles on different electrodes after 14 days of incubation in the bioelectrochemical system. Violin plots represent the percentage of the electrode area covered by cells, clusters, or colonies based on image analysis. Each point represents a single image field analysed under 100x magnification. Electrodes are grouped by polymerization level (control, 1 cycle, 5 cycles, 10 cycles of CV polymerization).

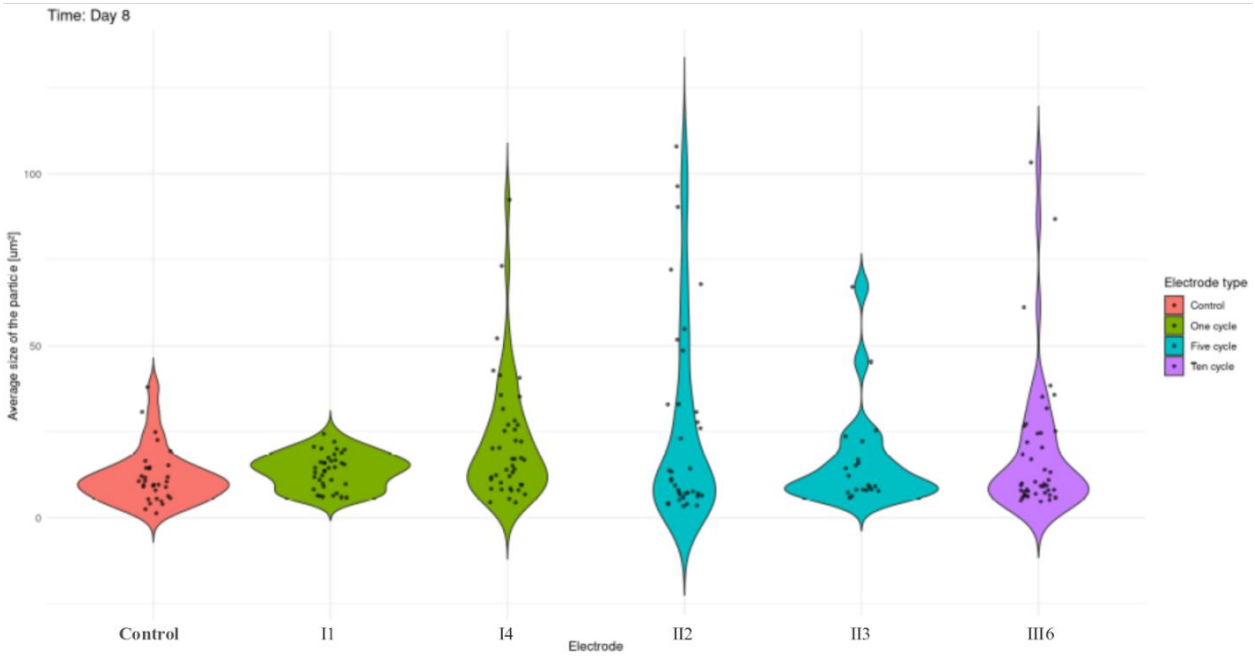

Figure 32. Average particle size on electrode surfaces after 8 days of incubation in the bioelectrochemical system. Violin plots show the distribution of average particle size (µm²) per image field for each electrode analysed under 100x magnification. Particles represent individual cells, clusters, or colonies detected by fluorescence imaging and image analysis. Electrodes are grouped by treatment type: control, 1 cycle, 5 cycles, and 10 cycles of cyclic voltammetry polymerization.

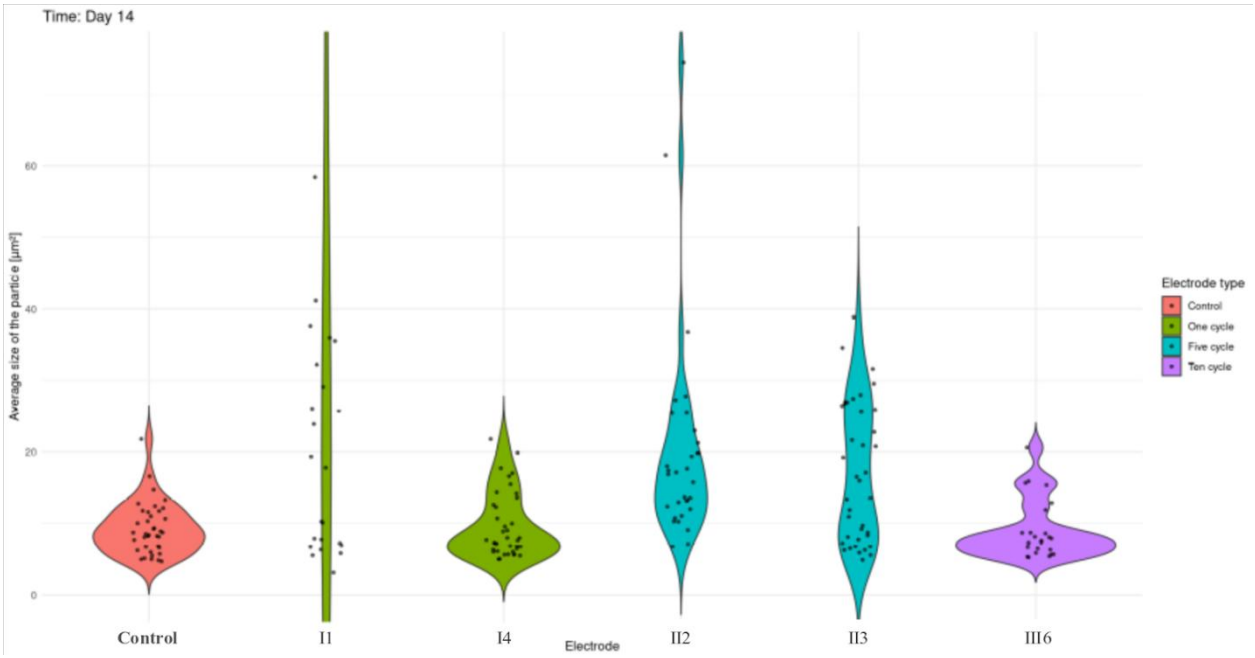

Figure 33. Average particle size on electrode surfaces after 14 days of incubation in the bioelectrochemical system. Violin plots represent the distribution of average particle size (µm²) on each electrode based on image analysis. Each dot corresponds to a single analysed field of view under 100x magnification. Electrodes are categorized by polymerization level (control, 1 cycle, 5 cycles, 10 cycles).

The CV plots of all modified graphite electrodes after cell attachment are presented in Figure 34. Notably, no redox peaks were observed in CV plots before cell attachment, considering -0.3 to +0.4V). Comparing CV results before and after cell attachment (Figure 34, CV at d0) reveals a

blocking effect across all modified electrodes post-inoculation, leading to an overall decrease in current response. This effect suggests that initial cell attachment influences surface conductivity. After bacterial attachment, the CV plots show distinct redox peaks, particularly for modified electrodes, which are indicative of electron transfer between *Shewanella* MR-1 and the electrode surface. The bare graphite electrode (control: C-d0, C-d1, C-d4, C-d6) does not exhibit well-defined redox peaks throughout the experiment. Instead, it shows a relatively low current response, indicating slow biofilm formation and weak extracellular electron transfer (EET). In the case of I1 and I4 (PPY-1 electrodes), CV curves show the gradual evolution and changing of two main redox peaks over time, particularly around -0.1 V and +0.08 V. These peaks could be attributed to flavin-mediated (-0.1 V) and contact-based (+0.08 V) EET pathways, commonly observed in *Shewanella* MR-1. Electrodes modified with 5 scan cycles polymerization (PPy-5: II2 and II3) exhibit clearer redox features and a stronger electrochemical response compared to PPy-1 electrodes. This suggests enhanced electron transfer, likely due to an optimal polymer thickness, which facilitates both bacterial attachment and conductivity. For PPY-10 electrode (III6), the redox peak at -0.1 V is not well-defined (d0). Initially, these electrodes may exhibit higher electrochemical activity due to direct electron transfer. However, as the biofilm forms (d1–d6), biofilm thickness increases, leading to a rise in charge transfer resistance (Rct), which in turn reduces the overall current output (Figure 34). Moreover, a drop in current over time (d1–d6) may be linked to (i) increased biofilm coverage and thickness, which raises resistance and limits electron transport. (ii) nutrient depletion, reducing metabolic activity and, consequently, electron transfer efficiency.

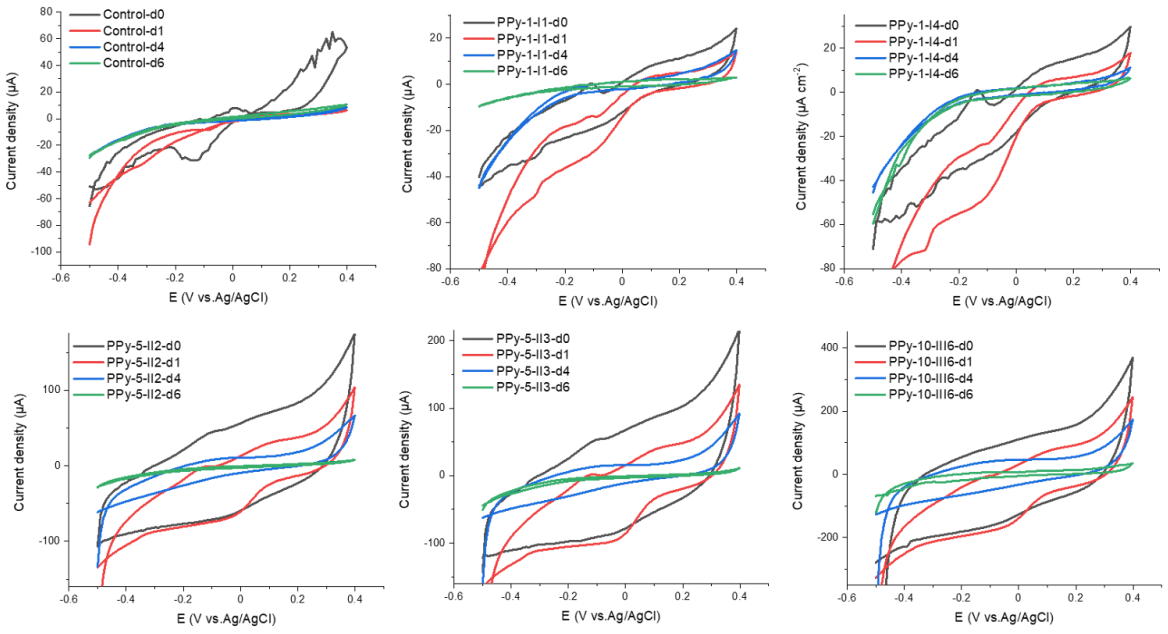

Figure 34.The CV plots (1mVs-1) of modified graphite electrodes with PPy after cell attachments at starting inoculation (d0) and d1, d4, and d6 of inoculation in anaerobic condition.

EIS was used to evaluate the charge transfer resistance (Rct) of the electrodes at different time points (Figure 35). The Nyquist plot of the bare graphite electrode exhibits a large semicircle, indicative of a high charge transfer resistance (Rct) and poor electron transfer efficiency. For modified electrodes, the Nyquist plots exhibit two semicircular regions, (i)high-frequency region which represents charge

transfer resistance (Rct) and (ii) low-frequency region corresponding to diffusion-related processes. Over time (d1 to d6), the semicircle size at high frequencies increases, suggesting a rise in charge transfer resistance due to increased biofilm coverage, which can affect electron transfer efficiency. Charge transfer resistance (Rct) trends across modified electrodes is III6 < II3 ≤ II2 < I4 ≤ I1. This trend indicates that III6 (10 scan cycles) has the lowest Rct, suggesting initial improvement in charge transfer due to polymer modification. 5 scan cycle modifications (II2, II3) provide a balance between adhesion and conductivity, supporting efficient biofilm development. 1 scan cycle modifications (I1, I4) exhibit higher Rct, suggesting less conductivity and possibly weaker biofilm-mediated electron transfer.

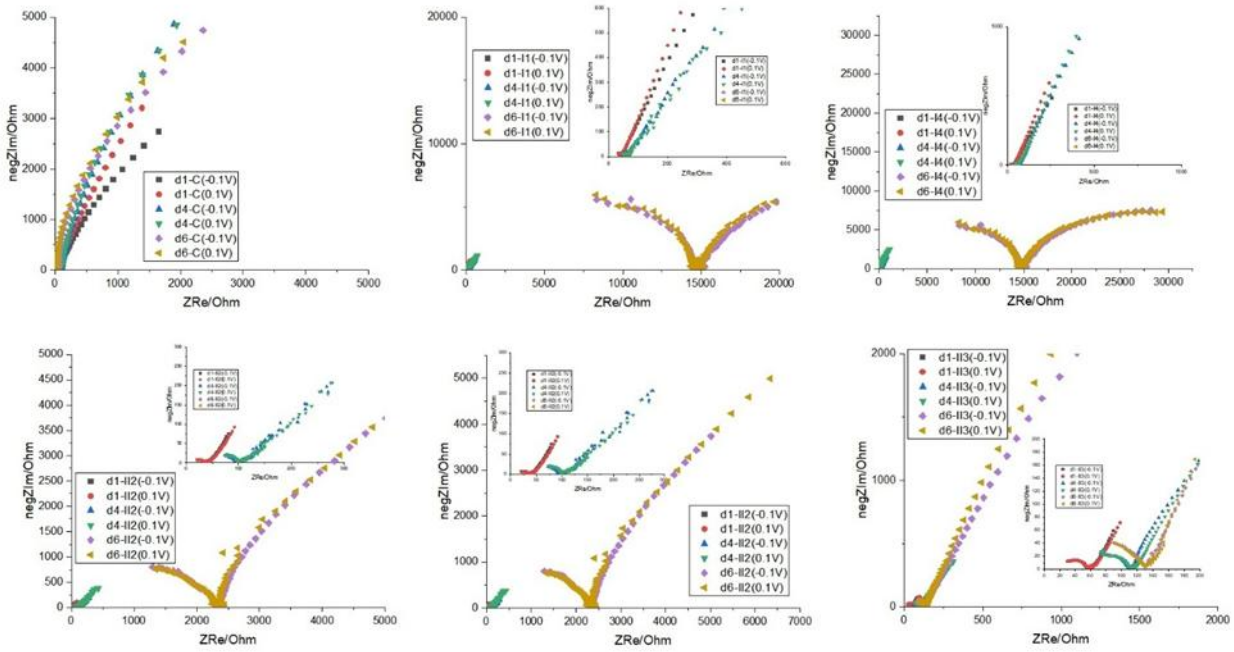

Figure 35. Nyquist plots of modified electrodes at starting inoculation (d0) and d1, d4, and d6 of inoculation in anaerobic condition.

It should be noted that Day 6 data should be interpreted with caution, as the observed decrease in medium volume may have exposed parts of the biofilm to air, potentially altering growth and increasing electrolyte resistance. This effect is particularly noticeable in some electrodes, such as I1, I4, II2, and II3. The loss of media volume introduces an external factor beyond biofilm-electrode interactions, which should be considered when analysing the results.

3.2 Structuring of Microalgal Biofilms on Electrode Surfaces

3.2.1 Introduction

Previous experiments established optimal electrode surface modification protocols and demonstrated enhanced initial bacterial attachment efficiency. However, these single-species attachment studies represent a simplified scenario compared to real-world applications, where multiple bacterial species compete for resources and form spatially complex multilayered biofilm structures. Such stratified

biofilms can exhibit superior pollutant degradation capabilities and enhanced electroactive properties compared to monolayer attachments.

To address this limitation and develop tools for controlling multilayered biofilm architecture, JSI developed a polyelectrolyte-assisted approach for engineering structured biofilms on electrode surfaces. This method was evaluated on different substrates (graphite electrodes and FTO glass) using electroactive microorganisms including *Chlorella sorokiniana* and *S. oneidensis* MR-1. The approach utilizes electrostatic interactions between charged polymers and microbial cell surfaces to control biofilm density, layering, and stability.

For *C. sorokiniana*, this strategy addresses inherent limitations in natural biofilm formation. The spherical morphology and multi-membrane chloroplasts of this microalga result in weak surface adhesion, extended electrode maturation times, and significant biomass washout in bioelectrochemical systems. The polyelectrolyte multilayer approach aims to achieve immediate stable adhesion and create conductive, photosynthetically active biofilms suitable for biophotoelectrochemical applications.

3.2.2 Methods

3.2.2.1 Microorganism Cultivation

C. sorokiniana cultures were maintained in TAP medium under controlled conditions: 150 µmol m^{-2} s^{-1} light intensity, 12:12 hour light/dark photoperiod, at 27°C. *S. oneidensis* MR-1 was cultured as described in previous sections, with fluorescent labelling using SYTO 11 and SYTO 64 dyes for visualization.

3.2.2.2 Polyelectrolyte Biocompatibility Assessment

Minimum inhibitory concentrations were determined for candidate polyelectrolytes: polyethyleneimine (PEI), acetylated PEI, poly(allylamine hydrochloride) (PAH) as positive polymers, and poly(sodium 4-styrenesulfonate) (PSS) as the negative polymer. Colony forming unit (CFU) assays assessed cytotoxicity across concentration ranges to identify optimal polymer concentrations.

3.2.2.3 Surface Preparation and Multilayer Assembly

FTO glass substrates were cleaned and UV sterilized prior to modification. Polyelectrolyte pretreatment involved immersion in PEI solutions (0.1–10 mg/mL) followed by incubation with algal suspensions at OD_{750} ≈ 6.0 for 10 minutes at room temperature or 4°C. Layer-by-layer (LBL) assembly utilized alternating deposition of PEI (positive) and PSS (negative) polyelectrolytes to build multilayer structures. For *S. oneidensis* experiments, same protocols were applied to graphite electrode surfaces and fluorescently labelled bacterial suspension of OD_{600} ≈ 2.5.

3.2.2.4 Microscopy and Image Analysis

Biofilm characterization employed bright-field, fluorescence, and confocal laser scanning microscopy (CLSM). Coverage analysis was performed on samples within 10 minutes of preparation, with biofilm thickness measurements up to ~25 µm. Image quantification utilized ImageJ/Fiji software for coverage percentage and structural analysis. Three-dimensional reconstruction of *S. oneidensis* biofilms on graphite surfaces was performed to visualize layered architecture.

3.2.3 Results

3.2.3.1 Polyelectrolyte Biocompatibility Screening

Colony forming unit assays revealed significant differences in cytotoxicity among the tested polyelectrolytes. Among the positively charged polymers evaluated, PEI exhibited the lowest inhibitory effects on *C. sorokiniana* growth and viability. Both acetylated PEI and PAH demonstrated higher toxicity levels, making them less suitable for biofilm engineering applications. The negatively charged PSS was excluded from further adhesion studies due to charge incompatibility with the predominantly negative cell surface of *C. sorokiniana*, which would preclude effective electrostatic binding. Based on these biocompatibility results, PEI at the highest non-toxic concentration was selected as the primary polymer for subsequent immobilization experiments (Figure 36).

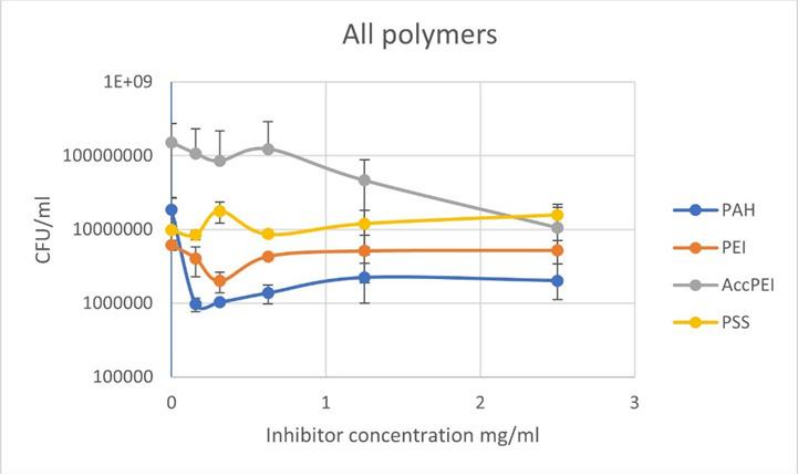

Figure 36. Inhibitory effects of tested polyelectrolytes on *C. sorokiana* culture

3.2.3.2 Initial Adhesion on Polyelectrolyte-Modified Surfaces

Preliminary adhesion tests were conducted using PEI concentrations of 2.5 and 10 mg/mL to coat both regular glass and conductive FTO glass substrates. The coating procedure involved 10-minute immersion at 4°C, followed by one-hour incubation with *C. sorokiniana* suspensions at two different cell densities: high loading (OD_{750} ~10) and low loading (OD_{750} ~1).

Visual inspection revealed marked differences between treated and untreated surfaces (Figure 37). PEI-coated substrates showed clear and extensive algal coverage, while uncoated control surfaces exhibited no visible cell attachment. Higher initial cell density (OD_{750} ~10) resulted in denser biofilm coverage across the surface, demonstrating a direct relationship between inoculum concentration and attachment efficiency. Interestingly, the difference between 2.5 and 10 mg/mL PEI concentrations did not produce perceptible changes in visible adhesion density, suggesting that 2.5 mg/mL provides sufficient surface modification for effective cell capture.

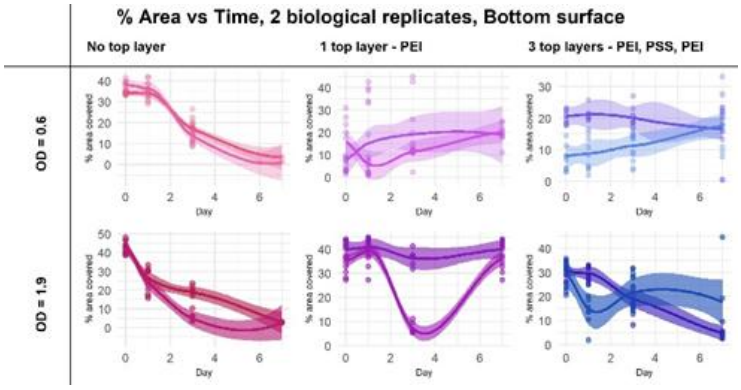

Figure 37. Temporal dynamics of biofilm surface area coverage by C. sorokiniana cultures at initial optical densities of OD_{600} = 0.6 (upper panel) and OD_{600} = 1.9 (lower panel). Biofilms were either unstabilized (red), stabilized with 1 polyelectrolyte (PE) layer (violet), or stabilized with 3 PE layers (blue)

Layer-by-layer assembly experiments demonstrated that biofilm stability could be significantly enhanced through additional polyelectrolyte deposition. Covering the initially formed biofilm with supplementary polyelectrolyte layers resulted in improved temporal stability, with reduced cell detachment over extended incubation periods. However, this approach revealed an optimal range for layer number. When three or more polyelectrolyte layers were applied above the biofilm, cell distribution became increasingly heterogeneous, with microalgae forming distinct clusters rather than maintaining uniform surface coverage. This clustering effect likely results from excessive surface charge density or physical constraints imposed by thick polyelectrolyte films.

To validate the layer-by-layer approach for electroactive bacteria relevant to BES applications (T3.2.2), multilayer assembly was performed using *Shewanella oneidensis* MR-1 on PEI-treated graphite electrodes. Sequential deposition following the protocol graphite-PEI-cells-PEI-cells was employed, with the first bacterial layer stained with SYTO 11 (green fluorescence) and the second layer with SYTO 64 (red fluorescence). Confocal microscopy analysis confirmed successful formation of distinct bacterial multilayers (Figure 38), with green-fluorescent cells positioned directly on the graphite surface and red-fluorescent cells localized exclusively on top of the first layer. No isolated single-color cell clusters were observed, confirming that multilayer formation was mediated entirely by polyelectrolyte bridging rather than direct cell-surface or cell-cell adhesion. Surface coverage remained incomplete (~70% based on representative imaging), indicating that optimization of deposition parameters may be required for complete electrode colonization in BES configurations. Complete surface coverage could not be achieved through polyelectrolyte-mediated attachment alone, regardless of initial cell density or polymer concentration. To reach full electrode coverage, cells required additional time for natural growth and proliferation on the modified surface, indicating that the polyelectrolyte approach provides enhanced initial attachment but must be combined with conventional biofilm maturation processes.

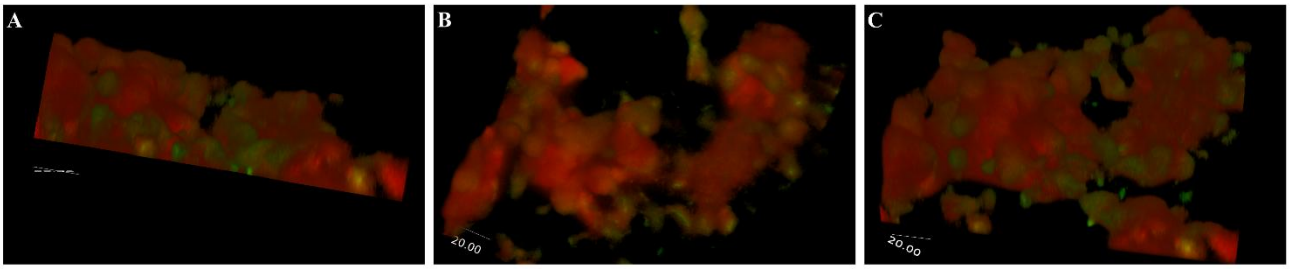

Figure 38. Confocal microscopy 3D reconstruction of multilayered Shewanella oneidensis MR-1 biofilm on PEI-treated graphite surface. First bacterial layer (green, SYTO 11) deposited directly on the electrode surface, second layer (red, SYTO 64) positioned on top of the initial layer through polyelectrolyte-mediated assembly. (A) Frontal projection, (B) top-down projection, (C) oblique view (30° rotation). Scale bar = 20 µm

3.3 Carbon brush modifications - electrochemical characterization

3.3.1 Introduction

Previous investigations focused on flat graphite electrodes to establish fundamental modification protocols and characterize microbial attachment mechanisms. However, real-world bioelectrochemical systems require electrodes with substantially larger surface areas to achieve commercially viable current densities and treatment capacities. Carbon brush electrodes are widely employed in scaled BES applications due to their three-dimensional architecture and high specific surface area, which can exceed that of flat electrodes by several orders of magnitude.

To bridge the gap between laboratory-scale flat electrode studies and practical applications, the established polypyrrole modification protocols were adapted for carbon brush electrodes. This extension represents the first step toward scalable electrode modification strategies that maintain the enhanced microbial attachment properties demonstrated on flat surfaces while providing the surface area advantages essential for industrial implementation.

3.3.2 Results

3.3.2.1 Electrochemical Characterization of Modified Carbon Brushes

Carbon brush electrodes were modified using the optimal PPy-5 conditions previously established for flat graphite electrodes (Figure 39 - A). Cyclic voltammetry analysis demonstrated that polypyrrole modification significantly enhanced the electrochemical properties of the three-dimensional electrode structure. The current density of PPy-modified carbon brushes increased substantially compared to unmodified controls (Figure 39 - B), indicating successful polymer deposition and improved charge transfer characteristics throughout the brush architecture.

The successful adaptation of the flat electrode protocol to the complex three-dimensional geometry of carbon brushes confirms the robustness of the electropolymerization approach across different electrode configurations.

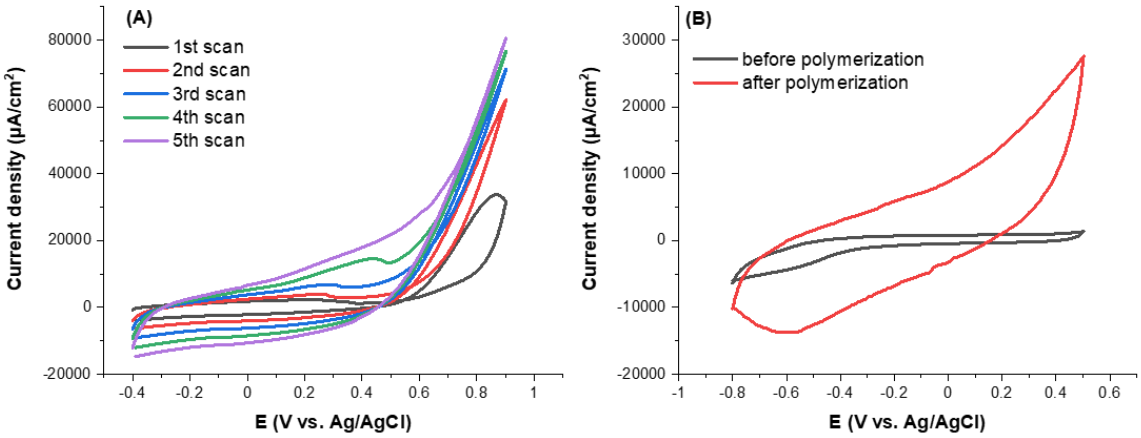

Figure 39. CV plots of pyrrole polymerization, during 5 cycles of scanning, on the surface of carbon brush electrode (A), and CV plots before and after polymerization of carbon brush (B) in Na2SO4 (0.5M)

3.3.2.2 Preliminary Cell Attachment Assessment

Initial evaluation of microbial attachment was conducted using the same protocols developed for *S. oneidensis* MR-1 on graphite electrodes, including identical incubation conditions and staining procedures. Scanning electron microscopy revealed successful polypyrrole modification of the carbon fiber surfaces and demonstrated enhanced cell attachment on modified brushes compared to unmodified controls (Figure 40).

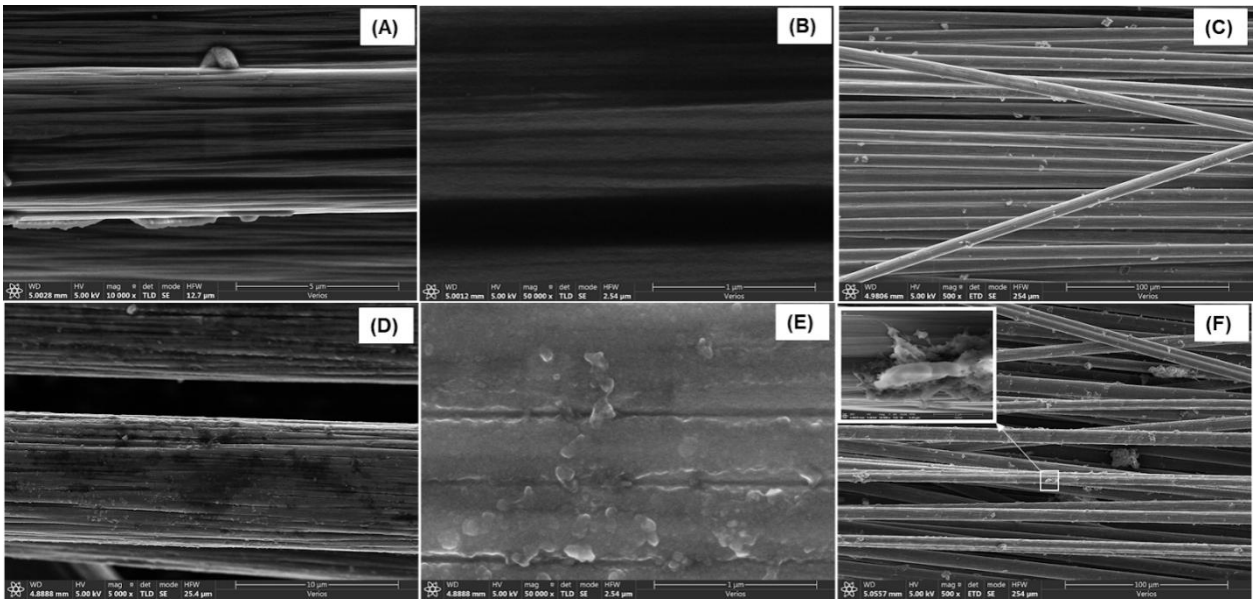

Figure 40. SEM images of bare carbon brush (A and B) and modified with polypyrrole (D and E), carbon brush (C) and modified carbon brush with polypyrrole (F) with attached cell

The SEM images confirm that the surface modification strategy translates effectively to the carbon brush platform, with visible increases in attached cell density on polypyrrole-treated fibers. This preliminary assessment suggests that the enhanced attachment properties observed on flat electrodes are preserved in the three-dimensional brush configuration.

3.3.3 Next Steps

In the further work under WP4 the comprehensive quantitative analysis of cell attachment efficiency on modified carbon brushes will be completed. Future work will include systematic cell counting, coverage analysis, and fluorescence microscopy characterization to establish quantitative comparisons with flat electrode performance. Additionally, long-term biofilm development studies and electrochemical performance evaluation under BES operating conditions will be necessary to fully validate the scalability of this modification approach for practical applications.

3.4 Modulation of redox potential on electrodes

LEITAT developed various protocols involving the modulation of the redox potential to enhance the selection and attachment of electrogenic strains on electrodes for the removal of different pollutants. This section describes the protocols applied to develop each type of biofilm, taking into account the expected pollutant removal pathways, and summarizes the main results achieved to date.

3.4.1 Biofilms for metals removal

Bioelectrochemical removal of metals is currently being studied as part of WP4 in three-chamber reactors (BES-M) treating groundwater from the well w8101 from Site 6 (see D1.1 and D4.1). These setups consist of an anodic chamber, separated from the cathodic chamber by a concentration (or saline) chamber (see D4.1).

In this case, as explained in the intermediate report (D3.2), metals removal occurs in the cathodic chamber, either by electrodeposition or indirect by-product precipitation due to oxygen reduction reactions (ORR). While microorganisms in the biofilm attached to the anode (anodic chamber) are not directly involved in metals removal, their electroactivity supplies the electrons required in the cathode for these reactions to take place. As such, work from WP3 involves the development of electroactive biofilms capable of catalysing the oxidation of organic matter and delivering the electrons generated from this degradation to the anode, to be later delivered to the cathode by an external electric circuit.

Results from a first inoculation in flat-plate reactors were previously discussed in D3.2. The present deliverable focuses on the outcomes of a second inoculation batch. The aim of this batch was to develop electroactive biofilms for metals removal in BES-M1 reactors, already operated by LEITAT (see D4.1). In this case, electro-stimulation was conducted under two different electrode configurations, which are detailed in the following sections.

3.4.1.1 Materials and methods

3.4.1.1.1 Laboratory setup and experimental conditions

The second inoculation batch was conducted in two flat plate reactors previously described in D3.2. Each reactor allocated two stacks of electrodes connected in parallel, i.e. 2 anodes and 2 air-cathodes of 100 cm^2 of surface each one. The anode material used was battery grade carbon felt (Sigracell® KFD2.5; SGL carbon). A general scheme of the setup is depicted in Figure 41.

The reactors were initially inoculated with concentrated biomass, containing a mixture (consortium) of microorganisms, from a long-term operating microbial fuel cell (MFC) which was initially inoculated using activated sludge from a wastewater treatment. Also, the effluent coming from the MFC was circulated during 3 days prior to polarization of the reactors.

After polarization and during the entire operation, the reactors were continuously fed with acetate based mineral medium with the following composition and physicochemical characteristics:

Table 1. Acetate based mineral medium composition and physicochemical characteristics

Component	Concentration	Unit
NaCl	450	ppm
$MgCl_2 \cdot 6H_2O$	165	ppm
$CaCl_2$	13.6	ppm
Mg_2SO_4	15.3	ppm
K_2HPO_4	128	ppm
$NaHCO_3$	8400	ppm
$NaCH_3COO$	2500	ppm
NH_4Cl	49.5	ppm
$FeCl_3$	0.65	ppm
$ZnCl_2$	0.07	ppm
H_3BO_3	0.006	ppm
$NiCl_2 \cdot 6H_2O$	0.024	ppm
$Na_2MO_4 \cdot 2H_2O$	0.036	ppm
$CoCl_2 \cdot 6H_2O$	0.238	ppm
$CaCl_2 \cdot 2H_2O$	0.087	ppm
$MnSO_4 \cdot H_2O$	0.0853	ppm
Biotin	0.01	ppm
Vitamin B5	0.025	ppm
Vitamin B-12	0.0005	ppm
4-aminobenzoic acid	0.0025	ppm
Thioctic acid (alpha lipoic)	0.025	ppm
Nicotinic acid/nicotinamide	0.025	ppm
Thiamine	0.025	ppm
Riboflavin	0.025	ppm
Pyridoxine HCl	0.05	ppm
Folic acid	0.01	ppm
HCl	0.60	ml/L
pH	7.5	-

Conductivity	11	mS/cm
COD	1.95	g-O_2/L

Feeding was carried out using a single buffer tank that was hydraulically connected to both reactors. The tank contained 5L of medium, which was weekly replenished with 3.5 L of fresh medium to ensure that the biomass had a sufficient carbon source. A peristaltic pump was used to distribute the medium through the reactors (see Figure 41)

3.4.1.1.2 Electrochemical operation

Electrostimulation was conducted under two different electrode configurations:

a) A 3-electrodes configuration, where the anode's potential was modulated in a controlled gradient from -0.1 V to -0.35 V vs Ag/AgCl M in -0.05 V increments, each step lasting for 79h. The protocol also includes electrochemical characterization techniques between potential steps such as open circuit voltammetry (OCV) and cyclic voltammetry (CV, from -0.1 V until -0.6 V vs Ag/AgCl with a scan rate of 10 mV/s). Electrochemical control in this case was performed by means of a potentiostat (VMP3, BioLogic's, France). This configuration was used for anodes inoculated in reactor 1 (A1 and A2).

b) A 2-electrodes configuration, in which the cell voltage (i.e., the potential difference between the anode and cathode) was gradually increased from 0.15 V to 1.2 V by means of a power source (72-2715, TENMA), in undefined time steps, with the anode potential and current increase serving as key control parameters. This configuration was used for anodes inoculated in reactor 2 (A3 and A4).

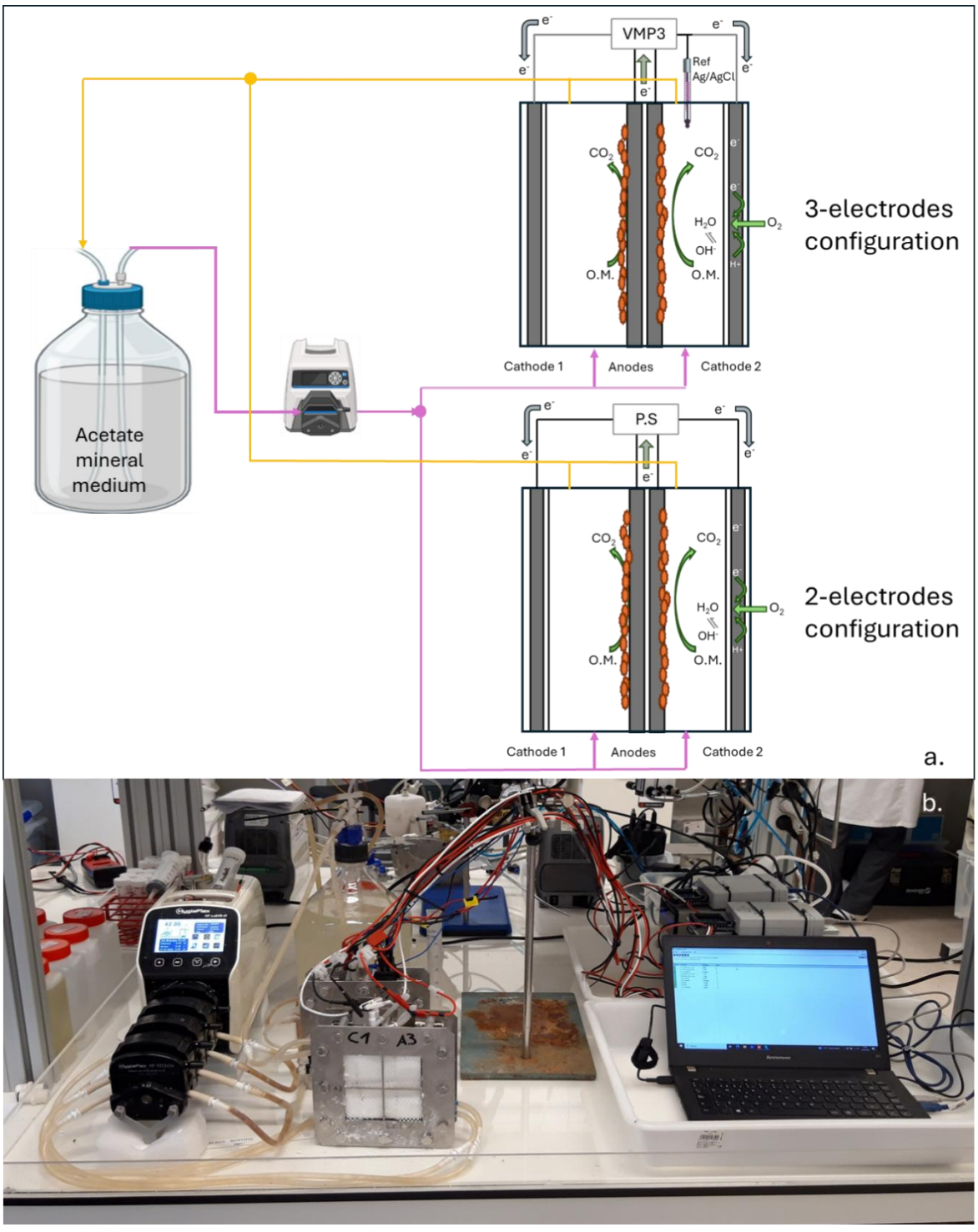

Figure 41. Scheme (a) and photograph (b) of the laboratory setup used for anodes inoculation

3.4.1.2 Results

Preliminary inoculation results from the 3-electrodes configuration were previously discussed in deliverable 3.2, while additional findings from both the 3-electrode and 2-electrode configurations will be reported in the present Deliverable.

3.4.1.2.1 Three-electrodes configuration

Figure 42 shows the temporal evolution of electrochemical potentials and current density for anodes 1 and 2, inoculated under a three-electrodes configuration. As seen in the figure, both anodes exhibited important electroactivity early in the inoculation process, producing an average current density of 0.11 ± 0.002 mA/cm^2 when the anodes potential was set at -200 mV vs Ag/AgCl 3M. This value corresponds to only 54% of the current density achieved during the first inoculation batch (0.21 mA/cm^2, see D3.2) under the same conditions, which could be directly related to a lower initial abundance of electroactive bacteria in this second batch. By the end of the inoculation (with the anodes potential set to -350 mV) the current density increased to 0.21 ± 0.001 mA/cm^2, closely approaching the density obtained in the first batch (0.25 mA/cm^2). As this current was considerably higher than 0.15 mA/cm^2 and remained stable for more than 7 days (data not shown), the anodes are considered successfully inoculated.

The cathode potential varied in response to the electrons supplied by the anodes, ranging from -650 mV to -1200 mV for anode 1, and -400 mV to -1200 mV for anode 2. Consequently, the cell potential fluctuated between 0.3–1.2 V for anode 1 and 0.2–0.9 V for anode 2.

Evidence of electroactivity from the beginning of inoculation is further supported by the Open Circuit Potential (OCP) of the anodes, which remained stable around -500 mV. This potential was also maintained during subsequent metal removal experiments reported in D4.1.

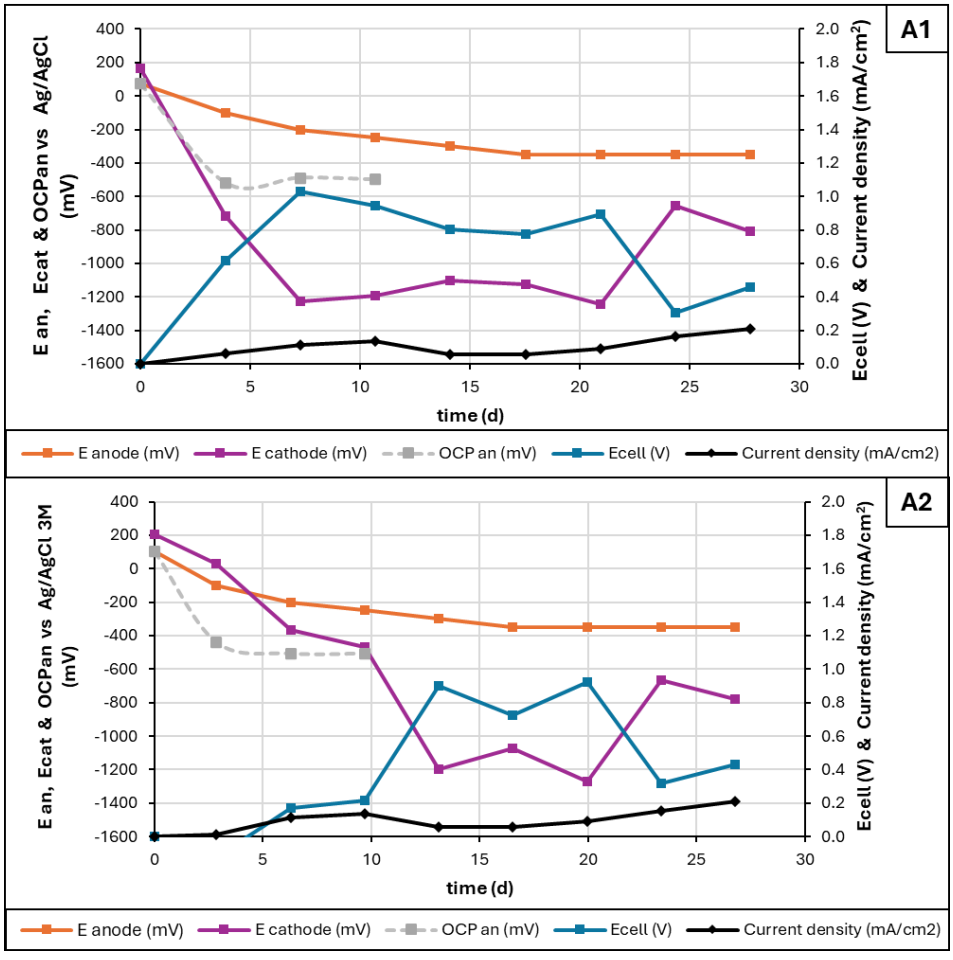

Figure 42. Temporal evolution of electrochemical potentials and current density in anodes 1 (A1) and 2 (A2) under a three-electrodes configuration. Ean=Anode's potential; Ecat=Cathode's potential; OCPan= Anode's potential in Open Circuit Potential.

In Figure 43 is depicted the current output in cyclic voltammetry for both anodes at the end of the inoculation period. As observed, both inoculation reactors deliver high current levels within the expected operating range of BES-M1 reactors (between -500 mV and -300 mV), further confirming the electroactivity of the biofilms. These results support their suitability for metal treatment applications in BES, as demonstrated in the experiments for Task 4.4, with initial results discussed in the intermediate report D4.1 and further analysis to be provided in the final report D4.3.

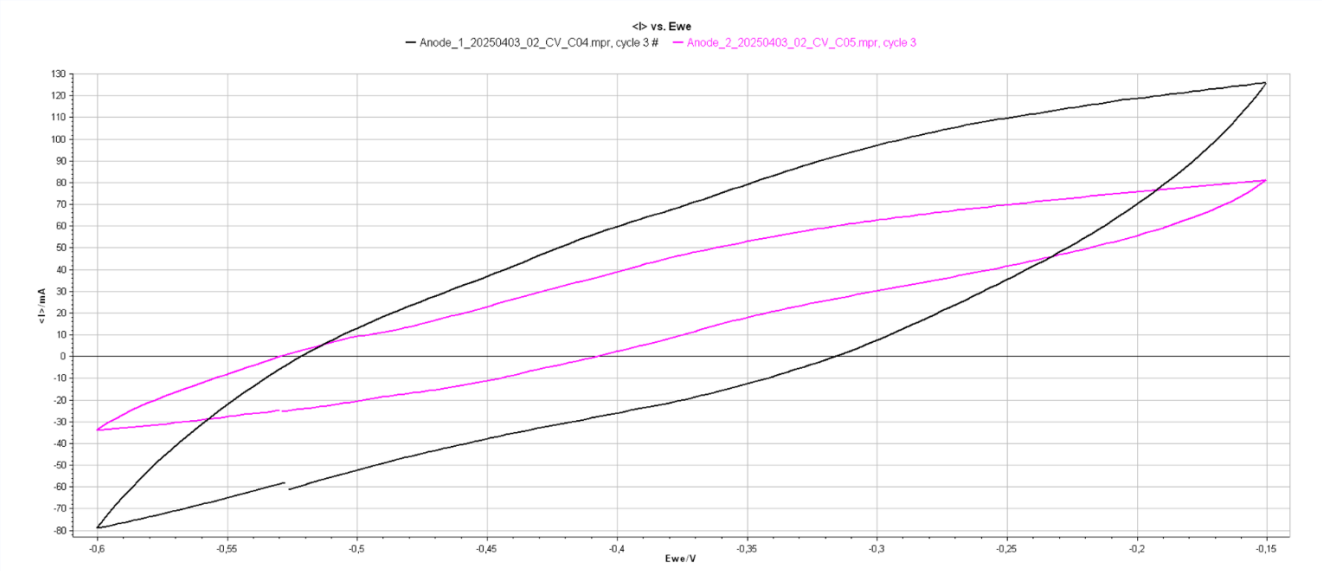

Figure 43. Cyclic voltammetry of anode 1 (black line) and anode 2 (pink line) after inoculation's last potential step (-350 mV)

3.4.1.2.2 Two-electrodes configuration

A two-electrodes configuration was tested at LEITAT as an alternative to the conventional three-electrodes setup traditionally used for inoculating electroactive biofilms. In this approach, inoculation was carried out by modulating the cell voltage between 0.15 V and 1.2 V using a power supply, with the anode potential and current increase serving as key control parameters. **Figure 44** shows the temporal evolution of electrochemical potentials and current density for anodes 3 and 4, inoculated under this configuration.

As shown in the figure, anode 4 reached a potential below -400 mV during the first ten days of inoculation at a cell voltage of 0.3 V. When the cell voltage was increased to 0.7 V, the anode potential remained stable. However, raising the voltage to 0.9 V caused a decrease in anode potential, likely due to initial stress experienced by the electroactive bacteria at these new conditions. A similar, but more pronounced drop was observed when the voltage was increased to 1.1 V. Nevertheless, the anode eventually recovered over time, forming a stable biofilm with a potential consistently below –400 mV. This stability was maintained when the cell voltage was further increased to 1.2 V. At this voltage, once the anode was stabilized, the current density fluctuated around an average of 0.2 mA/cm² (ranging from 0.17 to 0.26 mA/cm²).

Anode 3 required 34 days to reach a potential below -400 mV, which is why the cell voltage was kept at 0.4 V during this period. Once this threshold was achieved, the anode potential remained stable below –400 mV until the end of the experiment, where the cell voltage was changed sequentially until reaching a value of 1 V, obtaining current densities of more than 0.2 mA/cm^2 from day 48 onwards.

After 70 days of operation, two electroactive anodes with stable potentials were successfully obtained. These results demonstrate that inoculation using a two-electrodes configuration is a feasible approach. The effectiveness of these anodes for metals removal has also been validated and discussed in D4.1. Although this method certainly requires significantly more time than the 3-electrodes configuration (70 days vs 27 days), it offers a practical alternative when the use of a potentiostat is not possible.

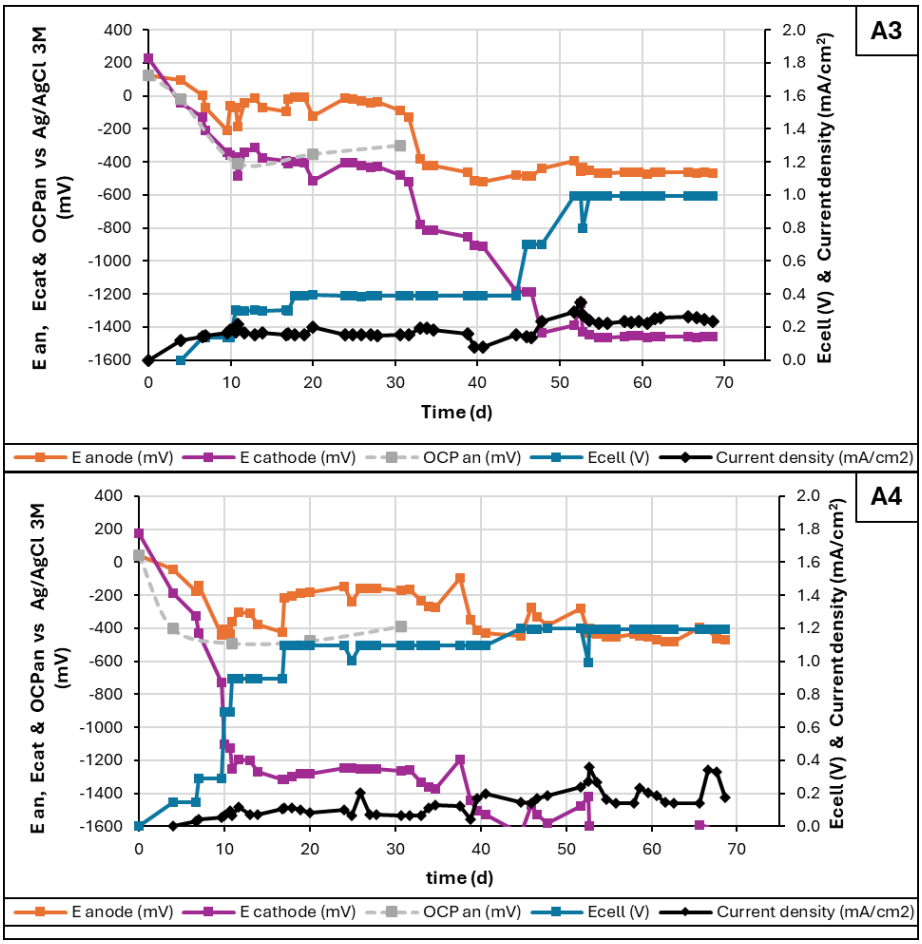

Figure 44. Temporal evolution of electrochemical potentials and current density in anodes 3 (A3) and 4 (A4) under a two-electrodes configuration. Ean=Anode's potential; Ecat=Cathode's potential; OCPan= Anode's potential in Open Circuit Potential.

3.4.2 Biofilms for hydrocarbons removal

The bioremediation of petroleum hydrocarbons requires multiple microorganisms, each one degrading specific hydrocarbons (i.e. microbial consortia). The use of indigenous bacterial consortia (isolated from the polluted site) is advantageous compared to bioaugmentation, as the bacteria are already adapted to the physic-chemical characteristics of the water/soil matrix. In alignment with Subtask 3.2.2 and Task 4.4 objectives, the collaborative work between LEITAT and JSI focused on selecting and characterizing bacterial consortia suitable for BES-based treatment of groundwater polluted with Total Petroleum Hydrocarbons (TPHs).

Single chamber reactors were selected to perform the enrichment of the microbial consortia existent on the selected groundwater Pz-39 from site 7, as reported on D3.2. The resulting biofilm was then used in the bioelectrochemical removal of hydrocarbons as reported in D4.1 The inoculation of the

electrodes was initially performed in H-type half reactors. For the second phase, a scale-up was performed in flat plate BES reactors. This change in cell architecture, from half H-type to flat plate cells, was performed for enhancing biomass growth stability.

3.4.2.1 H-type cells

3.4.2.1.1 Materials and methods

Reactors design

In the first inoculation phase, glass H-type Half reactors (VidraFoc, Spain) were used. Each reactor contained unidirectional carbon fibers (UDCFs, SGL, Germany) with an oxygen reduction catalyst (Precious-Metal-Free™ Catalyst from Pajarito powder) as a cathode (4.1 m^2 cathode/m^3 reactor) and, a carbon fibers brush as anode (9.7 m^2/m^3 reactor). The reactors were operated in 7-day cycles, with 300 mL groundwater as feed. Two different configurations were selected for testing, i.e., liquid-cathode and air-diffusion cathode. Duplicates were used for each (see Figure 45).

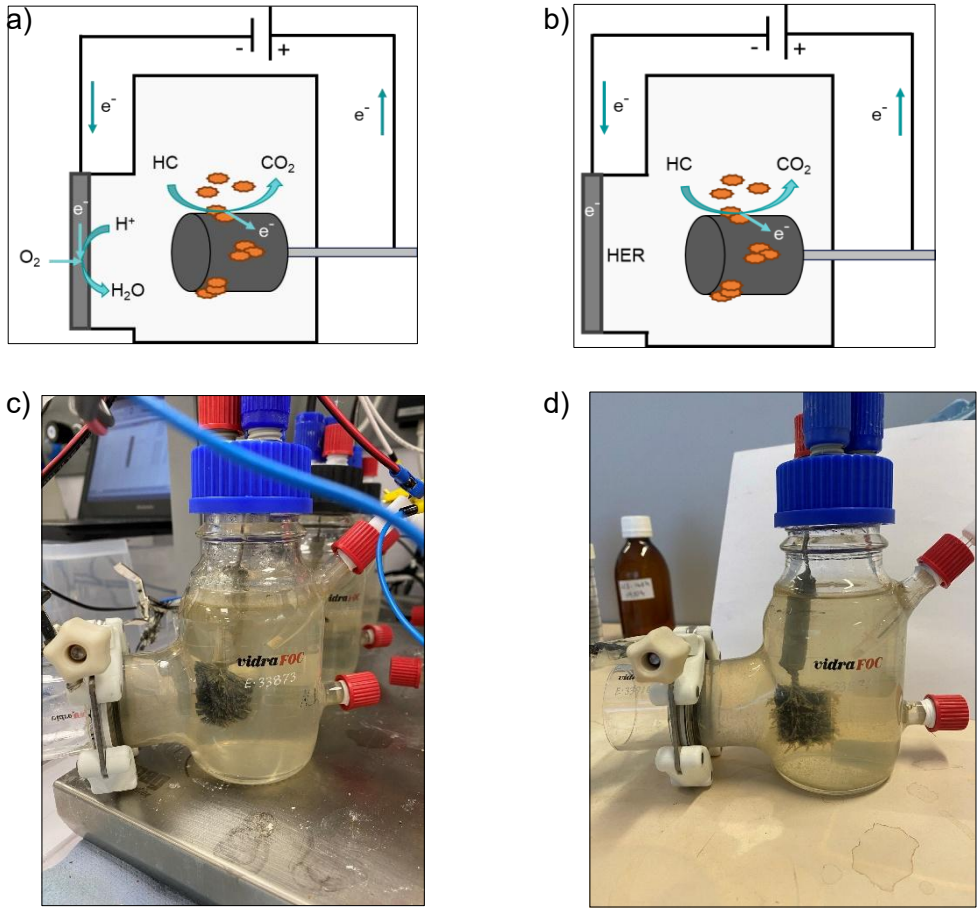

Figure 45 . H-type reactors used for the initial phase of inoculation. Air-diffusion cathode: a) and c); liquid-cathode: b) and d)

In total, two air-diffusion cathode reactors and two liquid-cathode reactors (see Figure 46) were assessed. Stirred at 140 rpm and at room temperature, the current density was monitored over weekly cycles. At the end of each cycle the reactors were emptied and refilled with groundwater from Pz-39.

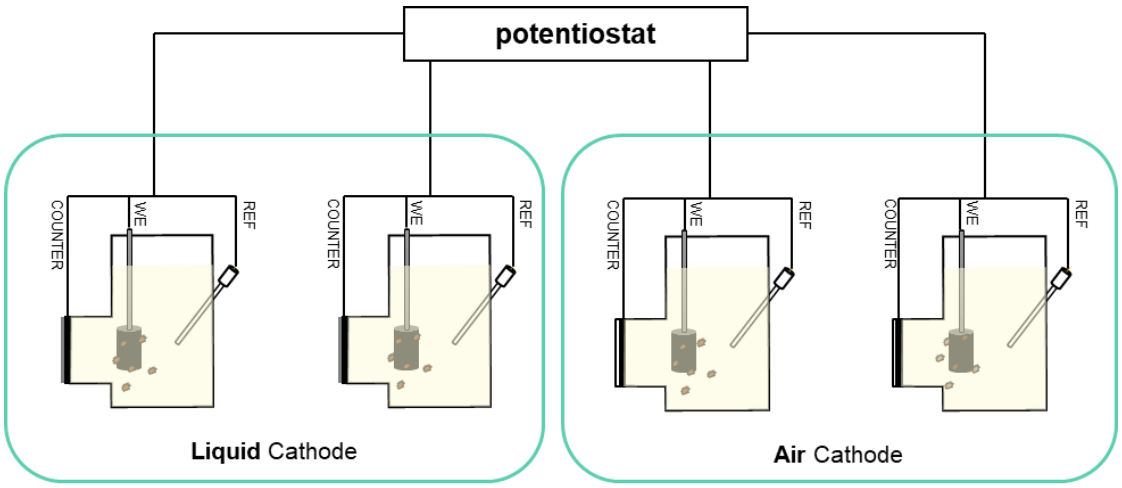

Figure 46. Schematic representation of the laboratory setup used for half H-type reactors setup

The experimental work was organized into four successive runs: in Run I, the feed was the Pz-39 groundwater from site 7. On Run II, 200 mL of Pz-39 feed were centrifuged at 1500 rpm (Thermo Scientific, Model SL1 PLS TX-400 TC PKG) and the resulting biomass was added to the feed; during Run III the feed was changed to Pz-39 again; on the course of Run IV, kerosene was added to the Pz-39 groundwater. A summary of the different Runs per Cycle can be found on Table 2.

Table 2. Summary of each cycle feed

Cycle	Run	Feed
1 - 10	I	Pz-39 GW
11 - 14	II	Pz-39 GW + concentrated biomass
15 - 16	III	Pz-39 GW
17 - 22	IV	Pz- 39 GW + Kerosene

Electrochemical operation

H-type reactors were analysed by a three-electrode setup, using an Ag/AgCl 3M reference electrode, a carbon fibre brush anode as working electrode and an air-diffusion cathode or a liquid-cathode as counter electrode depending on the reactor.

The electrochemical protocol included an open circuit voltage (OCV) stabilization for 1 minute, where the reactor was able to reach equilibrium before applying any potential. Cycle Voltammetry was then performed within the potential window of -0.5 V to + 0.9V vs Ag/AgCl 3M at a constant scan rate of 50 mV/s. Using this technique, we were able to identify redox processes and possible electroactive species formation within the biofilm during the inoculation phase, particularly those involved in hydrocarbon degradation.

A chronoamperometry was then conducted in all reactors. The working electrode was kept at a potential of 0.6 V vs Ag/AgCl 3M. This potential was maintained throughout the degradation cycle to drive the inoculation and the electrochemical oxidation of hydrocarbons. Current density was analysed to check if the reactor was inoculated, considering a threshold of 0.01 A/m^2 as indicator of the effectiveness of the process.

At selected cycles, cyclic voltammetry was also performed at the end of the inoculation period to monitor the progression of the bioelectrochemical system during the inoculation phase.

Hydrocarbons determination

TPHs and BTEX concentrations were determined by a laboratory accredited under the UNE-EN ISO IEC/17025 standard (Eurofins Iproma, Castellon, Spain). Samples were collected in glass containers provided by the laboratory, which contained H_2SO_4 for preservation. Immediately after collection, the samples were transported in isothermal coolers and delivered to the laboratory within 24 hours. Analysis was carried out with methods CGM/040 and CG/021-a. The first method is derived from ISO 20595:2018 and is used for analysing volatile organic compounds such as light HC and BTEX using gas chromatography-mass spectrometry (GC-MS). CG/021-a, based on UNE-EN ISO 9377-2 and UNE-EN ISO/TS 166558-2, targets heavier hydrocarbon fractions using gas chromatography with flame ionization detection (GC-FID). The detection limits can be found on Table 3.

Table 3. Limit of Quantification and method for different fraction of TPHs measured

Parameter	Method	Limit of Quantification (LOQ)
Hydrocarbons C5–C10 (GROs)	**CGM/040-a**	25 µg/L
Benzene	**CGM/040-a**	0.20 µg/L
Toluene	**CGM/040-a**	0.5 µg/L
Ethylbenzene	**CGM/040-a**	0.5 µg/L
o-Xylene	**CGM/040-a**	0.5 µg/L
m,p-Xylenes	**CGM/040-a**	1.0 µg/L
Hydrocarbons C5–C8	**CGM/040-a**	15 µg/L
Hydrocarbons >C8–C10	**CGM/040-a**	10 µg/L
Total Petroleum Hydrocarbons (C10–C40)	**CG/021-a**	40 µg/L
Hydrocarbons C10–C28 (DROs)	**CG/021-a**	30 µg/L
Hydrocarbons C29–C40	**CG/021-a**	10 µg/L
Hydrocarbons C10–C12 (*)	**CG/021-a**	10 µg/L
Hydrocarbons C12–C16 (*)	**CG/021-a**	10 µg/L
Hydrocarbons C16–C21 (*)	**CG/021-a**	10 µg/L
Hydrocarbons C21–C35 (*)	**CG/021-a**	10 µg/L
Hydrocarbons C35–C40 (*)	**CG/021-a**	10 µg/L
Total Petroleum Hydrocarbons (C5–C40)	**—**	65 µg/L
Xylenes (Ortho, Meta, and Para)	**CGM/040-a**	1.5 µg/L
BTEX (sum of Benzene, Toluene, Ethylbenzene, Xylenes)	**CGM/040-a**	2.7 µg/L

Microbial community analysis

Microbial community analyses were performed by JSI on biomass samples collected from air-cathode and liquid-cathode h-type reactors after operation. The DNA was isolated using a standardized protocol (IMMT ltd., Slovenia) and 16S rRNA amplified by PCR. Obtained amplicons were sequenced using nanopore technology by standard library preparation and sequencing (Nanopore Protocol - 16S Barcoding Kit 1-24, Version:16S_9086_v1_revL_14Aug2019), ONT ltd.). After sequences of amplicons were obtained, the following protocol was conducted: 1) DNA quality was checked using the FastQC software, 2) The reads were filtered and trimmed by Fastq quality trimmer by sliding window (Revision 4 - 2020-03-01; Galaxy project), 3) The reads were characterized by BLAST+

software (v2.14.0+, NCBI) using the 16S ribosomal RNA database (2023-07-11; NCBI), and 4) Microbial community analysis was performed using the MEGAN software (v6.24.23).

3.4.2.1.2 Results

Feed groundwater analysis

Groundwater feed samples were initially analysed to track the contaminant levels introduced into the reactors. Figure 47 shows the evolution of contaminant levels in the feed throughout 22 cycles, divided into four experimental runs. In Run I (Cycles 1 to 10), the feed shows a higher concentration of hydrocarbons on the first cycles performed immediately after receiving the fresh samples (Cycle 1 and Cycle 9, highlighted by a dashed line). These concentrations gradually declined over the subsequent cycles, due to degradation, volatilization of sorption processes during the storage of the sample. In Run II (Cycles 11 to 14), as expected, the biomass addition correlated with a continuous decrease of every contaminant in the GW. However, when conducting Run III (Cycles 15 and 16) where Pz-39 was reintroduced as feed, the concentrations were once again similar to previous cycles, indicating that the stored feed may have reached a baseline or steady-state in terms of hydrocarbon content.

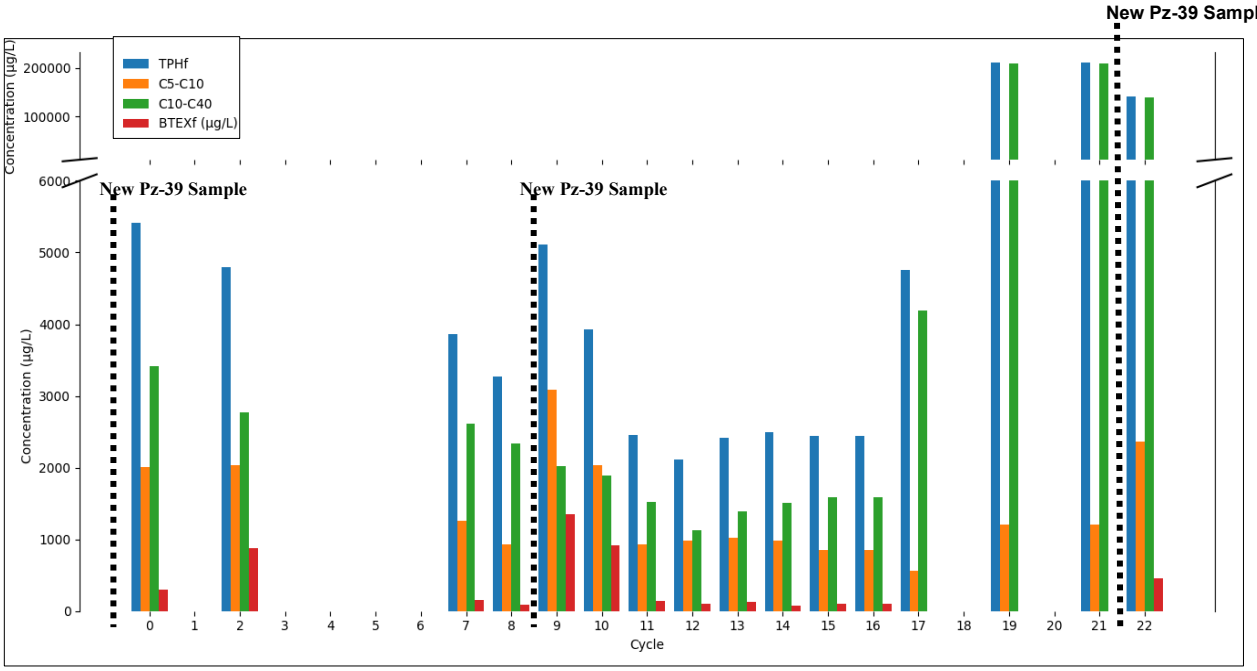

Figure 47 Feed hydrocarbon concentrations over cycles for reactors inoculation

When kerosene was added in Run IV (Cycles 17 to 22) a large spike in hydrocarbon concentrations was noticed, particularly in C10 – C40 TPHs, reaching values above 100,000 µg/L. This confirmed kerosene as a substantial new source of hydrocarbon input. Although a new Pz-39 sample was introduced in Cycle 22, its addition only increased the concentration of C5-C10 TPHs and BTEX.

Chronoamperometry

Figure 48 presents the current density evolution throughout the inoculation phase of four bioelectrochemical reactors: two with air-diffusion cathodes (AC1 and AC2) and two with liquid cathodes (LC1 and LC2). Across 22 cycles the cathodes were kept at a potential of +0.6 V vs Ag/AgCl 3M, but varying feed compositions as shown in the previous section. During Run I (Cycles 1

to 10), where only Pz-39 was fed, AC2 showed an initial current density above the defined threshold (0.01 A/m^2) but after cycle 5 fell below this value, a behaviour that was maintained throughout the rest of the Run. The remaining reactors: AC1, LC1 and LC2 showed low but slightly fluctuating current densities, mostly below the activity threshold of 0.01 A/m2, suggesting a limited bioelectrochemical activity.

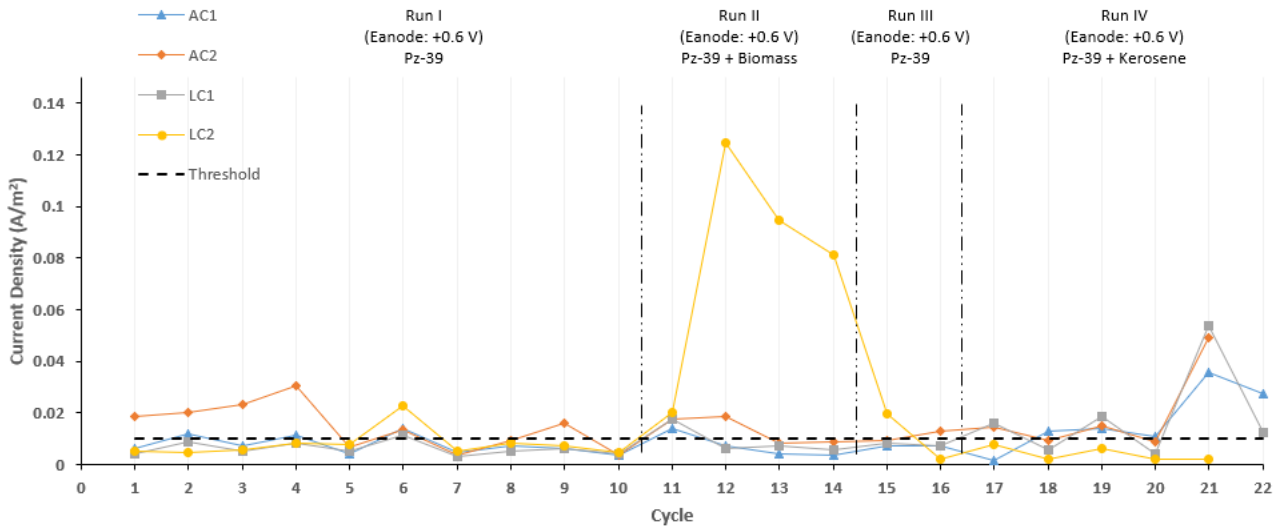

Figure 48. Current density evolution during bioelectrochemical reactors inoculation phase: AC1, AC2, LC1 and LC2

Due to the results obtained on Run I, biomass was added to the reactors in Run II (Cycles 11 to 14). During this Run, LC2 showed a sharp peak in current density after Cycle 12. Despite it was initially thought that this indicated elevated bioelectrochemical activity, it was confirmed that the main reason were corrosion issues (see **Error! Reference source not found.**Figure 49). In contrast, AC1, AC2 and LC1 initially showed promising results, with cycle 11 being the first where all reactors were maintained above the 0.01 A/m^2 threshold. Nonetheless, the subsequent cycles displayed a drop in the current density and at cycle 14 every reactor, except for LC2 due to the previously described issue, were below the threshold line. These results suggest biomass didn't increase or boost the electroactive microbial activity.

In Run III (Cycles 15 to 16), Pz-39 was kept as feed without any addition. LC2 anode was fixed and protected against corrosion issues, but the reactors failed to maintain above the threshold value.

For this reason, in Run IV (Cycle 17 to 22), Kerosene was added to the reactors feed. All reactors except LC2 displayed a noticeable increase in current density, particularly AC1, AC2, and LC1 in cycle 21. This suggests that the addition of kerosene can boost the electroactive microbial activity in some reactors.

Overall results show that during inoculation of these reactors the behaviour is highly variable with isolated high-activity events. This can be due to the process of emptying the reactors completely, leading to losing of suspended biomass particles, which might be important for this inoculation and degradation process.

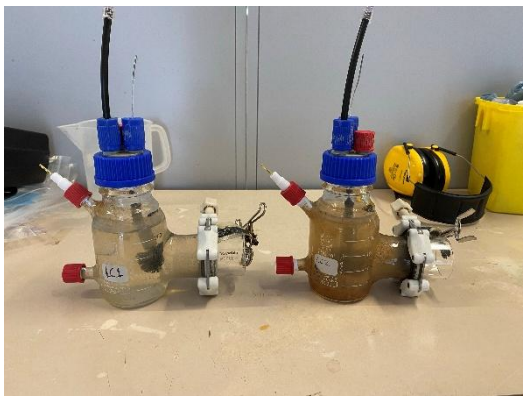

Figure 49. Comparison between LC1 and LC2 reactors after Cycle 14.

Cyclic Voltammetry characterization

The electrochemical evolution of the bioelectrochemical systems during the inoculation phase was also monitored through cyclic voltametries at the start and at the end of some representative cycles. For clarity and comparison, only two CVs are shown for each reactor: one from an early cycle (Cycle 2) and one from a later stage (Cycle 19).

Air-cathode diffusion reactors (AC1 and AC2) in Cycle 2 (see Figure 50) show positive currents up to 0.3 $A.m^{-2}$ at potentials >0.3 V vs Ag/AgCl 3M at the end of the cycle, which correspond to the oxidation of hydrocarbons. This current is higher than the value obtained at the same potentials at the beginning of the cycle which indicates that, during this cycle, biofilm growth and accumulation of exoelectrogenic bacteria may have occurred. AC2 presented a slightly larger current than AC1, indicating better initial activity. Liquid cathode reactors, LC1 and LC2, also showed higher current densities at the end of the cycle at oxidative potentials when comparing with its start. This also suggests that during the first cycles there was an accumulation of exoelectrogenic bacteria on the groundwater that acted as electrolyte.

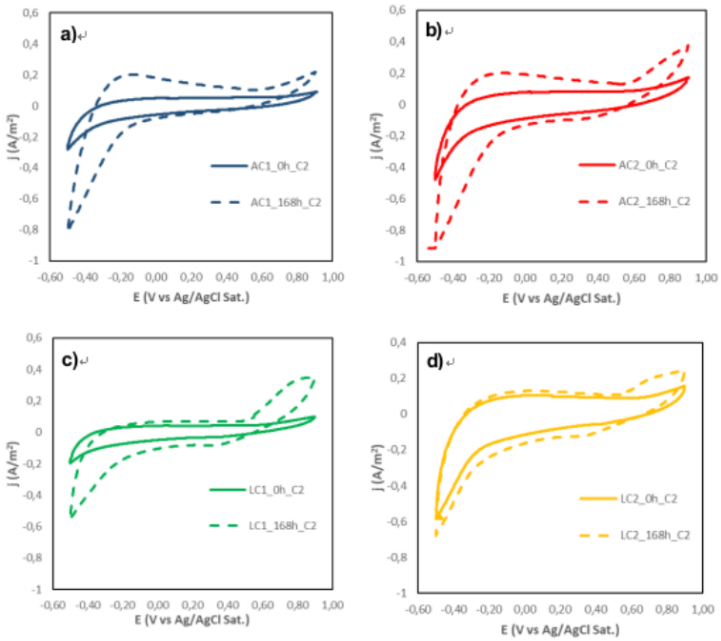

Figure 50. Cyclic Voltammetries performed to all the reactors at the start (0h) and at the end (168h) of the 2nd cycle

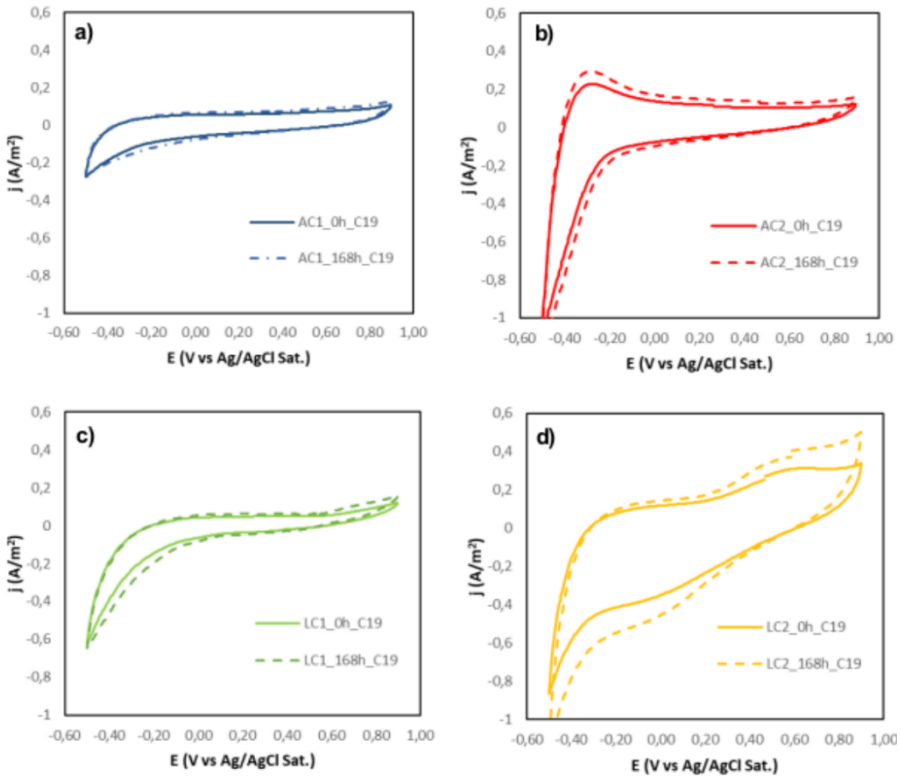

Figure 51 Cyclic Voltammetry's performed in cycle 19 at the start (0h) and at the end (168h) of for all the reactors

At cycle 19 (see Figure 51), air-cathode reactors CV show severe attenuation with positive currents reaching less than 0.1 $A.m^{-2}$, indicating that the hydrocarbon oxidation seems to be less active. Long-term deterioration of bioelectrochemical systems often arises from biofilm build-up and salt precipitation on the anodes, which can cause fouling and diffusion limitations, potentially reducing electron transfer rates and substrate availability.

Analysing Liquid Cathodes CV's at cycle 19, LC1 shows a slight reduction in oxidation current densities, but LC2 shows an improvement, with higher current densities. This suggests that liquid cathodes preserve the anodic biofilm, allowing continued hydrocarbon oxidation.

One factor that can influence these long-term trends seen in the chronoamperometry and cyclic voltammetry data is the handling of suspended biomass and particles when the reactor is emptied between cycles. When the reactor is drained and refilled, some suspended exoelectrogenic bacteria and fine biofilm fragments are washed out, and the system restarts with a lower inoculum. Together with fouling and diffusion limitations this can explain the decline, or plateau, in anodic activity during the 22 studied cycles.

Analysis of the microbial community

In alignment with subtask 3.2.2 and task 4.4 objectives, the collaborative work between LEITAT and JSI focused on selecting and characterizing bacterial consortia suitable for BES-based treatment of polluted groundwater. The primary goal was to identify consortia possessing both electroactive and TPH-degrading properties simultaneously.

Biomass samples were collected by LEITAT from air-cathode and liquid-cathode h-type reactors after cycle 22 of operation, from both (i) electrode-attached biofilms and (ii) planktonic communities. In these samples JSI then analysed the bacterial composition using molecular techniques explained in the previous section.

Results for microbial community analyses from the h-type reactors are displayed in Figure 52 and Figure 53. These results revealed significant differences between bacterial communities that evolved separately on carbon brush surfaces versus liquid phases. The cathode type also significantly influenced community composition, making the electrode-related samples clearly distinguishable from the other micro-environments in the reactor.

As shown in Figure 52, planktonic communities present in the liquid phase closely resemble the original groundwater composition, with the LC reactor being the most similar. This suggests that non-electroactive bacteria continued to dominate the bulk liquid phase in these reactors. However, the taxonomy profiles of the liquid samples (Figure 53) show an increased abundance of *Sphingobium* and *Extensimonas*, known for having efficient hydrocarbon degradation capabilities. These genera were particularly present in the liquid-cathode reactors. Additionally, the liquid-cathode reactor exhibited a higher abundance of *Thiobacillus*, also capable of hydrocarbons degradation, in both the liquid phase and the brush.

On the other hand, communities, attached to the surface of the electrodes showed enrichment of sulfate-reducing bacteria with electrogenic properties (refer to D4.1), which suggest that electro-stimulation can selectively promote the abundance of bacterial genera important for both hydrocarbon degradation and sulfur cycling. However, while electrogenic bacteria such as *Geobacter*, *Shewanella*, and *Desulfuromonas* were detected on the electrodes, their relative abundance remained low, indicating that the applied operational conditions were insufficient to favour their proliferation, matching with results from the cronoamperometry and cyclic voltammetries performed at one of the final cycles of inoculation (cycle 9), as discussed in the previous section. Taking all of these results into consideration, it was decided to change the reactor configuration to flat-type cells, in order to avoid biomass loss due to washing out when GW is renewed in the reactors.

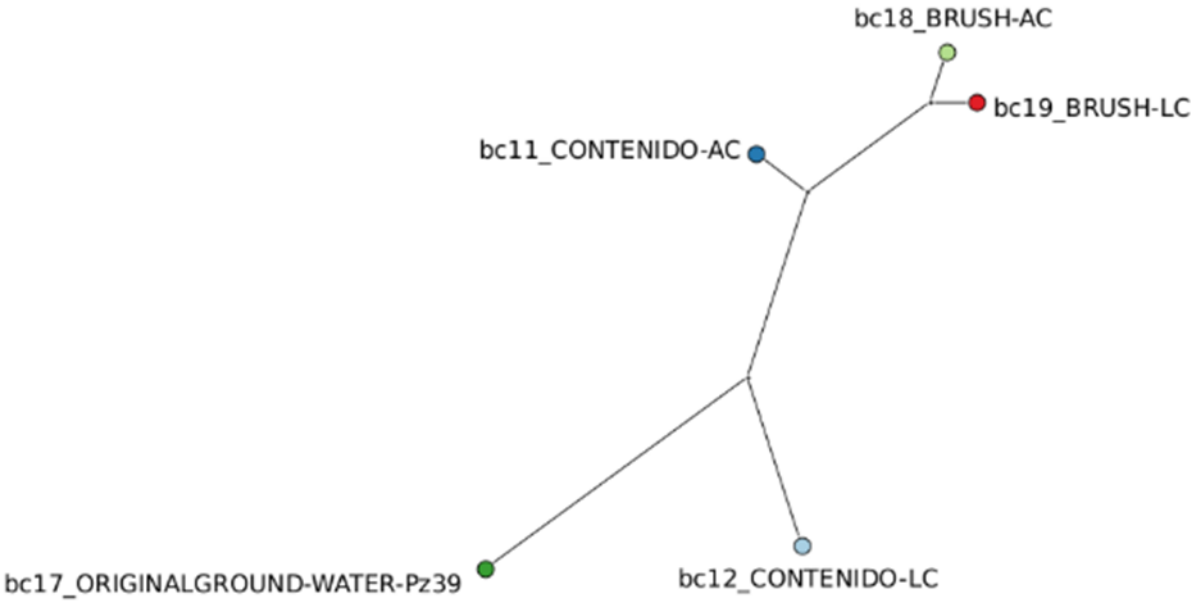

Figure 52. Neighbor joining network based on the UniFrac weighted matrix for comparison of microbial communities between samples of carbon brush (BRUSH), liquid from the BES (CONTENIDO) and original groundwater sample. LC - liquid cathode, AC – air-cathode. Sampling level: Genus.

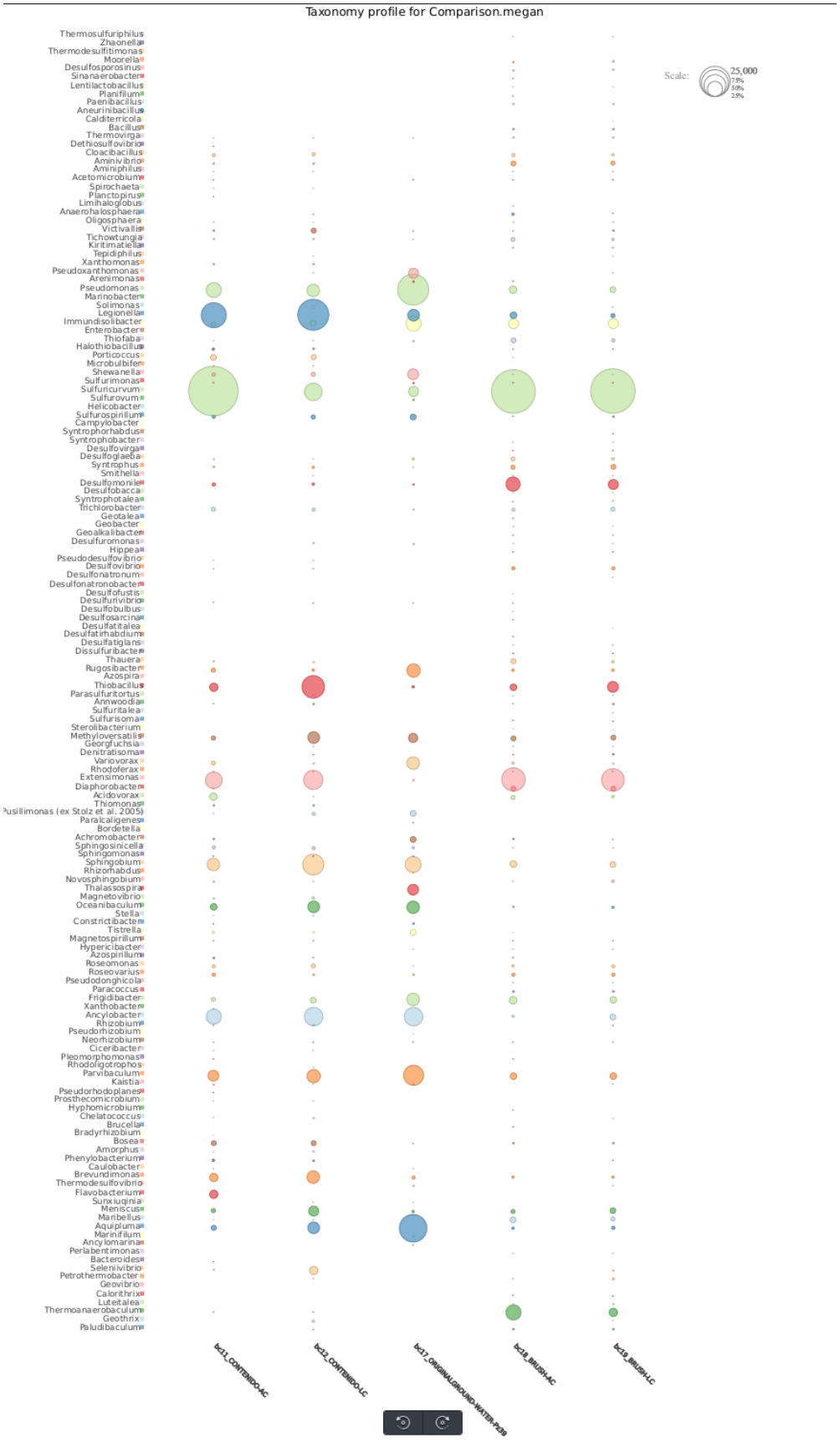

Figure 53. Taxonomy profile comparing microbial communities between samples of carbon brush (BRUSH), liquid from the BES (CONTENIDO) and original groundwater sample. LC - liquid cathode, AC – air-cathode. Sampling level: Genus

3.4.2.2 Flat type cells

3.4.2.2.1 Materials and methods

For the second phase, two flat plate BES reactors were used, using once again carbon fiber brushes as the anode (64.6 m^2 anode/ m^3 reactor) and a liquid-cathode of UDCFs + catalyst (6.6 m^2 cathode/ m^3 reactor). A scheme and dimensions of the reactors are displayed in Figure 54.

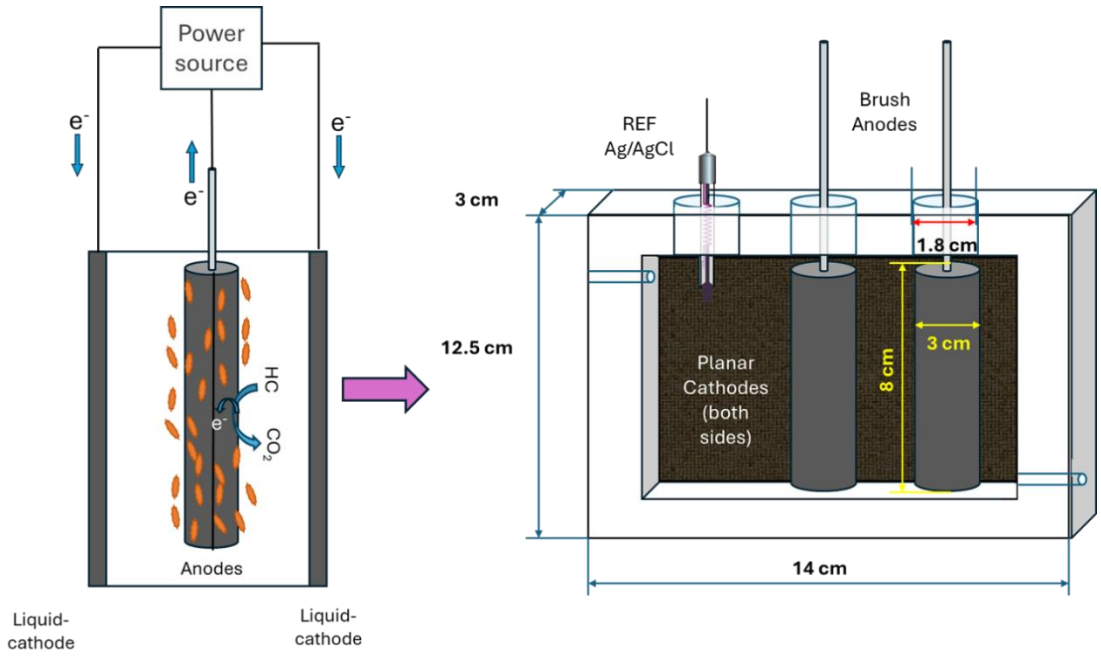

Figure 54. Schematic representation of the laboratory setup used for flat-type reactors setup.

Each reactor was connected to a 3 L buffer tank containing the contaminated groundwater, via polyethylene tubing with an internal diameter of 4 mm. The water was continuously pumped from the buffer tanks to the reactors at a flow of 100 mL/min. The reactors were operated at room temperature.

Electrochemical operation was conducted following the same method as in the half H-type reactors, where the anode was initially polarized at +0.6 V vs Ag/AgCl. Afterwards, the anode potential was set to +0.45 V vs Ag/AgCl as further explained in the following section

3.4.2.2.2 Results

Feed Groundwater Analysis

Groundwater feed samples were collected after 15-minute recirculation loop through the entire flat-type setup (including reactors LC1 and LC2), prior to analysis. This recirculation period, although relatively short, is considered sufficient to potentially influence contaminant concentrations due to processes such as volatilization of light hydrocarbons, sorption to tubing or reactor components, and early microbial activity. Sampling was performed at the start of each cycle, except for cycle 3. New Pz-39 groundwater samples were received more frequently when compared to the previous H-type experimental phase, i.e. one drum of 25 L per month.

As shown in Figure 55, total TPHs concentration was relatively low in cycle 1, but remained stable between 1500 and 2000 µg/L throughout most other cycles (2, 4, 5, and 7). The component

distribution across TPH C_5-C_{10}, TPH C_{10}-C_{40} and BTEX remained proportionally consistent in these cycles, with BTEX concentrations ranging from 500 to 750 µg/L.

An exception occurred in Cycle 6, where differences between LC1 and LC2 feed concentrations were observed. These variations could be attributed to non-homogeneous sampling, concentration fluctuations during recirculation, or minor bioelectrochemical interactions occurring in the tubing or reactor setup.

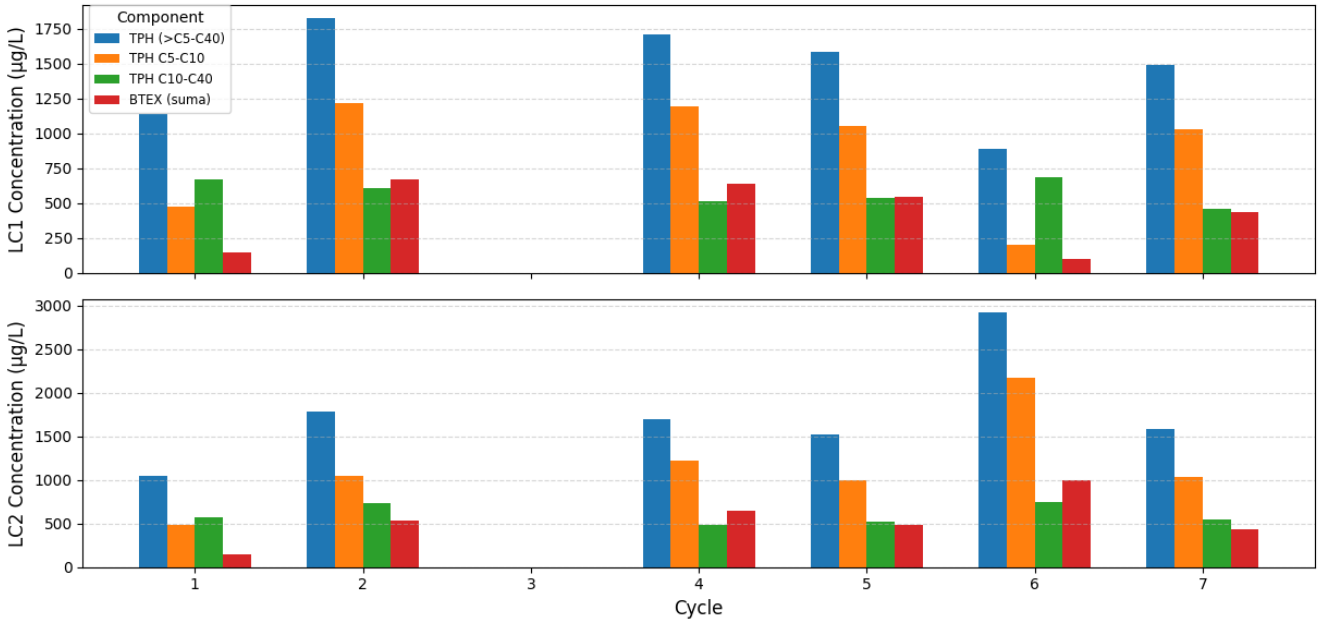

Figure 55. Feed groundwater contaminants concentration over the duration of the flat-type LC1 and LC2 inoculation.

The composition and trends across hydrocarbon groups are largely consistent, suggesting that the feed groundwater was reasonably comparable between reactors, which validates the comparison between the cycles and the reactors across these cycles. Any differences in electrochemical or microbial behaviour are therefore more likely due to reactor-specific dynamics, not inconsistencies in feed composition or contaminant loading.

Chronoamperometry

Flat-type reactors inoculation was carried out with the anode polarized at a potential of +0.6 V vs Ag/AgCl 3M, consistent with the procedure used in the H-type reactors. Based on prior performance and design advantages (see D4.1), liquid cathode was the preferred configuration for this phase. Two reactors were fabricated, LC1 and LC2, and the current density was monitored over weekly cycles for a total of seven weeks. The objective was to evaluate whether each system could reach and maintain current densities above the inoculation threshold of 0.01 A/m^2, which had been previously identified as a benchmark for successful inoculation.

Figure 56 shows both reactors failed to maintain a current density average value above the threshold during cycle 1, indicating limited electroactive biofilm development during the first week. However, from cycle 2, LC2 exhibited a significant and sustained increase in current density, maintaining values

well above the threshold throughout the rest of the experiment. In contrast, LC1 showed more moderate performance. While exceeding the threshold in Cycle 2 and 6, it remained just below the threshold during cycles 3, 4 and 5, showing a slight gradual upward trend.

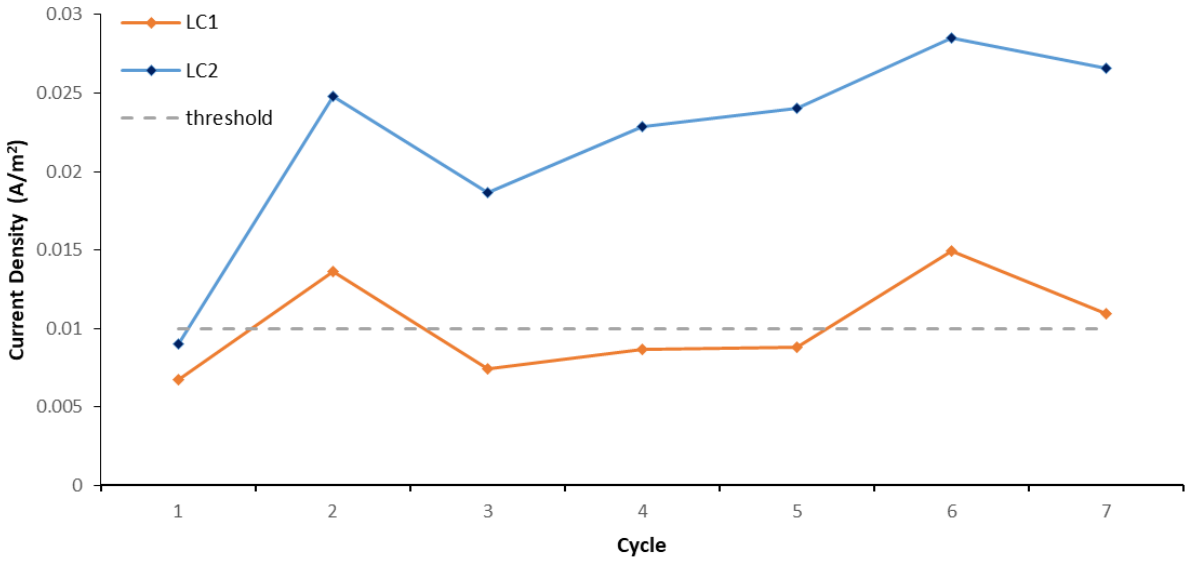

Figure 56. Current density evolution during bioelectrochemical flat-type reactors inoculation: LC1, and LC2.

These results suggest that the transition from H-type to flat-type reactors managed to achieve notable improvements in inoculation efficiency and electrochemical performance. Several factors may explain this improvement, including the enhanced retention of suspended particles, improved mass transport, and an architecture that supports microbial attachment and biofilm formation. The consistent performance of LC2, indicated that the new configuration provides a more suitable environment for bioelectrochemical activity during the initial stages of operation.

Cyclic voltammetry characterization

Cyclic voltammograms were obtained at the start of every cycle for flat reactors inoculation. Figure 57 shows the electrochemical behaviour of LC1 (Figure 57a) and LC2 (Figure 57b) at the first and last cycle. Both graphs show current density (A/m^2) in function of electrode potential (V vs Ag/AgCl sat.), indicating the presence and evolution of electrochemical activity at the carbon-brush anode.

LC1 and LC2 reactors show an increase in anodic current density at cycle 7 across the entire positive sweep, peaking around 0.4 $A.m^{-2}$, when compared with cycle 1 which peaked at around 0.2 $A.m^{-2}$ for LC1 and 0.3 $A.m^{-2}$ for LC2. The shape obtained at cycle 7 is more defined and wider, suggesting improved electron transfer processes and greater electroactive biofilm maturity.

This progression indicated that bioelectrochemical activity improved between cycles, with increased current density. The anodes at cycle 7 for both reactors are likely developing a more stable and active biofilm, indicating enhanced anodic activity over time.

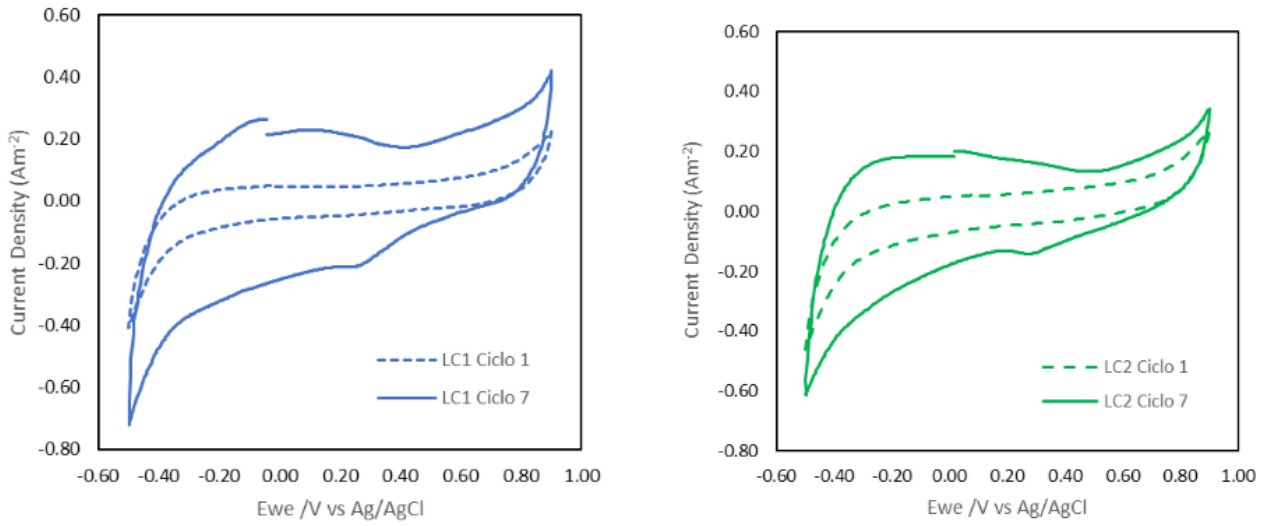

Figure 57. Cyclic Voltammetry (CV) analysis of the liquid cathode flat-type reactors: (a) LC1 and (b) LC2 at cycle 1 (dashed line) and cycle 7 (solid line)

Voltage shift

While flat-type reactors exhibited better electrochemical performance than H-type reactors at an anode potential of +0.6 V, hydrocarbon degradation showed no significant differences between electrochemical and control reactors. These results suggested that biological processes played a predominant role in overall hydrocarbon removal under the tested conditions (see D4.1). The likely reason for this is the limited growth of electroactive bacteria at the applied electrochemical conditions, also consistent with microbial community analyses performed by JSI on H-type reactors.

Thus, an alternating lower voltage of +0.45 V was applied to reactors LC1 and LC2 to promote a better development of electroactive bacteria. This value was chosen based on a) evidence from literature and b) its being the lowest potential at which the reactors could operate while maintaining a positive current density. The voltage was applied for two weeks, and cyclic voltammetry measurements were carried out before and after this period. The results are shown in Figure 58.

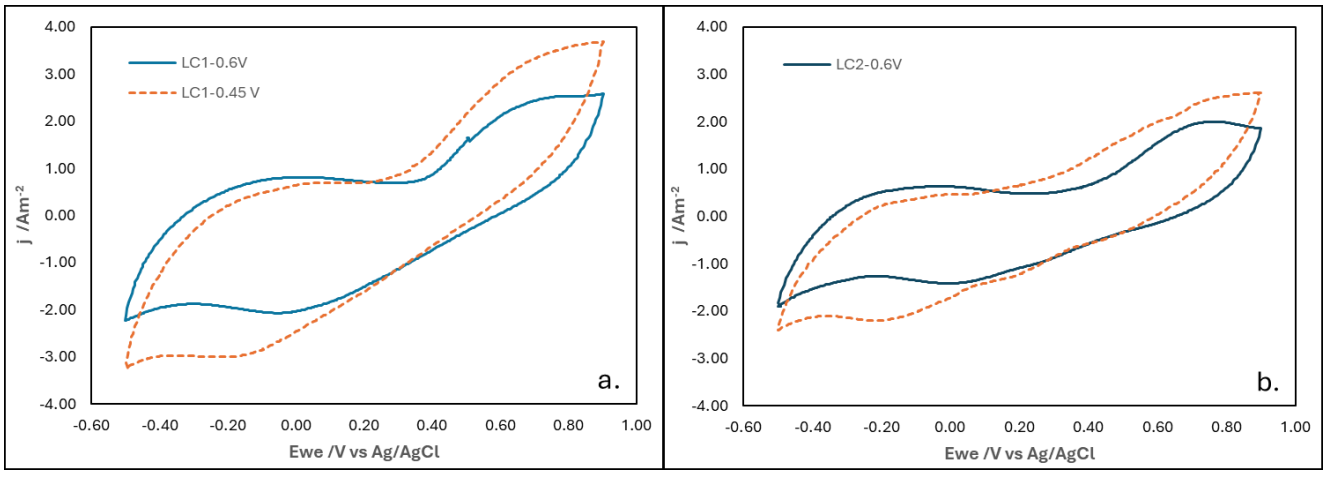

Figure 58. Cyclic voltammograms of reactors LC1 (a) and LC2 (b) at an anode's potential of +0.6V and after two weeks of enrichment at an Ean= 0.45V

As seen in the figure, both reactors exhibited a substantial increase in the anodic current density, even at an anode potential of +0.6V, compared to the results in Figure 58. This is likely due to the time elapsed between the end of cycle 7 (see previous section) and the moment the cyclic voltammograms were recorded, suggesting further maturation of the electroactive biofilm. Moreover, the application of a lower voltage led to an additional increase in current density and produced more clearly defined voltammograms, indicating the presence of a more stable and electroactive biofilm with improved electron transfer processes.

The most significant outcome relates to the impact of electroactive bacteria promotion on hydrocarbon degradation. Under the new conditions, electroactive reactors achieved 1.4-1.7 times higher TPH removal than the control reactor, marking the first substantial performance difference between reactor types and representing a step forward in optimizing the process for future pilot-scale applications. These degradation results are preliminary and will be further addressed in the final deliverable D4.3. Biofilm samples obtained after enrichment at this voltage have been recently sent to JSI for microbial characterization, with results still pending.

3.4.3 Biofilms for chlorinated ethenes removal

The removal of chlorinated ethenes (CE) by BES (task 4.1, see D 4.1), requires the establishment of both aerobic and anaerobic conditions. This necessitated the development of a bioanode and a biocathode.

At the anode, oxygen evolution occurs, supporting the growth of aerobic microorganisms capable of oxidizing chlorinated compounds with carbon chains longer than C_2. These microbes utilize the produced oxygen to degrade such compounds into of CO_2 and chlorinated ethenes (i.e. TCE, PCE, and VC) which can then be reduced to ethane in the cathodic compartment.

At the cathode, hydrogen evolution takes place under anaerobic conditions. In this environment, the organohalide-respiring bacteria (OHRB) *Dehalococcoides mccartyi* can be a key degrader, having the ability to completely reduce chlorinated compounds such as perchloroethylene (PCE), vinyl chloride (VC), and trichloroethylene (TCE), to ethene (Löffler et al., 2013), utilizing electron donors (i.e. hydrogen) (Dell'Armi et al., 2022). Therefore, promoting the selection and enrichment of *D. mccartyi* on the cathode surface is key to developing highly efficient dechlorinating biocathodes.

The initial step involved testing the enrichment of dechlorinating microbial communities on electrode surfaces using contaminated groundwater. This was followed by the addition of a commercial dechlorinating inoculum. To this end, flat-plate electrolysis cells were operated with real groundwater from Site 9, continuously recirculated for over 50 days, while monitoring current density.

3.4.3.1 Materials and methods

3.4.3.1.1 Laboratory set-up and experimental conditions

Biomass enrichment was performed in three double-chamber flat-plate electrolysis cells constructed from polymethylmethacrylate. Each chamber had a volume of 612.5 cm³ and was separated by a Cathion Exchange Membrane (CEM; CMHPP, RALEX®). Two different cathode materials were evaluated: stainless steel wool (SSW; AISI 434, RASKO, Germany) and synthetic graphite granules (Grade 2908, Graphexel Ltd, UK). In addition, since hydrogen evolution is necessary for the reductive dichlorination of CE (in which chlorine atoms will be replaced by hydrogen), a control reactor was

included, using non-conductive plastic fillings as the cathode. This setup also prevented hydrogen evolution.

All reactors employed a mixed metal oxide (MMO) anode, with both anode and cathode having an exposed surface area of 121 cm². Titanium wire and rods were used as current collectors.

A schematic of each reactor is shown in Figure 59.

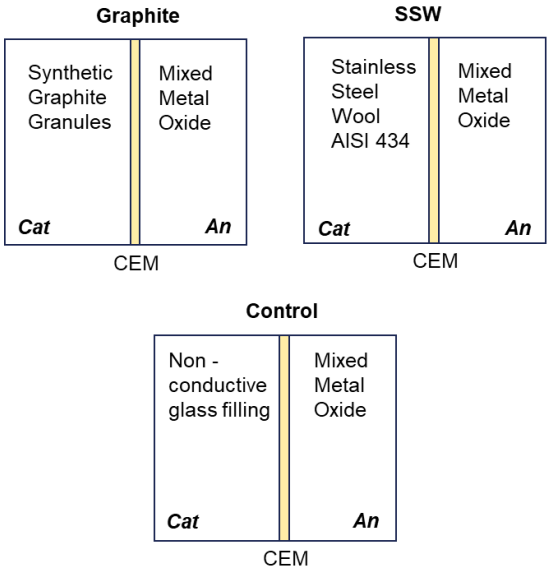

Figure 59. Scheme of flat-type reactors used for CE removal

GW from site 9 was used as both the anolyte and catholyte in all tested reactors, more specifically, GW from Pz-62 and Pz-53. The waters from these two sources were mixed in equal proportions (50:50) to balance microbial activity potential and contaminant load. Pz-62, showing signs of natural attenuation with relatively low concentrations of chlorinated ethenes (CEs), was considered favourable for microbial enrichment. In contrast, Pz-53 exhibited higher CE concentrations, making it suitable for evaluating dichlorination activity.

The reactors operated in batch mode, with both anolyte and catholyte composed of the same 1:1 mixture of groundwater from Pz-62 and Pz-53. Each reactor was connected to external catholyte and anolyte buffer tanks containing 1 L of the mixed GW, continuously recirculated at a flow rate of 100 mL/min using peristaltic pumps. A photograph of the experimental setup is depicted in Figure 60.

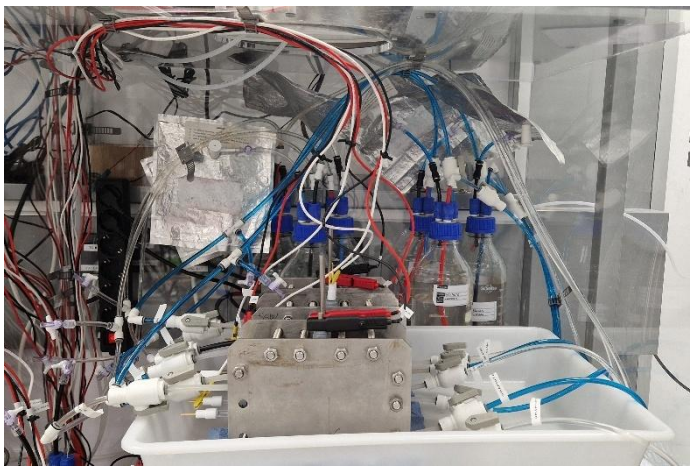

Figure 60. Experimental setup used for CE removal

3.4.3.1.2 Electrochemical operation

A three-electrode configuration was used, where the cathode was poised at a potential of -0.6 V vs Ag/AgCl 3M in all 3 reactors, with a preliminary phase (4 days) at -0.4 V. On day 39 the cathodic chambers of the experimental reactors were also bioaugmented with a custom blended bioaugmentation culture formulation able to completely degrade chlorinated solvent mixtures under anaerobic conditions (KB-1 Plus, SiREM, USA) in the presence of hydrogen. Throughout the enrichment current density was monitored, while cyclovoltammetries were conducted at specific times.

3.4.3.1.3 Results

Figure 61 shows a time-dependent profile of the volumetric current density (in mA/L cathode) as a function of time (days) for three different experimental conditions: SSW as cathode, graphite as cathode, and a control reactor with non-conductive plastic fillings as the cathode. The cathode potential was initially set at -400 mV, and on day 4 it was changed to -600 mV, causing shifts in the current density, particularly in the SSW and Graphite conditions. Around day 39, bioaugmentation with KB-1 was also performed. As the cathode was used as the working electrode, current density values were negative, as the electrons flow from the cathode to the anode. Thus, in this case, a more negative current density implies more electroactivity within the reactor.

The control reactor, maintained a near-zero current density throughout the entire experiment, indicating no significant electrochemical activity, as expected by the addition of non-conductive fillings. Conversely, the SSW reactor showed a varying current density, starting with values near -2 mA/L cathode. After the potential was changed to -600 mV, the current density further decreased, eventually stabilizing near -8/-10 mA/L cathode. After bioaugmentation current density fluctuated around -10/-14 mA/L cathode, showing a slight enhance of the electroactivity.

The graphite reactor started with a high negative current density (around -8 mA/L cathode), considerably higher than the SSW reactor. However, after the potential change to -600 mV, the current density increased to values around -4mA/L cathode. Following bioaugmentation on day 39, the current density rapidly decreased to -16 mA/L cathode, stabilizing however at values near -4 mA/L cathode.

Considering these results, the SSW reactor outperformed the graphite reactor regarding current density values obtained from the start of the inoculation. This might also be directly related to a

slightly enhanced removal of CE in this reactor (see D4.1). However, further studies are needed to optimize the applied voltage and more clearly establish the relationship between current generation and CE degradation.

Interestingly, bioaugmentation appeared to have a greater impact on the SSW reactor than on the graphite reactor, suggesting that the electrode material significantly influences microbial activity. Nonetheless, findings from D4.1 indicate that anaerobic conditions were not consistently maintained across the reactors. Therefore, additional experiments will be conducted to address this issue and ensure more reliable results.

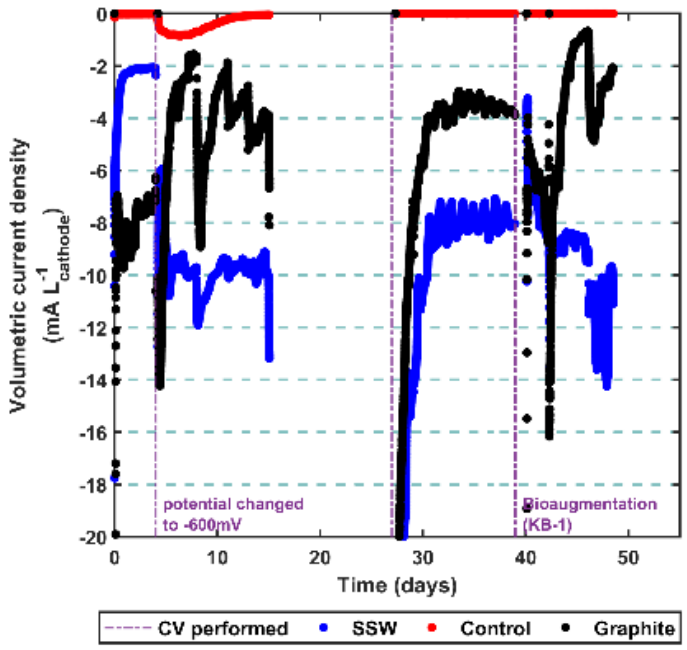

Figure 61. Temporal evolution of the volumetric current density (mA/L cathode) for three different experimental conditions: SSW as cathode (blue dots), graphite as cathode (black dots), and a control reactor (red dots) with non-conductive plastic fillings as the cathode. Vertical dashed lines indicate when a CV was performed. Significant events throughout experimentation (change of cathode's potential to -600 mV and bioaugmentation) at specific times are also highlighted in the figure.

4 Conclusions

The work developed in Task 3.2 allowed the successful development of strategies for spatial structuring of microbial consortia through synthetic aggregates and biofilms, including electroactive variants, building on consortia from WP1 Task 1.3 and aligning with WP3 objectives for consortia aggregation, immobilization, and biofilm enhancement. This included protocols for robust multicellular aggregates enabling aerobic-anaerobic niche separation (e.g., SRB cores with *Cobetia marina*), vaterite-based carriers for hydrophobic pollutants (e.g., PAHs, atrazine, lindane) with demonstrated consortium stability (e.g., I18-S0211 maintaining core genera over 14 days), planar biofilm delivery to plant roots, controlled electrostatic aggregation for 2D/3D architectures, and flow cytometry assays for GMO strain growth assessment on pesticides.

For electroactive biofilms, polypyrrole modifications (optimal at 5 cycles) enhanced attachment and performance (e.g., reduced charge transfer resistance, higher current densities up to 0.4 A/m²), with polyelectrolyte layering enabling multilayered structures for *Shewanella* and *Chlorella*, and carbon brush adaptations improving scalability. Redox modulation protocols yielded electroactive biofilms for metals (stable at 0.2 mA/cm² using three/two-electrode configurations), hydrocarbons (kerosene-boosted currents >0.01 A/m² in flat-plate reactors, with SRB enrichment but low electrogen abundance), and chlorinated ethenes (SSW cathodes at -600 mV post-bioaugmentation reaching -10/-14 mA/L, emphasizing strict anaerobism needs). The development of electroactive biofilms for metals removal through redox potential modulation proved feasible both under three-electrodes configuration and two-electrodes configuration, with the latter providing an alternative and practical methodology for anodes inoculation.

Electroactivity was observed in reactors during the enrichment of CE-degrading microorganisms in groundwater from site 9, using either stainless steel wool (SSW) or graphite cathodes. However, the SSW reactor exhibited higher current density from the start of inoculation, indicating greater electroactivity compared to the graphite reactor. While bioaugmentation can enhance electroactivity, its effectiveness appears to be strongly influenced by the choice of electrode material, with the SSW reactor again showing superior performance. To ensure the optimal efficiency of the commercial KB-1 consortium, it is essential to maintain strict anaerobic conditions throughout the reactors.

In this deliverable, innovative approaches like µLUME and iACME were extended for consortia isolation and structuring, screening combinations for electrogenic and degradation capabilities, though challenges in hydrocarbon systems (e.g., variable electroactivity, reliance on biomass retention) highlight optimization gaps relative to WP3 promises for improved efficiencies.

Link with other WPs:

- The developed aggregated consortia and biofilms fulfil WP3 Subtask 3.2.1-3.2.2 objectives and will be integrated into WP4 for rhizosphere phytoremediation (T4.1, e.g., root delivery methods), estuarine sediment treatment (T4.3, e.g., immobilized inocula), and BES groundwater remediation (T4.4, e.g., electroactive biofilms for metals/organics), with protocols validated for lab-scale scalability toward WP5 field trials (TRL 5).
- Selected consortia and strains will be analysed via metagenomic WGS to identify metabolic pathways and interspecies interactions, supporting WP2 Task 2.2 constraint-based models for simulating biodegradation and guiding further enhancements, though pending characterizations (e.g., post-enrichment samples) may refine predictions.

- Electrode modification and redox protocols directly support WP4 Task 4.4 objectives for low-energy BES reactors treating mixed pollutants, enabling simultaneous oxidative/reductive pathways, with preliminary degradation results (e.g., 1.4-1.7x control for TPHs) aligning with WP3 promises but requiring verification in WP5 replication scenarios.
- Plant root delivery methods link to WP3 Task 3.1 and WP4 Task 4.2, facilitating PGP consortia testing for metal tolerance and organic pollutant degradation in poplar-microbe systems, addressing WP3 objectives for phytoremediation improvement while noting assumptions on field transferability (e.g., ignoring matrix complexities) to be tested in WP5.

Overall, the spatial engineering tools bridge WP1 microbial resources with WP4/5 bioremediation, meeting WP3 expectations for biosystem optimization, but hydrocarbon and anaerobic control challenges suggest iterative feedback with WP2 models for wider implementation in WP5 Task 5.3.

5 References

Dell'Armi, E., Zeppilli, M., Di Franca, M.L., Matturro, B., Feigl, V., Molnár, M., Berkl, Z., Németh, I., Yaqoubi, H., Rossetti, S., Papini, M.P., Majone, M., 2022. Evaluation of a bioelectrochemical reductive/oxidative sequential process for chlorinated aliphatic hydrocarbons (CAHs) removal from a real contaminated groundwater. J. Water Process Eng. 49, 103101. https://doi.org/10.1016/j.jwpe.2022.103101

Löffler, F.E., Yan, J., Ritalahti, K.M., Adrian, L., Edwards, E.A., Konstantinidis, K.T., Müller, J.A., Fullerton, H., Zinder, S.H., Spormann, A.M., 2013. Dehalococcoides mccartyi gen. nov., sp. nov., obligately organohalide-respiring anaerobic bacteria relevant to halogen cycling and bioremediation, belong to a novel bacterial class, Dehalococcoidia classis nov., order Dehalococcoidales ord. nov. and family Dehalococcoidaceae fam. nov., within the phylum Chloroflexi. Int. J. Syst. Evol. Microbiol. 63, 625–635. https://doi.org/10.1099/ijs.0.034926-0

Rybkin I, Gorin D, Sukhorukov G and Lapanje A (2019) Thickness of Polyelectrolyte Layers of Separately Confined Bacteria Alters Key Physiological Parameters on a Single Cell Level. *Front. Bioeng. Biotechnol.* 7:378. doi: 10.3389/fbioe.2019.00378